Thai coast project report

Work Package 1

Baseline assessment of hydro-meteorological boundary conditions.

Jerome Curoy[1], Raymond Ward[1,2] and John Barlow[3].

[1]Centre for Aquatic Environments, University of Brighton, UK; [2]Department of Landscape Management, Estonian University of Life Sciences, Estonia; [3]Department of Geography, University of Sussex, UK

Edited: Cherith Moses[4], Kanchana Nahapakorn[5]

[4]Edge Hill University, UK [5]Mahidol University, Thailand

The **Thai-coast project** is funded through the Newton Fund Understanding of the Impacts of Hydrometeorological Hazards in South East Asia programme, funded by the Economic & Social Research Council (ESRC) and Natural Environment Research Council (NERC) and Thailand Social Research and Innovation (TSRI). Project reference: NE/S003231/1.
www.edgehill.ac.uk/nerc-tcp

Table of contents

1 Aim

Aim: to characterise the recent past (~ 150 - 20 years) and present, coastal geomorphology, coastal protection & flood conditions, together with sedimentary processes including mass movements in river catchments, flood responses and deposition/erosion at the coast. During extreme hydro-meteorological events there are, potentially, two consecutive phases of geomorphic process: first, immediate, severe erosion and flooding on the coast via sediment removal and shoreline retreat; second, subsequent sediment provision to the coast through sediment pulses delivered from the catchment by rivers (e.g., via mass movements/landslides and/overland flow erosion caused by the increased rainfall). These operate within the constraints of historic and current coastal protection including distribution of natural ecosystems, such as mangroves, that protect the shoreline. Establishing and understanding the hydro-meteorological boundary conditions will facilitate scenario modelling under future predicted climate change scenarios (climate and flood modelling, Work Package 2 and coastal vulnerability assessment, Work Package 4).

2 Summary

Coastal provinces in Thailand need immediate solutions to counter coastal erosion and flooding. Both issues affect over 11 million people (17% of the population). These issues are only going to be exacerbated in the future for environmental, human and financial aspects by the impacts of climate change and sea level rising as predicted by the Thai's Office of Natural Resources and Environment Policy and Planning. This project is focusing on two highly touristic provinces in Southern Thailand with economies highly linked to coastal activities: the Krabi province and the Nakhon Si Thammarat (NST) province. We are particularly interested to develop (i) trends in frequency of hydro-meteorological events over the last 20 years and (ii) discharge and sediment budgets for events of low, medium and high magnitudes. This is to quantify how much water and sediment moves in the fluvial-coastal system during hydro-meteorological events of different magnitudes. This information is important to understand the impact of particular hydro-meteorological events on the shoreline, in terms of both erosion and flooding, and to predict the impact of future events under different climate change scenarios (WP2).

Hydrological, storm and tidal data are collected from Thailand's Meteorological Department through our data usage agreement, and the Permanent Service for Mean Sea Level. Part of the historical shoreline change data are provided by the project partner DMCR and completed by this study using satellite images processing to a much smaller timescale over the last 30 years. Sedimentation data within estuaries are collected utilising a range of techniques including: $^{210}Pb/^{137}Cs$ dating to identify recent historical (~150 years) sediment accretion rates in predominantly depositional settings, laser particle size analysis to identify changes in granulometry, influenced by depositional energy and/ or sources and geochemical impulse dating using known dates of inputs of heavy metals. This enables the dating of the extent and magnitude of extreme sediment deposition events in the historic past e.g., related to hydro-meteorological events, to help assess potential future impacts. Topographic and optical data, derived from high-resolution aerial photographs and satellite imagery are used to quantify the sediment cascade associated with high-magnitude hydro-meteorological events over the past two decades. To quantify the volumetric flux associated with mass wasting, a landslide inventory is created for each available year from which volumetric estimates of erosion are derived based on well-established relationships between landslide area and volume. Total volumetric flux associated with mass wasting are then modelled using the negative power law scaling of each landslide inventory's magnitude-frequency distribution. Once completed, the volumetric fluxes associated with high magnitude hydro-meteorological events are being compared to those measured between events to understand the significance of high-magnitude events within the sediment cascade.

The main outputs from this study show that mangrove environments in Southern Thailand

erode much faster and recover much slower than sandy beaches while anthropic activities have a noticeable impact on shoreline position. The coastline in the NST province is also very reactive to storminess and extreme weathers. The sediment volumes released during the catastrophic events of 2011 in the Krabi province to the catchments are estimated in some catchment as being 10 times greater than any other year when measurements were possible. This year's events were also very clearly marked in the sedimentary records of the Krabi's mangrove and seagrass environments by an increase of sedimentation rates. A positive correlation between the size or the activity of the landslides and rainfall intensity is identified especially in the catchments of the Krabi province. The El Nino-Southern Oscillations (ENSO) have been identified as the main parameter influencing the sediment distribution made available to the coastal environments throughout the rivers over time while sudden short time-scale events such as extreme rainfall, flood events and typhoons are at the origin of sudden peaks of sedimentation rates.

3 Introduction-Desk Study

Coastal areas in Thailand are heavily populated and represent a tremendous resource for the country in regard to recreational, economical, farming, environmental and tourism activities. Within the context of climate change and coastal change, economies are under threat and the study of shoreline position is a key parameter to understand the past evolution of coastal environments (Splinter et al., 2018).

The stability of coastal environments is a direct consequence of the interplay between sediment replenishment from rivers, the introduction of marine sediment and the remobilisation these sediment mixtures by the coastal currents. Sediment supplied by rivers to the coastal environments originates from their whole catchment area.

Landslides, which are terrestrial mass movements of slope sediment, are common geomorphologic features in Thailand (Soralump, 2010; Yumuang, 2006; Ono et al., 2014). They may often occur suddenly causing property damage and human casualties. In recent years, Thailand has experienced several landslide events claiming hundreds of lives and causing millions of Baht in economic losses. Landslides in Thailand are typically associated with heavy rainfall (Soralump, 2010) which global climate change is predicted to exacerbate (Gariano and Guzzetti, 2016). The sediment material from these terrestrial mass movements may constitute the principal material of the sediment cascade within the river catchments contributing to the coastal sediment supply, particularly to depositional environments such as mangroves. The latter are excellent sediment sinks that enable the investigation of variations in sediment characteristics to reveal past hydrodynamic/weather conditions.

The topography of the South of Thailand can be generalised as high relief mountains backing a wide, flat, low-lying coastal plain making coastal communities prone to flood events. These disasters have had significant impact in Thailand in recent decades, both in terms of economical and human impacts. In 1993, a tropical depression caused flooding in the Nakhon Si Thammarat province resulting in 23 deaths and 1.3 billion baht in damage (Daly et al., 2016). The 2004 tsunami claimed over 5000 lives and economic damage was estimated at more than 40 billion baht (Daly et al., 2016). In 2010, a total of 8,970,653 people (some 2,612,472 households) were affected, and 258 people died due to flooding (IFRC, 2011) with billions of baht lost to the economy. In 2011, floods throughout Thailand resulted in the loss of over 800 lives and more than 1236 billion baht in damage (Daly et al., 2016). In 2016, floods in southern Thailand left 11 dead and affected 350,000 people. A month after in 2017, another 21 people were reported dead by Thailand's Department of Disaster Prevention and Mitigation (DDPM) (Floodlist.com, 2020). The study and modelling of such events improves understanding of how and when they occur and helps in mitigating or preventing their future occurrence and impacts.

Often, historical field data on shoreline, river and landslide behaviour are scarce or non-existent depending on location and sometimes sites are very remote or inaccessible. For these reasons coastal scientists and managers have turned their attention towards the use of satellite imagery to facilitate observations. This study has adopted such approach and provides an evaluation of coastal evolution along the coastlines of the Krabi and the Nakhon Si Thammarat (NST) provinces in the South of Thailand from 1990 to present. To facilitate those observations and collect data on the study sites we (1) regrouped all freely available appropriate satellite imagery and (2) used up to date satellite imagery analysis tools to determine the shoreline position over a range of time periods.

A similar approach based on the use of free satellite and aerial imagery has been used to collate data on mass movements over the last 15-20 years and develop a landslide inventory within six river catchments in both provinces. The catchments of interest were for the rivers: Pak Nam Krabi, Kam and Phela within the Krabi province; and, Thung Sai, Hin and Cha Mao within the NST province.

Sediment characteristics such as grain size, bulk density, sorting coefficient, organic matter contents as well as radio-isotopic activity were measured within vertical profiles of cores taken from mangroves within each of these six river catchments. Additionally, three seagrass sites located just outside the river mouth of the Phela river were part of this analysis. The aim of this analysis is to (1) characterise the sediment transported by the rivers within each study site and their catchment; (2) be able to identify a significant change in grain size distribution linked to extreme or increased flash flood periods with higher sediment discharge and stream competency; (3) investigate the link between organic matter content and broader hydrometeorological conditions through the linkage of organic matter deposition; (4) calculate sedimentation rates over the last 50 years.

3.1 Topography and geology

The geology of the Malay Peninsula in Thailand consists of a succession of Paleozoic and Mesozoic sedimentary and metamorphic rocks, intruded by Late Paleozoic to Mesozoic igneous rocks, and covered by Cenozoic sedimentary rocks or sediments (Nazaruddin and Duerrast, 2018). The main mountain chains are formed in granite (Ridd et al., 2011). In the context of tectonics, this area is located on the intra-plate of the Eurasian plate. It is regionally affected by the interaction of the plate boundary between the Indian and the Burman plates. Two active faults cut through Southern Thailand in a SSW-NNE direction, the Ranong Fault and the Khlong Marui Fault. The Ranong fault zone extends from the Andaman Sea towards the Gulf of Thailand through the Ranong, the Prachuab Kirikhan and Chumpon provinces with a total onshore length of about 440 km (Nazaruddin and Duerrast, 2018). Some parts of the fault zone follow the channel of the Kraburi River, and subsidiary faults cut Late Cretaceous and Palaeogene granites and Cenozoic sedimentary rocks (Nazaruddin and Duerrast, 2018). The Khlong Marui Fault has a length of 210 km cutting thought the inflection of the Thai Peninsula. This fault cuts across the Phuket province, the Phang Nga Bay and the Ban Don Bay on the Andaman Sea and then follows the Khlong Marui channel to the Gulf of Thailand through Surat Thani province (Nazaruddin and Duerrast, 2018). Geologically this fault cuts through Late Cenozoic to Palaeogene granites and Paleozoic sedimentary rocks (Morley et al., 2011; DMR, 2014) (Figure 1).

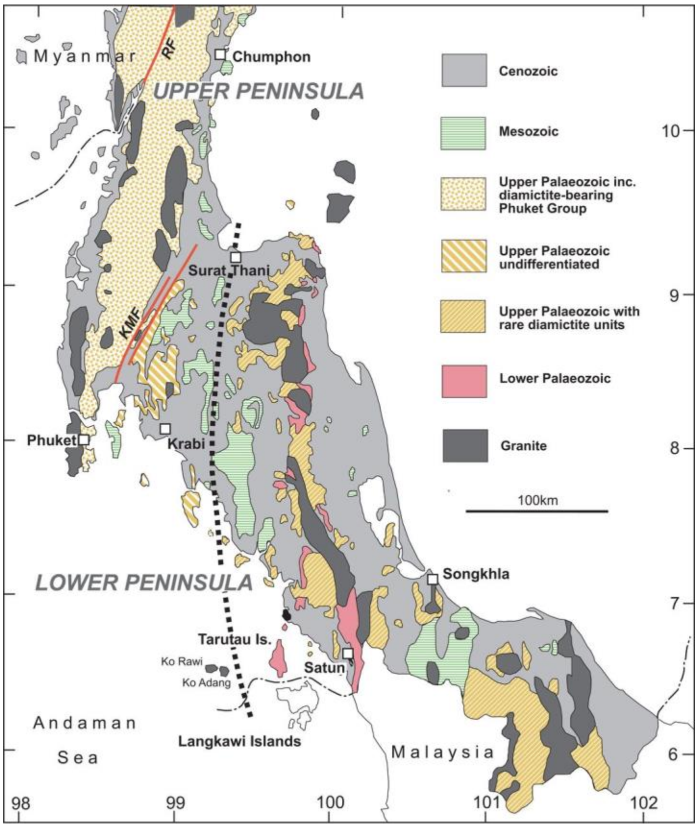

Figure 1: Geological map of Southern Thailand. (Red lines: KMF, Khlong Marui Fault; and RF, Ranong Fault; Ridd, 2016).

The South of Thailand can be divided into three main topographic areas (Figure 2): the Southern mountain ranges, constituting the high elevation points at the back of the studied areas; the coastal plain of the Gulf of Thailand and the coastal plain of the Andaman Sea, where our study areas are located.

There are three Southern mountain chains comprised of (North to South):

- ✓ The Phuket mountain chain; starting from the bottom-end of the Tenasserim mountain chain in the Ranong province, running south across the Surat Thani province, the Phang Nga province, and then the Surat Thani province again to finish in the Phuket and the Krabi provinces. This chain is 200 km long (North to South) and 50 km wide (East to West) at its greatest extent (https://km.dmcr.go.th/, 2013). Its highest elevation is the Khao Langkha Tuek with an elevation of 1395 m.
- ✓ The Nakhon Si Thammarat Mountain Range starting from Ko Tao and extending to the South all the way to the Satun province, creates a natural boundary between the Nakhon Si Thammarat province, the Surat Thani province and the Trang province. It is 319 km long (North to South) and 45 km wide (East to West, https://km.dmcr.go.th/, 2013). its highest peak, the Khao Luang, is 1780 m high making it the highest peak of Southern Thailand.
- ✓ The Sankalakiri mountain range starts from the coast of the Satun province and stretches 528 km to the southeast along the Thailand-Malaysia border. This also runs through the Songkhla, the Yala, and the Narathiwat provinces and ends in the Waeng District, Narathiwat province. The highest peak is called the Hulu Tippacha, height 1,535 m (https://km.dmcr.go.th/, 2013).

The coastal plain of the Gulf of Thailand on the East of the peninsula extends from the Chumphon province to the Narathiwat province. This area used to be a shallow seashore and was transformed into land by Quaternary deposits (mud, sand and gravel) brought to the coast by fluvial and sea currents (https://km.dmcr.go.th/, 2013; Figure 2).

The Andaman coastal plain on the West of the peninsula is narrow where large embayments, short narrow beaches and Permian limestone islands or rock cliffs are key features (https://km.dmcr.go.th/, 2013).

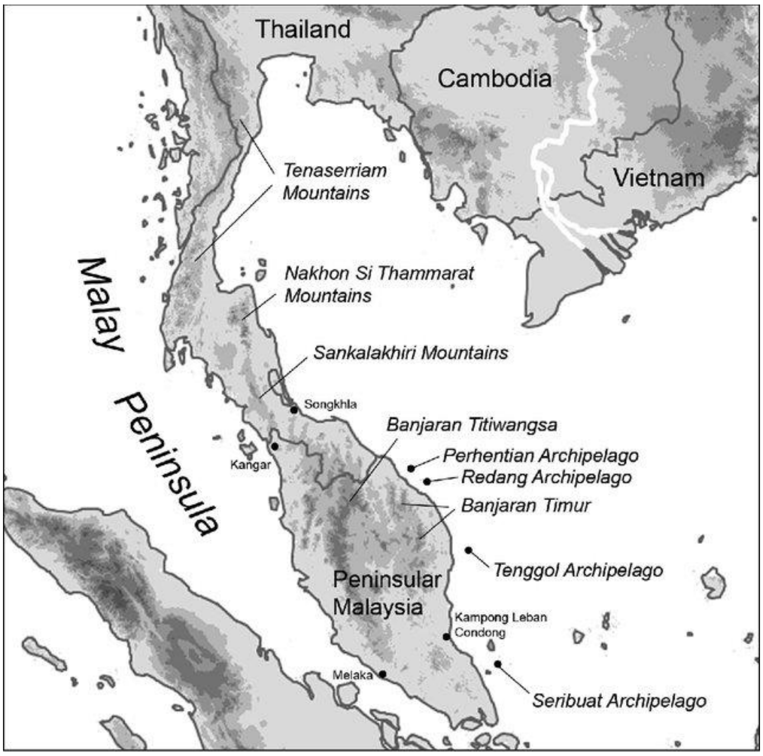

Figure 2: Major mountain ranges of the Malay Peninsula of southern Thailand (Grismer et al., 2011).

3.2 Coastline types and Coastal erosion

Southern Thailand is located between the Gulf of Thailand and the Andaman Sea. The Gulf of Thailand is a semi-enclosed bay located in the South China Sea consisting of 1,878 km of the East Coast of Thailand. The Gulf is 380 km wide on average, 540 kilometres at its widest and 810 km long (Robinson, 1974). Its average depth is approximately 44 m while its deepest depth is approximately 86 m (Robinson, 1974), quite a shallow bathymetry. The Gulf's seafloor is characterised by a gentle slope covered with deposits of clay, silts, sand or a mixture of those along the coast of Nakhon Si Thammarat (Figure 3).

The Andaman Sea has a length of about 1200 km from North to South and is at its widest (West to East) of approximately 650 km wide, bordering 2815 km of the Thai coastline. Its average depth is 870 m and is at its deepest of about 3,777 m deep. In the area of the Krabi province, the seabed of the Andaman Sea has a very gentle sandy slope and the continental shelf has a depth of < 300 m (https://km.dmcr.go.th/, 2013; Figure 4).

The total coastline length of both areas of interest is 236.82 km long for the Nakhon Si Thammarat province, and 203.79 km for the Krabi province (Table 4; Department of Marine and Coastal Resources, 2018). The elevation of coastal areas along Nakhon Si Thammarat ranges from 0-4 m above the mean sea-level (http://www.dmr.go.th/, 2015), highlighting the risk of coastal flooding from storm surges, coastal erosion and sea level rise.

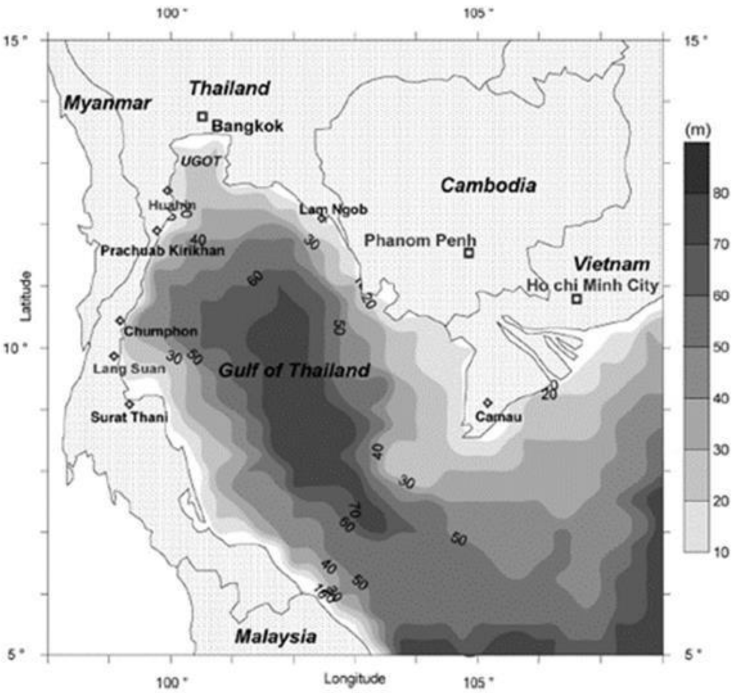

Figure 3: Bathymetry in the Gulf of Thailand (Sojisuporn et al., 2010).

(A)

(B)

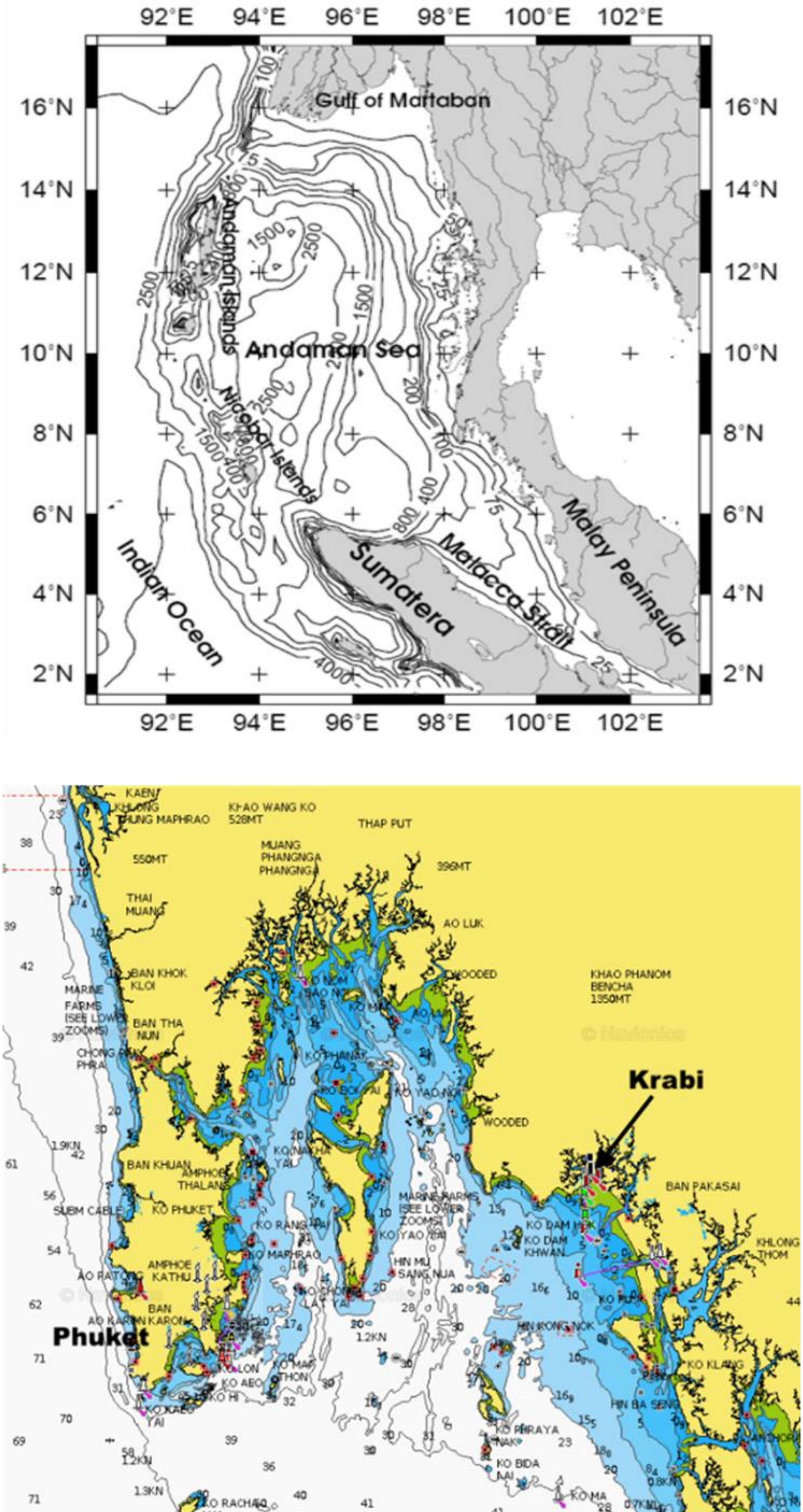

Figure 4:Bathymetry of the Andaman Sea (A) and in the proximity of the Krabi province (B) ((A)Rizal et al., 2012; (B)https://brittany-kayaking.com/, 2020).

Province	Area (km^2)	Coastal length (km)	Number of islands	Population (people)	Number of fishing households
Nakhon Si Thammarat	9,942.50	236.82	9	1,557,482	6,260
Krabi	4,708.51	203.79	154	469,769	1,212

Table 1: Human and coastal characteristics of the Nakhon Si Thammarat and Krabi provinces (National Statistical Office, Ministry of Information and Communication Technology, 2013).

The shape of the coastline in Southern Thailand is very sinuous along the Krabi province creating more shelter from incoming waves on some sections of its coastline. In contrast, the Nakhon Si Thammarat province coast is much more straight and as a consequence is subject to the full strength of incoming waves. Both coastlines present a variety of environments: rocky cliffs; sand or gravel beaches; lagoons; wetlands; estuaries and tidal flats (Figure 5). The latter environments are often colonised by mangroves and seagrasses, both valuable conservation areas for the South of Thailand. Pressures from tourism, recreational activities, fisheries/aquaculture industry and the sensitivity to changing environmental conditions have resulted in these areas being subject to conservation law protection.

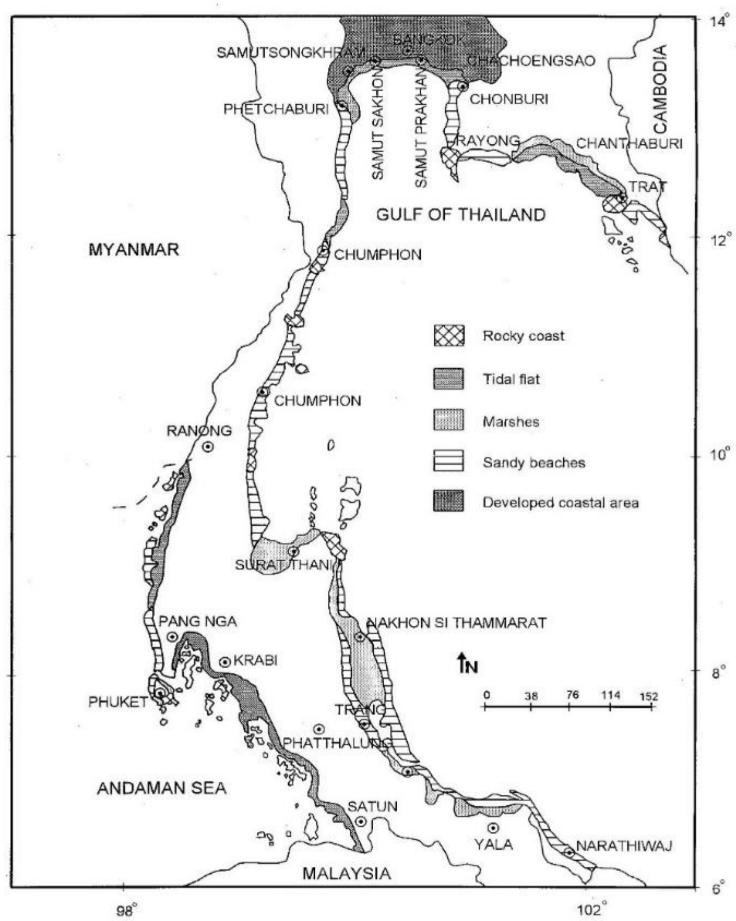

Figure 5: Type of coasts observed in Thailand (http://www.dmr.go.th/, 2015).

Prior to this study, erosion of the coastline along Nakhon Si Thammarat was classified as critical, with reported erosion rates of more than 5 m per year in the South of NST and erosion rates ranging from 1 to 5 m in the North of Nakhon Si Thammarat. The coastline along the Krabi province is mostly eroding at a rate of 1 to 5 m per year with localised areas eroding at more than 5 m per year (Department of Marine and Coastal Resources. Marine and Coastal Resource Database, 2011 *in* http://www.Km.dmcr.go.th, 2013; Figure 6).

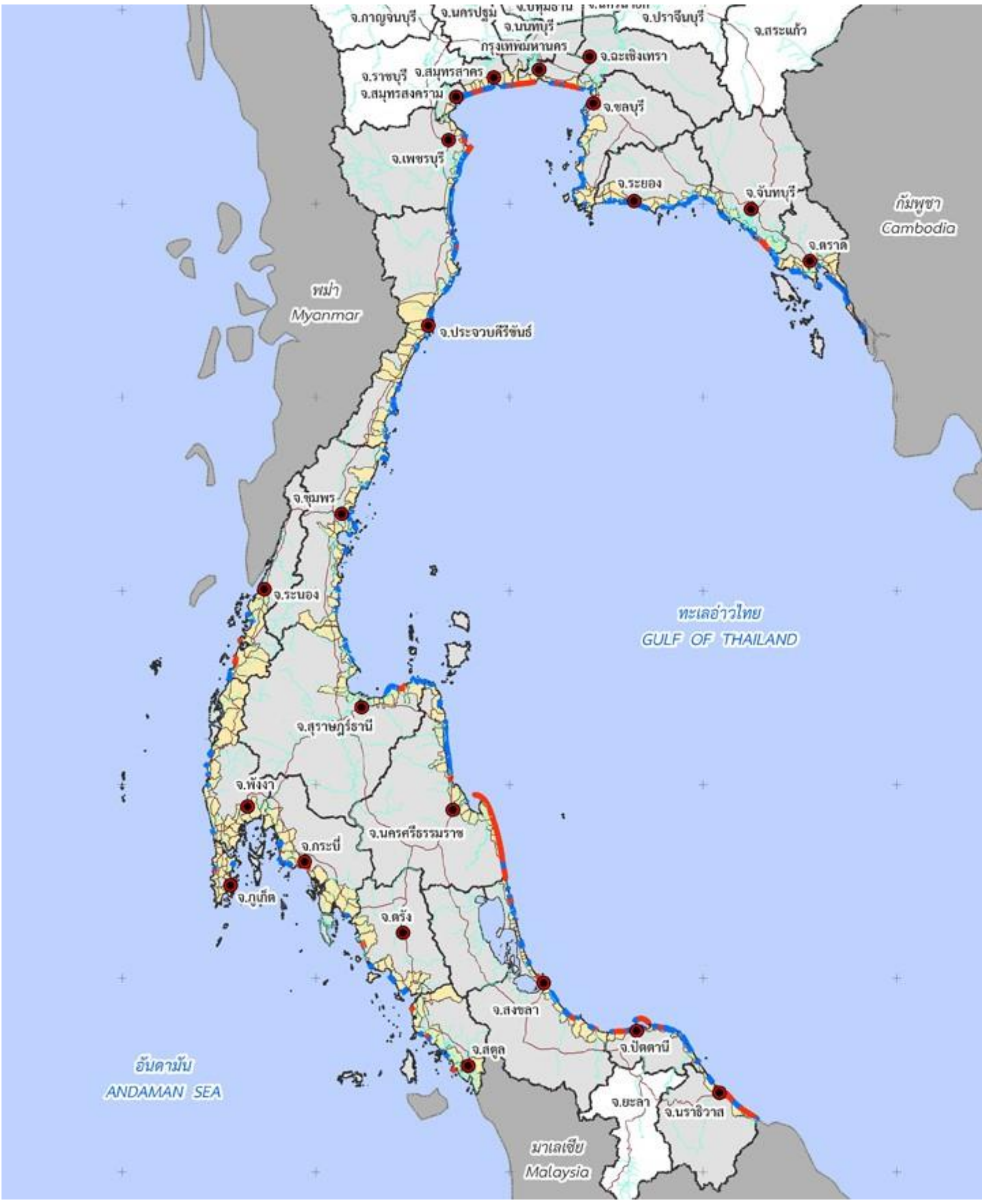

Figure 6: Situation of Coastal Erosion in 2011. Moderate erosion, 1 - 5 meters per year; Severe erosion, > 5 meters per year (Department of Marine and Coastal Resources. Marine and Coastal Resource Database, 2011 in http://www.mkh.in.th/, 2020).

Province	Severe erosion (>5m)	Moderate erosion (1 to 5m)	Little erosion (<1m)	Modified area (km)	Included erosion area (km)	Other areas (no erosion yet, km)	Total length of shore (km)
Nakhon Si Thammarat	4.48	-	9.23	47.77	61.48	175.34	236.82
Krabi	-	0.45	1.76	9.99	12.20	191.59	203.79

Table 2: Coastal erosion for the studied province areas in 2017, showing the length of shoreline affected (Department of Marine and Coastal Resources, 2018 in http://www.mkh.in.th/, 2020).

The causes of coastal change are the result of both natural processes and anthropogenic activities.

Natural processes include the effects of waves, winds, tides and vegetation. The complexity of the weather in Thailand, with the regular occurrence of storms/typhoons and two monsoons per year greatly influences the redistribution of sediment along both coasts (http://www.mkh.in.th/, 2020). Along the Eastern coast of Southern Thailand, coastal sediment is redistributed towards the South during the Northeastmonsoon and that sediment is returned towards the North during the Southwest monsoon. The morphology and bathymetry of the Gulf of Thailand allows strong winds from the China Sea to build large waves that hit the Nakhon Si Thammarat coastline causing significant erosion. On the other side the peninsula the gently sloping and relatively shallow bathymetry of the Andaman Sea, in contrast to the Indian Ocean, allows a much more efficient wave energy dissipation so that only waves from extreme events reach the Krabi coastline. Wave dissipation is amplified by the presence of the Phuket peninsula and the various islands that shelter the Krabi coastline.

Over the years, anthropogenic activities have had a dramatic effect on sediment transport and redistribution along the rivers and the coastline of both the Krabi and the Nakhon Si Thammarat provinces. The main anthropogenic activities influencing sediment transport in Thailand are:

- ✓ The construction of dams, weirs and other upstream structures preventing the “natural” transit of sediment from the mountains to the estuaries and ultimately the coast;
- ✓ The excavation of considerable amounts of sediment for the construction of large-scale building developments such as the construction of deep-water ports or buildings have reduced sediment availability;
- ✓ The development of large coastal tourism developments such as hotels and associated infrastructure have been very intrusive in coastal areas preventing the natural flow of sediment in those areas;
- ✓ The development of aquaculture especially in mangroves has disrupted sediment deposition patterns and the “natural flows” (historical patterns) of the coastal currents and waves;
- ✓ Climate change factors such as sea level rise, changes to rainfall patterns and extreme weather events influence coastal erosion and coastal flooding.

In Thailand, two main type of coastal defence management strategies are used (https://km.dmcr.go.th/, 2013) (Figure 7):

- ✓ One is based on a “natural” approach, protecting and restoring natural fauna and flora along the coast such as mangroves, seagrasses or coral reefs, which reduces wave energy to the shore or promotes sediment deposition/stabilisation. Sediment recycling or recharging are also currently practiced supporting the “natural” flow of sediment in the context of continental sediment supply shortfalls;

- ✓ Another strategy is based on the engineering of solid structures such as breakwaters, groynes and sea walls. These constructions have the effect of slowing longshore sediment transport along key stretches of coast.

Figure 7: Different types of coastal management used in Thailand. (A) & (B) Sea walls, respectively courtesy of https://km.dmcr.go.th/ and the ThaiCoast Project; (C) Recharging and recycling of beach sediment, courtesy of https://www.bangkokpost.com/; (D) Breakwaters, courtesy of https://km.dmcr.go.th/; (E) Groyne, courtesy of the ThaiCoast Project; (F) other type sea defense aiming at reducing wave energy and trapping sediment, courtesy of https://km.dmcr.go.th/.

3.3 Climate

The climate along the coast of Thailand is tropical and characterized by two monsoonal winds (Figure 8). The Southwest monsoon occurs from May to October bringing moderate to heavy rains to the studied regions and strong winds. During that period wave conditions are generally more dynamic along the South-Eastern and the South-Western coasts. The retreat of the Southwest monsoon in September/October is frequently accompanied by extreme stormy weather and tropical cyclones or even hurricanes along the Nakhon Si Thammarat coast. These high wind events usually occur three to four times a year carrying heavy rain (http://www.dmr.go.th., 2015), causing flash flooding and enhancing coastal flooding. Strong winds from those events generate high energy waves traveling from the China Sea and breaking directly on the Southern coast of Thailand. In contrast, the cyclone period along the Andaman coast occurs in May (Sojisuporn, 2003) during the Southwest monsoon.

From November to April, the winds of the Northeast monsoon generate very small waves along the East coast of the southern peninsular of Thailand (http://www.dmr.go.th, 2015). The South-western coast of Thailand is still characterised by rain until December due to the monsoon that blows through the Gulf of Thailand carrying humidity from the sea. The weather is drier from January to April as Thailand experiences summer and the winds come from the South or Southeast. Sometimes clashes occur between the cold air mass coming from China and the hot air mass that covers Thailand causing thunderstorms and gusts of wind ("summer storms") (http://www.mkh.in.th, 2020).

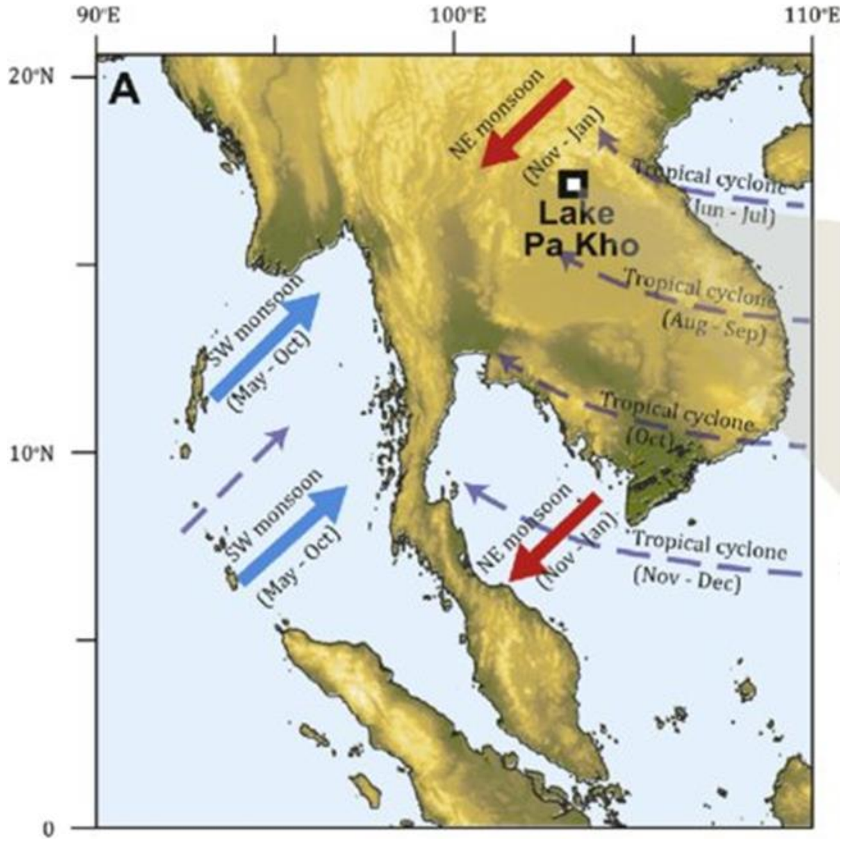

Figure 8: Representation of the Northeast and the Southwest monsoons (http://www.vcharkarn.com/vblog/51575/6).

Average annual rainfall in the region around Krabi town varies from approximately 1730 to 2900 mm, averaging 2330 mm per year. In the centre of the Nakhon Si Thammarat province, average annual precipitation varies from 2070 to 4230 mm, averaging approximately 3870 mm per year (based on the Thai Meteorological Department website data from 2007, https://www.tmd.go.th/).

Records of wind information are also available from the Thailand Meteorological Department. In Krabi town, winds predominantly come from the Southwest; they are also the strongest in the region (Figure 9) with gusts up to 53.6 km/h in 2018, associated with the Southwest monsoon. Winds from the East and Northeast are the second most prominent and the second strongest in the Krabi province (Figure 9) with gusts up to 41 km/h in 2018 associated with the Northeast monsoon. In Nakhon Si Thammarat winds predominantly come from the East and East-Southeast. The strongest gusts during the Northeast monsoon are up to 48.6 km/h in 2018. The second most prominent winds come from the West. Gusts during the Southwest monsoons were up to 46.8 km/h in 2018.

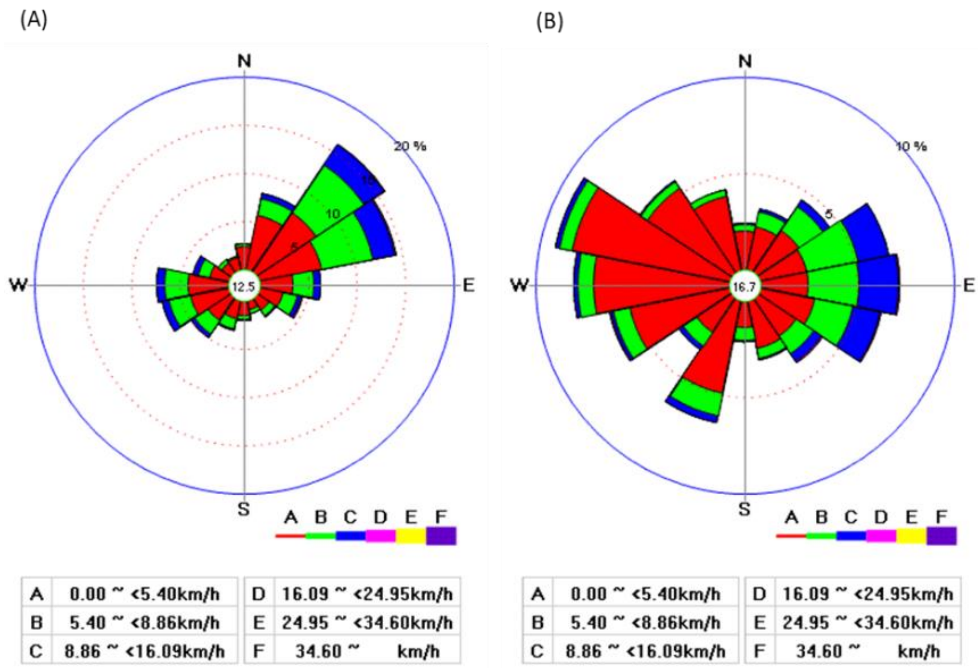

Figure 9: Wind roses in 2018 for (A) Krabi Town and (B) Nakhon Si Thammarat (Source: Thai Meteorological Department, 2020; http://www.aws-observation.tmd.go.th/).

3.4 Waves, tides and currents

Coastal processes in Thailand are mainly controlled by waves and tides (Sinsakul, 1992). A Swan Model, developed for the representation of significant wave height in the Andaman Sea and the Gulf of Thailand by Kompor et al. (2018) over a period of 10 years between 2005 and 2015, showed that significant wave heights in the region were generally <2 m, confirming Choowong et al. (2008) observations in the Andaman Sea (Figure 10). Because of the morphology of the Western coast of Thailand, wave conditions near Phang-Nga Bay are calm (Scheffers et al., 2012), this observation can be extended to the Krabi province coastline. On the West coast, waves are most active during the Southwest monsoon from May to October with an average significant wave height of 1.17 m (Table 3). The action of the Northeast monsoon is prevalent on the East coast from November to March with an average significant wave height varying from 0.23 to 0.51 m dependent on location along the Nakhon Si Thammarat coast. Those models also confirm that both monsoons induce an increase in significant wave height on both the East- and West-facing coastlines in southern Thailand regardless of their orientation (Figure 10, Table 3).

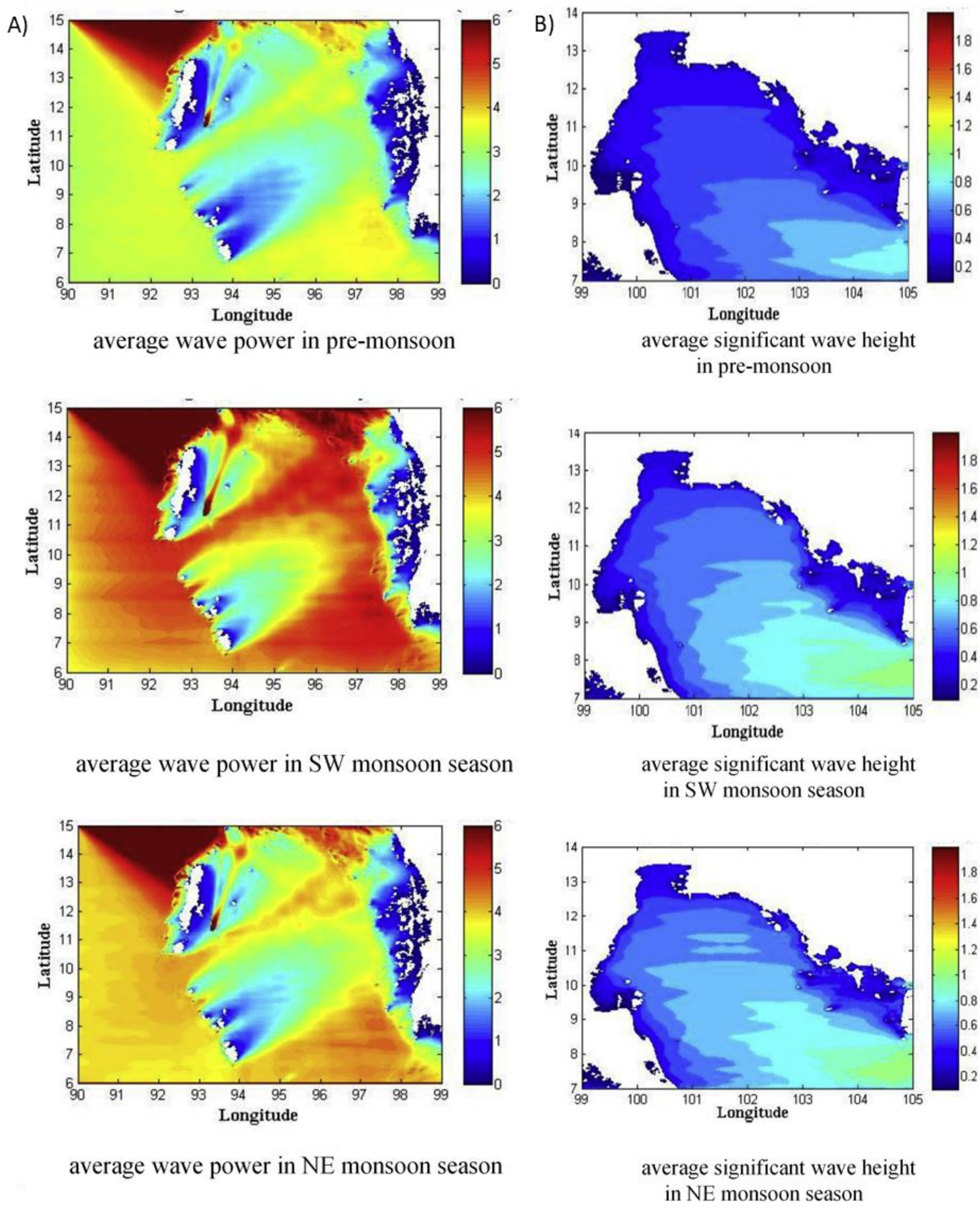

Figure 10:Swan model of the average significant wave height in A) The Andaman Sea and B) the Gulf of Thailand for the time-period spanning from 2005 to 2015 (Kompor et al., 2018).

Station	Average significant wave height (m)			Average wave power (kW/m)		
	Pre-monsoon	SW monsoon	NE monsoon	Pre-monsoon	SW monsoon	NE monsoon
Nakhon Si Thammarat province						
Station in the proximity of Thung Sai	0.11	0.21	0.23	0.04	0.1	0.13
Station in the proximity of Tha Sala	0.23	0.3	0.39	0.15	0.21	0.39
Station in the proximity of Hua Sai	0.24	0.33	0.51	0.18	0.25	0.52
Krabi province						
Station in the proximity of Ko Pu	0.74	1.17	0.81	2.14	3.95	2.34

Table 3: Summary table of the average significant wave height and average wave power modelled by Swan along the Coasts of the Krabi and the Nakhon Si Thammarat provinces for the time period between 2005 and 2015 (Kompor et al., 2018).

The tidal characteristics along the coasts of Thailand are very intricate with three types of tide: diurnal, semidiurnal and mixed semidiurnal type (Siripong, 1984a; Siripong, 1985; Ganin, 1991; Aungsakul et al., 2007). The tides along the studied coasts are mixed semidiurnal and the tidal range on the Krabi coast varies from micro- to mesotidal whereas on the Nakhon Si Thammarat coast it is mainly microtidal. Along the Krabi coastline the average mean spring tidal range is about 2.5 m whereas along the Nakhon Si Thammarat coast it averages 1.5 m (Sinsakul, 1992).

Currents in the southern part of the Gulf of Thailand are complex resulting from the interaction of various parameters including the tide, the winds, the monsoons and the China Sea currents (Figure 11). Tidal currents flow predominantly northward during high tide and reverse as the tide changes. The strength of those currents varies with the tidal range, however Yanagi and Takao (1998) concluded that tidal currents contributed very little to the net circulation within the Gulf. In fact, the predominant monsoonal winds cause eddies, mixing and the exchange of water mass in the Gulf (Robinson, 1974; Siripong, 1984b; Buranpratheprat and Bunpapong, 1998; Yanagi and Takao, 1998; Sojisuporn et al., 2010). During the Northeast monsoon period, the strong Northeast winds build a strong South-westwards flow at the Gulf entrance. When these currents encounter the West coast, they deviate Northward following the coast. During the Southwest monsoon the strong West to Southwest winds from the Indian Ocean cause northward flows leading water and currents outside of the Gulf. The circulation pattern during this period goes from North to South along the Nakhon Si Thammarat coast (Sojisuporn et al., 2010).

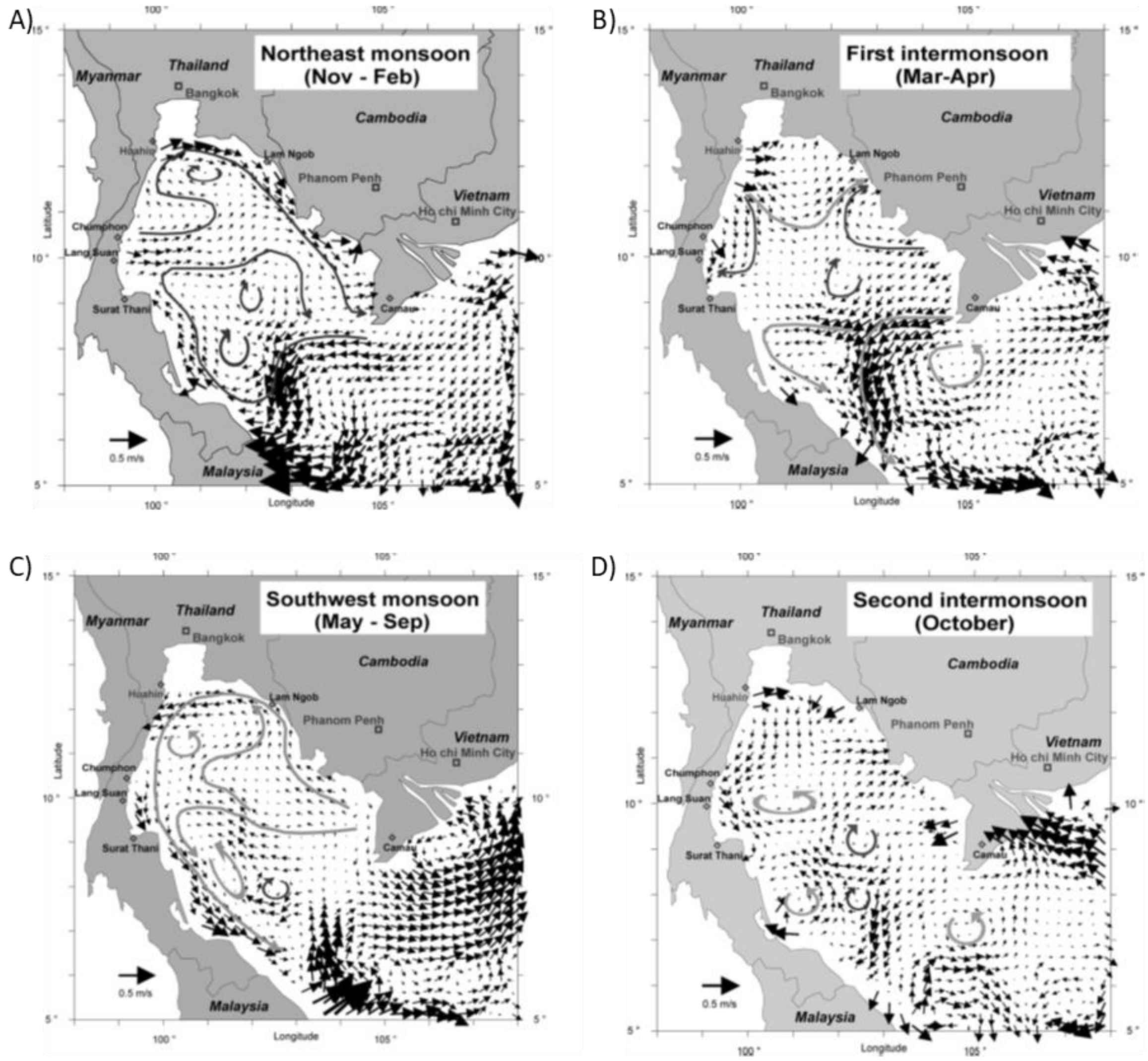

Figure 11: Seasonal variations of the mean currents in the Gulf of Thailand (Sojisuporn et al., 2010).

In the Andaman Sea, tidal currents are dominant in the Malacca Strait (Rizal et al., 2012) and therefore along the Krabi coast (Figure 12). Surface currents in the Andaman Sea and the Malacca Strait are also influenced by seasonal monsoons. However, in the more local context of the Krabi coast surface flow is always directed North-westward towards the Andaman Sea, for both Southwest and Northeast monsoons (Wyrtki, 1961; Rizal et al., 2012). This was explained by Wyrtki (1961) as being a consequence of the sea surface elevation in the Southeast domain (South China Sea) being higher than in the Andaman Sea all year long.

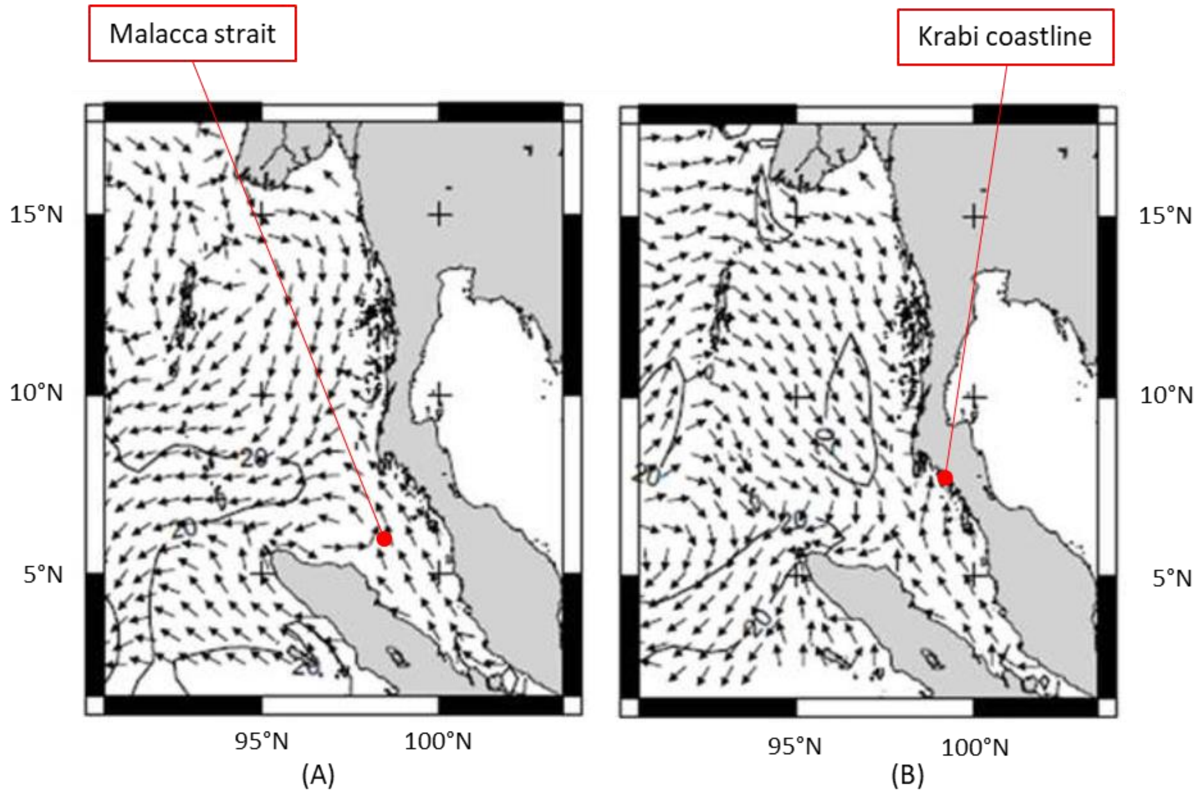

Figure 12: The climatology surface currents caused by tides, wind and heat flux derived from long-term (1985-2003) (a) February and (b) August average based on HAMSOM in the Andaman Sea. Contour values show mean magnitude of velocity in cm/s (Rizal et al., 2012).

3.5 Sea level

Sea level changes along the coast of Thailand have been the focus of interest from coastal researchers since the late 1980s and a lot of that attention has been directed on coastal areas around the Gulf of Thailand (Punpuk, 1992; Sinsakul, 1992; Neelasri et al., 1988; Vongvisessomjai, 2006; Niemnil, 2008; Trisirisatayawong et al., 2011; Sojisuporn et al, 2013). Over the last 20000 years until the late 1980s, it was estimated that the sea level had raised by 120 m (Fairbanks, 1989). However, since then the scientific community has identified the issue of climate change and its influence on sea level rise. Thailand is already suffering from alarming issues of coastal erosion and land subsidence; and climate change related sea level rise compounds the pressure coastal areas are already under. Sojisuporn et al. (2013) investigated variations in sea level measured all along the Gulf of Thailand between 1985 and 2009. Their conclusions indicated that net sea level rise in Southern Thailand is approximately 1.4 mm/year.

3.6 Reported Landslides in the Krabi and Nakhon Si Thammarat (NST) provinces

This study created a landslide event log based on information available from the Department of Mineral Resources (DMR) (Table 4). Since 2012 no reports on landslide events within the provinces of interests have been published. This study assumes that the damages were not sufficient to be reported by the DMR since then.

Landslide event log			
	The location	**Date**	**Damages/Casualties**
NST Province	Ban Thathun Nuea, Phipun District, Nakhon Si Thammarat Province	22-Nov-88	Approximately 230 people injured and killed, about 1500 houses damaged, agricultural area of approx. 9.8 km^2, worth about 1000 million baht.
	Baan Kiriwong, Lan Saka District, Nakhon Si Thammarat Province	22-Nov-88	12 people killed and 152 houses damaged and some 210 damaged.
	Ban Nai Plau Monastery, Village No. 8, Khanom Subdistrict, Khanom District, Nakhon Si Thammarat Province	March 26, 2011	2 deaths
	Khao Noi Subdistrict, Sichon District, Nakhon Si Thammarat Province	March 26, 2011	No damage reported.
	Ban Huai Phan, Village No. 2, Krung Ching Subdistrict, Nopphitam District, Nakhon Si Thammarat Province	29-Mar-11	Some roads have been cut.
	Ban Thap Nam Thao Village, Village No. 8, Krung Ching Sub-district, Naphit Tam District, Nakhon Si Thammarat Province	1-5 January 2012	Caused damage to agricultural and livestock areas, utilities and damage
Krabi province	Ao Nang Subdistrict, Mueang District, Krabi Province	17-Oct-04	14 guest houses were damaged in soil flows, 10 rooves, fences and walls were damaged, totalling over 10 million baht.
	Orange Fire Ban Khao Muang Krabi on the vehicle.	18-Oct-04	3 people were killed and 1 injured. 25 houses were damaged.
	Ban Huai Nam Kaew, Village No. 6 and Ban Ton Han, Village No. 7, Khao Khao Subdistrict, Khao Phanom District, Krabi Province	March 28, 2011	8 people died and many houses and agricultural areas were damaged.
	Ban Thep Phanom, Village No. 10, Khao Phanom Subdistrict, Khao Phanom District, Krabi Province	30-Mar-11	10 houses damaged, 1 broken bridge

Table 4:Log of the major landslide events reported for the areas of interests on the DMR website (http://www.dmr.go.th/, 2012).

4 Methodology

4.1 Sediment characteristics, Organic matter content and radio-isotopic dating

A total of eighteen cores were collected within mangrove and seagrass environments across both provinces of interest (see Section 3). Three mangrove and three seagrass sites were selected within the Krabi province, and three mangrove sites were selected in Nakhon Si Thammarat province, where seagrasses are largely absent (Figure 13).

75 mm diameter, 40 cm deep cores were removed from each site, taking care to ensure minimal compaction and maintain the stratigraphy. After extraction, cores were frozen for conservation during transport and storage.

In the laboratory, cores were extruded and the outer layer of the core was removed to prevent downcore contamination.

Cores were then cut in 1 cm thick subsamples. Each sample was weighed and then dried at a temperature of 40°C for at least a month to remove moisture.

After the sediment samples reached constant weight, they were then re-weighed to determine the level of moisture within each sample.

Soil organic matter content was calculated using the loss on ignition method (Schulte, 1995). After disaggregation, 2 to 4 g of sediment from each sample was burnt in a muffle furnace for 24 hours at a temperature of 450°C and the remaining sediment was used for radio-isotopic dating. These samples were then re-weighed to determine the weight of organic matter. That same sample was then used for grain size measurements.

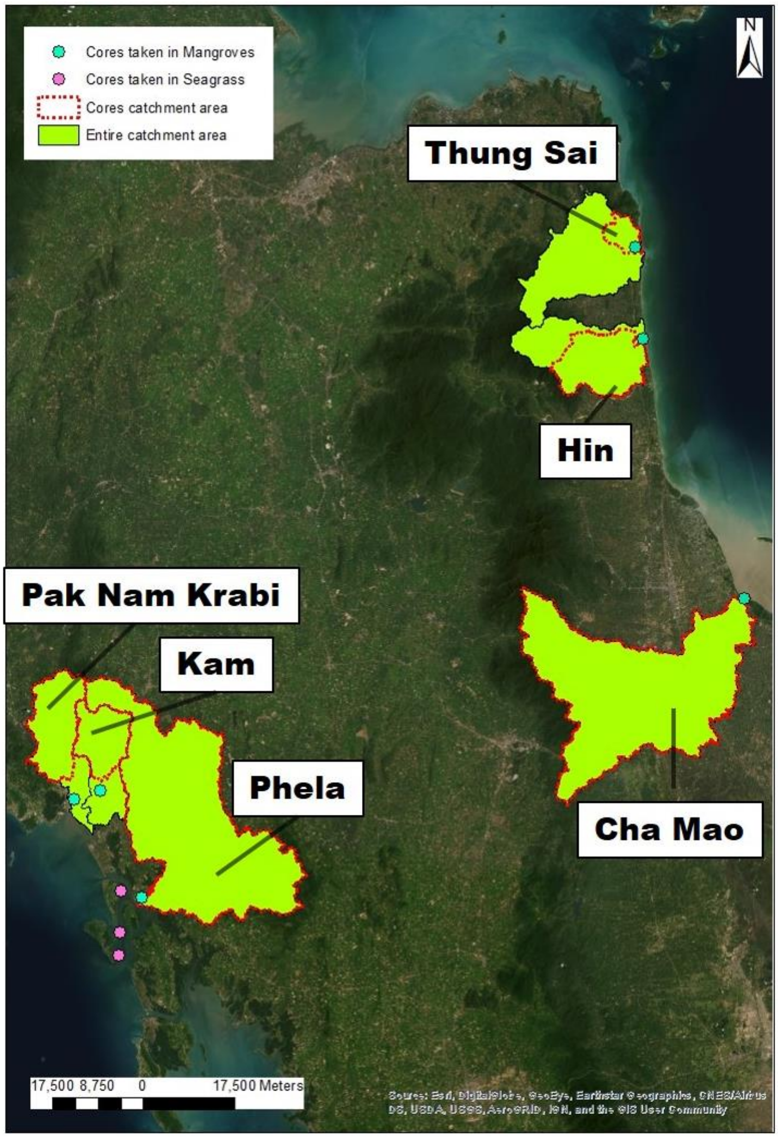

Figure 13: Location of the study sites.

Over 300 samples were analysed for grain size using a laser particle size analyser (Horiba LA960). Each sample was stirred for 30 minutes in Calgon (a combination of sodium hexametaphosphate and sodium carbonate) prior to particle size analysis in order to disperse the sediment particles within each sample. Each sample was then placed in the particle analyser in a sufficient quantity so that it was within the thresholds of obscuration as required by the manufacturer's software. Each sample was then submitted to 3 minutes of ultrasound to further disperse the particles. Samples were then measured 3 times under different wave lengths and an average grain size distribution was produced. Results were measured according to the standardised Wentworth (1922) grading system.

Standard grain size statistical values were calculated from the measurements:

- The D_{10}, D_{50} and the D_{90}.
- The sorting coefficient which is defined by SQRT(D_{75}/D_{25}), which indicates the degree of sorting.

Proportions of clay, silt, sand and gravels in each sample were also represented.

The portion of the sediment that was selected for radio-isotopic dating was placed in cylindrical vial and entered into the gamma ray spectrometer Canberra measurement chamber. The gamma spectrometer measures activities of radio-isotopes contained within the sediment, especially those of ^{137}Cs (661.65 keV), ^{214}Pb (351.92 keV) and ^{210}Pb (46.54 keV) that this study is relying on. To achieve a reliable measurement of the radio-isotopic activity within each sample, samples were left in the measurement chamber for at least 48h providing the instrument to reduce detection error to 5% or less. The age of the samples and the sedimentation rates were determined using the CRS model (Constant Rate of ^{210}Pb Supply; Appleby & Oldfield. 1978; Robbins, 1978) based on laminae counting of the ^{210}Pb decay in sediment deposits. The use of ^{137}Cs also permitted independent determination of sedimentation rates. This method relies on the input of ^{137}Cs, which occurred during atmospheric nuclear testing, mainly in the late 1950s and mid-1960s. It uses this injection as a marker to identify soil and sediment particles laid down post 1963 and allowing the determination of sedimentation rates between then and now. Because of the impact of COVID19 on the re-opening of the laboratories, radio-isotopic measurements were prioritised for a single core at each site. These measurements were then extended to the second core until the publication of this report, hence explaining why some sites only have one core with radio-isotopic measurements.

4.2 Landslide inventory

4.2.1 Landslide detection

Two remote sensing methods were used to create landslide inventories for the studied areas. One used high-resolution imagery from Google Earth historical imagery (resolution <5 m), aerial imagery (resolution <5 m), Earth Observatory (EO-1 ALI, resolution of 10m) and THEOS satellite imagery (resolution of 2 m). In this case, terrestrial mass movements were identified visually and delimited using polygons in ArcMap or Google Earth. High resolution imagery allows the rapid identification and mapping of landslides, even the smallest ones. All these images have the advantage to be georeferenced and rectified to compile all the data with no further processing or correction. The amount of high-resolution imagery data made available for this study allowed the creation of an exhaustive time series of landslide, resulting in a time series of images and therefore landslides predominantly between 2011 and 2019 (Table 5).
Because of the paucity of data from the high-resolution imagery, a second method was also used based on low-resolution satellite imagery. Low resolution satellite imagery offers a consistent dataset throughout time going back to the 1980s. However, the compromise in the resolution of the images (30m) made visual recognition of mass movements in the studied areas problematic, as most landslides in the surveyed areas are debris flows with a thin and long shape. Google Earth Engine is a brand-new platform for satellite imagery distribution and automated image analysis. Thanks to the data availability for Landsat 7 and Landsat 8, this study was able to collect imagery data from as early as 2000 to 2019 (Table 5). All images within the same year were compiled in a single image mosaic by calculating the median value for each individual pixel. Undertaking this compilation helped in creating full cloudless images. To resolve the issue of visual identification, it was decided to use Normalized Difference Vegetation Index (NDVI) maps to delineate areas with no vegetation (Lo et al., 2015) and then use a series of steps to increase the overall precision of the landslide identification. The semi-automated approach involved the following steps:

1. Creation of NDVI maps from the LandSat 7 & 8 yearly images;
2. Filter slope by excluding areas with a slope <5º angle (based on a 5 m resolution DEM);
3. Filter unvegetated areas by excluding urban, industrial, farming and cultured areas (GIS data supplied by Thai partners);
4. Filter roads and motorways by excluding buffers areas of respectively 9 m and 28 m around these features;
5. Filter topography by excluding low elevation areas (based on a 5m resolution DEM and a contour map).

The resulting maps were then visually inspected to quality assess the identification of the filtered unvegetated areas. These areas were then assumed to correspond to potential land mass movements or sediment sources.

High Resolution (<10m resolution)		Low Resolution (10 to 30m resolution)	
Data Imagery	**Catchment and Collection date**	**Data Imagery**	**Collection date**
Google Earth	**Pak Nam Krabi**: 03/03/2007, 03/01/2014, 24/01/2014, 17/02/2014, 09/03/2014, 29/01/2015, 11/01/2015, 05/04/2016, 04/03/2017, 17/11/2017, 20/11/2017, 18/02/2018, 21/03/2018, 09/01/2019, 05/02/2019, 11/02/2019, 25/02/2019, 02/03/2019, 10/03/2019. **Kam**: 24/01/2014, 02/02/2014, 09/03/2014, 11/01/2015, 29/01/2015, 20/03/2016, 10/04/2016, 04/03/2017, 11/03/2017, 21/03/2018, 25/02/2019, 04/03/2019. **Phela**: 13/02/2007, 03/03/2007, 25/02/2014, 09/03/2014, 29/01/2015, 24/02/2016, 25/03/2016, 09/02/2017, 04/03/2017, 17/02/2018, 25/07/2018, 24/11/2018, 11/02/2019, 25/02/2019, 02/03/2019, 21/03/2019. **Thung Sai**: 27/03/2013, 22/07/2015, 02/05/2016, 27/12/2016, 10/04/2017, 29/06/2018, 23/03/2019. **Hin**: 03/03/2001, 25/12/2007, 18/03/2013, 25/06/2013, 22/07/2015, 21/04/2016, 12/05/2016, 12/06/2016, 27/12/2016, 20/07/2017, 13/04/2018, 23/07/2018, 23/03/2019, 03/06/2019. **Cha Mao**: 06/03/2002, 25/12/2007, 18/03/2013, 16/03/2015, 18/03/2015, 17/07/2015, 02/04/2016, 21/04/2016, 12/05/2016, 06/06/2016, 12/06/2016, 27/12/2016, 08/02/2017, 06/07/2017, 10/08/2017, 23/07/2018, 08/03/2019.	**Landsat 7**	All catchments 2000 to 2013.
Aerial pictures	**Pak Nam Krabi**: 15/04/2011. **Kam**: 15/04/2011. **Phela**: 15/04/2011. **Hin**: 31/07/2009.	**Landsat 8**	All catchments 2013 to 2019.
Theos satellite imagery	**Pak Nam Krabi**: 09/12/2012, 13/02/2015. **Kam**: 09/12/2012, 13/02/2015. **Phela**: 09/12/2012, 24/02/2014, 01/03/2014, 08/02/2015, 13/02/2015, 16/03/2015. **Thung Sai**: 21/09/2009, 16/10/2010. **Cha Mao**: 30/03/2012, 17/07/2012.		

Table 5: List of the remote sensing imagery collected by the study.

Both ways of detection (low and high resolution) delivered two landslide inventories. 1523 landslides were detected using high resolution imagery mostly between 2013 and 2019 while more than 180 000 were identified with low resolution data between 2000 and 2019. These inventories cover a total area of 2314.38 km^2 across the six different catchments of interest.

Unfortunately, although the method based on the use of NDVI images was accurate for detecting areas with no vegetation in normally highly forested high-altitude environments, these models over-estimated the number of landslides identified visually when using high-resolution imagery. Even when fine tuning the various filters such as selecting steeper slope angles and/or smaller NDVI index ranges, these models still largely over-estimated the number of landslides. For these reasons, it was decided not to use the inventory derived from the low-resolution imagery for further landslide investigation.

4.2.2 Landslide area and landslides volume calculations

Calculations of the surface area of the landslides (A) was operated on ArcMap. Estimations of landslide volumes (V) were undertaken using a globally derived formulae developed by Larsen et al. (2010):

$$V=\alpha A^{\gamma}$$

Where the constants α and γ are respectively the values of the intersect and the scaling exponent. The landslides have a variety of shape, size and types. As a result, we used the "all landslide" parameters (γ= 1.332±0:005; $\log_{10}(\alpha)$ =-0:836±0:015) when $A < 10^5$ m^2, and the "bedrock" parameters (γ= 1.35±0.01; $\log_{10}(\alpha)$ = -0.73±0.06) for larger landslides (Larsen et al., 2010, Odin et al., 2019).

4.2.3 Frequency volume and Negative Power Law scaling.

Landslide erosion was modelled using an approach based upon the negative power law scaling properties of rockfall magnitude–frequency distributions. Because of the frequency of the landslide and rainfall data, the clear difference in rainfall between seasons in Thailand and the close relationship between rainfall and landslide occurrence in Thailand, the scaling properties of their frequency density under a seasonal time-series was considered most appropriate.

Negative power law scaling of rockfall magnitude–frequency distributions are modelled using (Brunetti et al., 2009):

$$f\,(V_R)= sV_R^{-\beta}$$

where $f\,(V_R)$ represents the frequency density, V_R is the event magnitude, and s and β are empirically-determined constants.

The constant s of the negative power law gives an overall indication of the level of activity within an inventory where the constant β is a marker of the relative importance of high-magnitude events (Barlow et al., 2012). To determine the constants s and β, the frequency densities were normalized by both time and area (events $km^{-2}.yr^{-1}$). The rockfall magnitude–frequency was plotted against logarithmically binned data and both axes were logarithmically scaled (Barlow et al., 2012). The plotted data were then censored for the smallest events when using low-resolution satellite imagery. The identified threshold corresponded to the resolution of the imagery i.e. 30 m. From the interpolation of the trend line drawn for the uncensored data, s and β were calculated (e.g. Figure 41).

4.2.4 Derivation of the sediment volumes made available per year

The total volumetric erosional flux (VT) of rock between a minimum and maximum magnitude can be calculated via the following formulae (Barlow et al., 2012):

R

$$VT = \int_{min}^{max} sV_R - \beta + 1\, dV_R$$

$$VT = \frac{sV_{Rmax}^{2-\beta}}{2-\beta} - \frac{sV_{Rmin}^{2-\beta}}{2-\beta}$$

Where V_{Rmax} is the event of the greatest magnitude and V_{Rmin} is the event of the lowest magnitude. Because of the high-resolution of the imagery data and the good fit of the power law equations at the tail ends, V_{rmin} was simply set to zero; and s and β are the empirically-determined constants from the power law equations.

4.2.5 Rainfall data

Rainfall information was acquired from various sources in order to get the best representation of local climates within each catchment in the study. The Thailand Meteorological Department (DMR) local stations (AWS) have daily records of rainfall since 2007 for most stations, these records have considerable lags of missing data (up to a year-long) making this information difficult to use even at a seasonal time scale sometimes. On the other hand, the Royal Irrigation Department (RID) of Thailand has fewer weather stations near the studied regions but their records are more complete on a monthly basis since 1987. The stations selected to investigate the rainfall are (Figure 14):

- Krabi province: the AWS station in Krabi and the Royal Irrigation Department of Thailand stations of PhangNga (340231) and Trang (650141);
- Nakhon Si Thammarat province: the AWS stations of Kanjanadit, Nakhon Si Thammarat and Banjak were used as well as the station of Klong Klai (270401) in Nakhon Si Thammarat from the Royal Irrigation Department of Thailand.

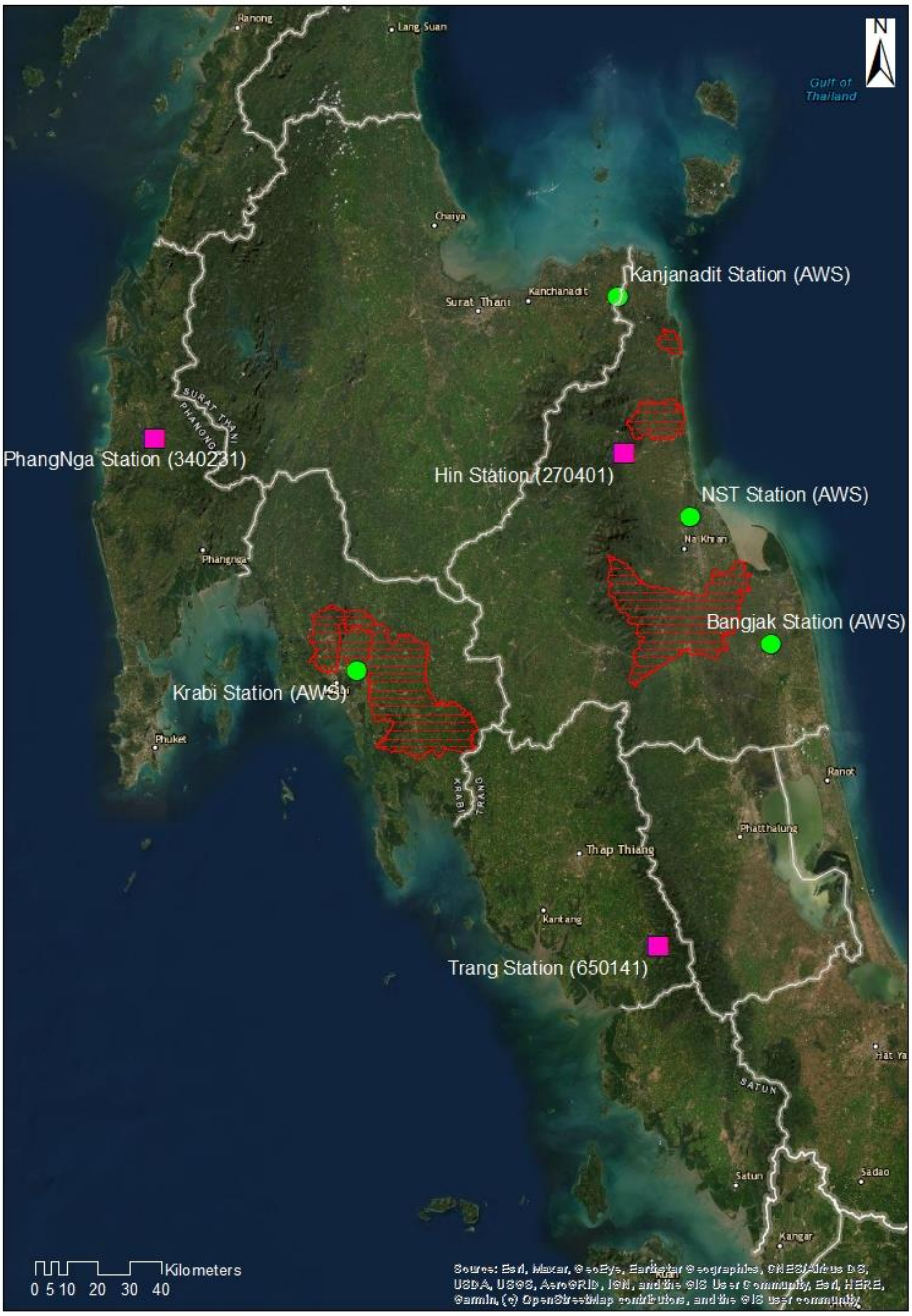

Figure 14: Weather stations locations. The green points correspond to the AWS stations and the purple squares are the RID stations. The red dashed areas represent the extent of the studied catchments.

In order to link shoreline changes and sedimentary records in the mangroves or seagrass environments to weather conditions or recorded natural disasters, an inventory of extreme weather events was created including all land falling tropical storms and intense rainfall events that occurred during the survey period and the 2004 tsunami (Figure 15). This inventory was created based on a conglomerate of news reports, the IBTrACTS data available on the National Oceanic and Atmospheric Administration (https://www.ncdc.noaa.gov/ibtracs/).

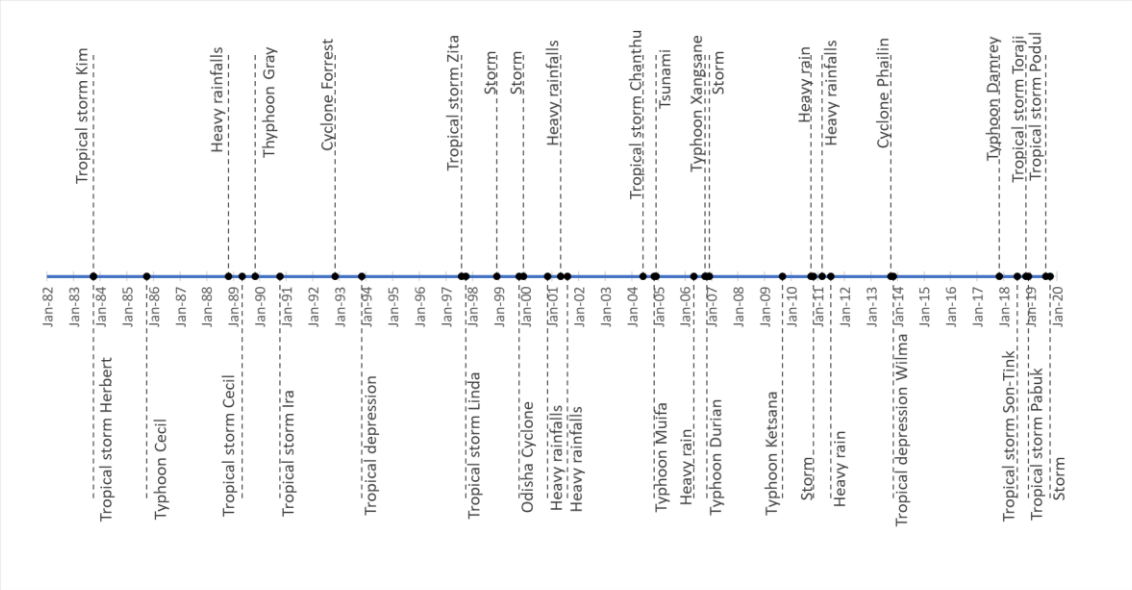

Figure 15: Extreme weather inventoried for Thailand from the 1980s.

5 Results and discussions

5.1 Sediment characteristics

5.1.1 Variations of the D_{10}, D_{50} and D_{90}.

5.1.1.1 Mangrove cores in the Krabi Province

The core from the lower mangrove (core 1) in Krabi town (Pak Nam Krabi catchment) presents a D_{10} varying from 0.04 to 0.9 microns, a D_{50} varying from 5.6 to 23.1 microns and a D_{90} varying from 35.6 to 132.7 microns. The upper mangrove core (core 2) shows variations of the D_{10} from 0.16 to 8.28 microns, variations in the D_{50} from 12.2 to 84.96 microns and variations of the D_{90} from 59.72 to 544.98 microns (Figure 16).

The core from the lower mangrove (core 1) at Krabi Airport (Kam catchment) presents a D_{10} varying from 0.5 to 7.2 microns, a D_{50} varying from 22 to 74.6 microns and a D_{90} varying from 121.1 to 517.8 microns. The upper mangrove core (core 2) presents variations of the D_{10} from 3.95 to 14.55 microns, variations of the D_{50} from 32.04 to 117.91 microns and variations in the D_{90} from 49.16 to 445.27 microns (Figure 17).

The core from the lower mangrove (core 1) in the Phela catchment presents a D_{10} varying from 0.4 to 6.7 microns, a D_{50} varying from 16 to 43.4 microns and a D_{90} varying from 57 to 187 microns. The core from the upper mangrove (core 2) shows variations in the D_{10} from 4.03 to 11.17 microns, variations in the D_{50} from 29.41 to 76.08 microns and variations in the D_{90} from 102.75 to 281.31 microns (Figure 18).

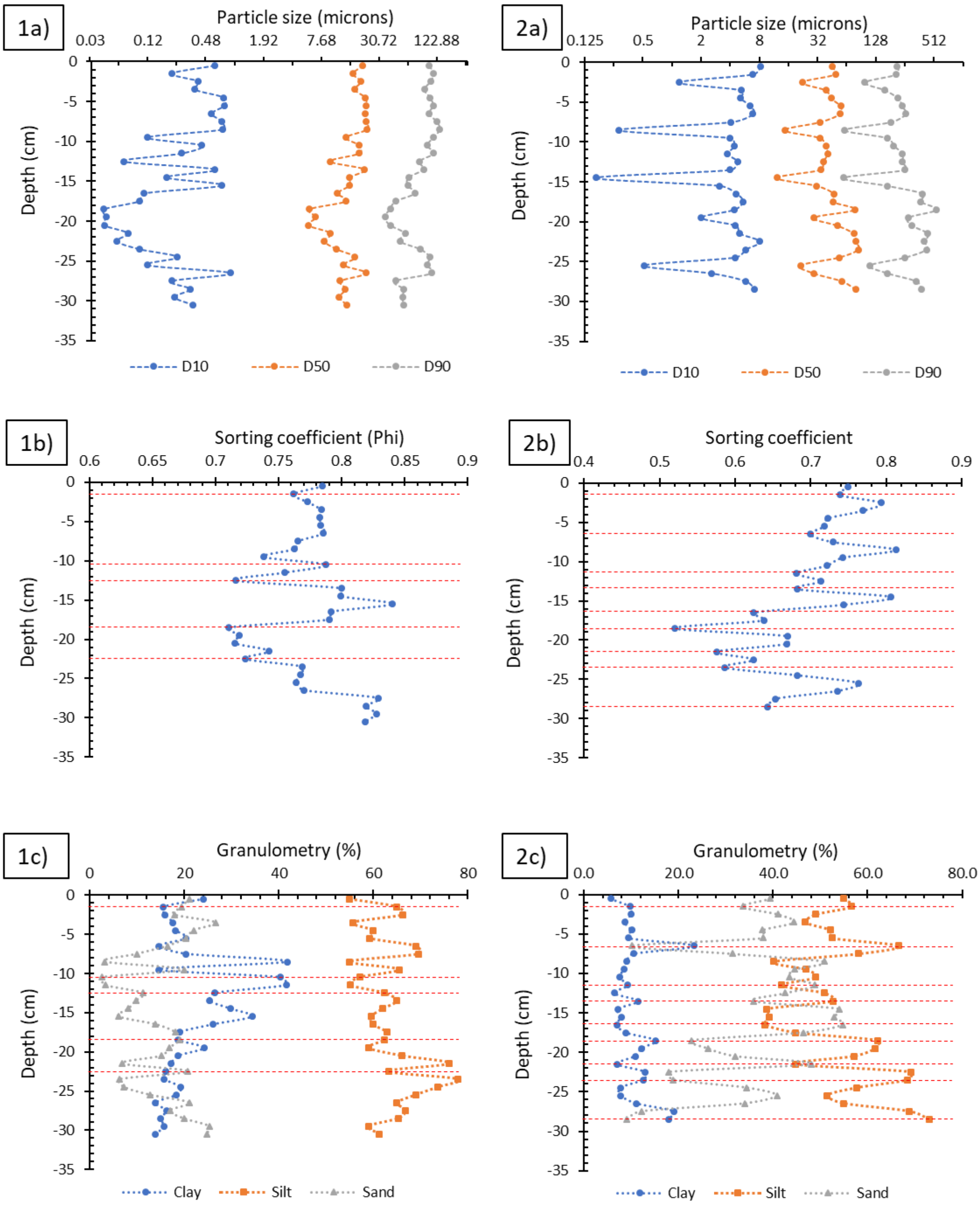

Figure 16: Characterisation of the sediment records in the Pak Nam Krabi river mangrove ("Krabi Town"). 1) Results of the first core and 2) Results from the duplicate core. a) Variations of the D_{10}, D_{50} and D_{90}; b) Variations of the sorting coefficient; c) Variations of the percentages of clay, silt and sand. The red dashed line are markers of drops in the sorting coefficient associated to significant changes in the grain size distribution.

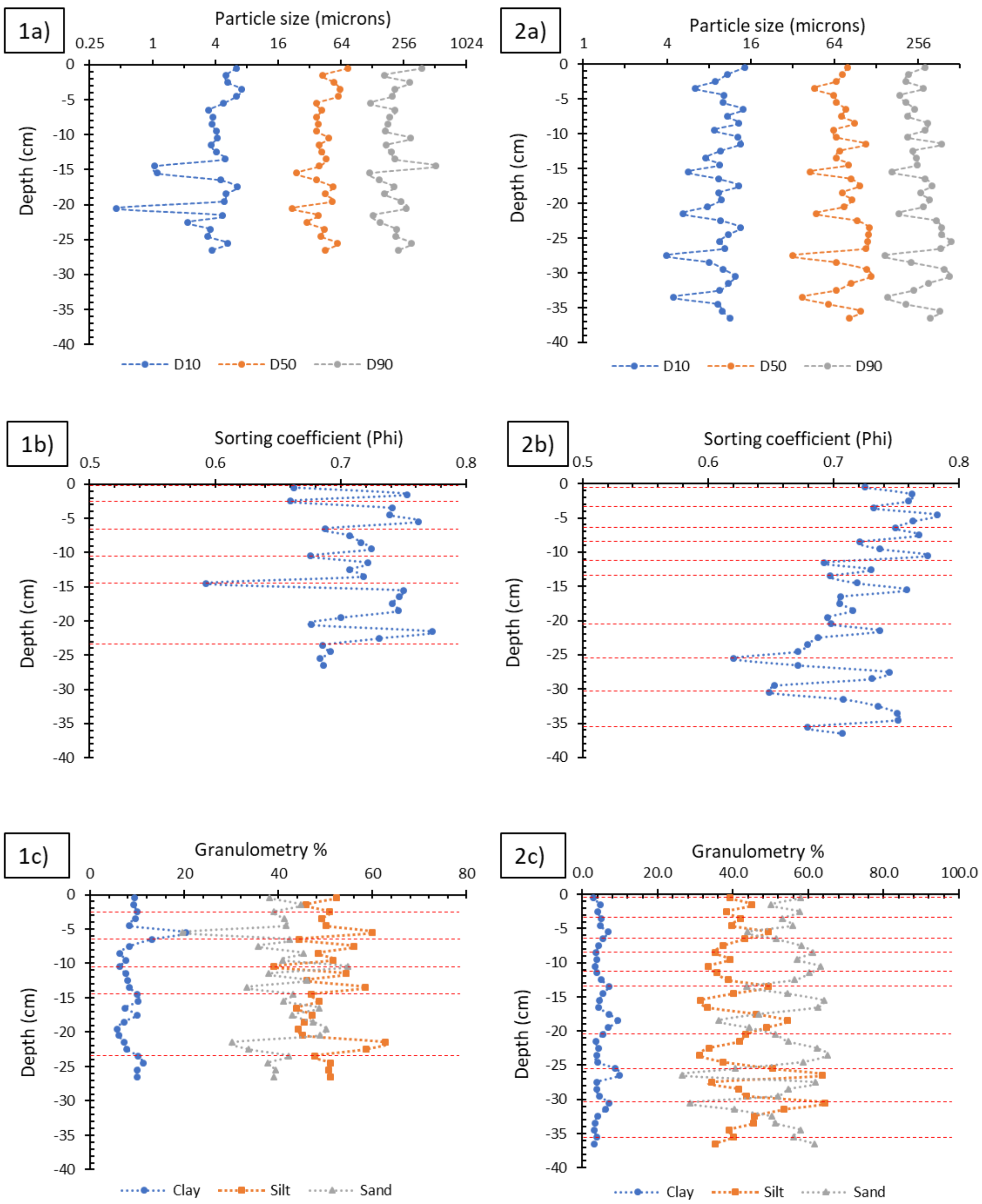

Figure 17: Characterisation of the sediment records in the Kam river mangrove ("Krabi Airport"). 1) Results of the first core and 2) Results from the duplicate core. a) Variations of the D_{10}, D_{50} and D_{90}; b) Variations of the sorting coefficient; c) Variations of the percentages of clay, silt and sand. The red dashed line are markers of drops in the sorting coefficient associated to significant changes in the grain size distribution.

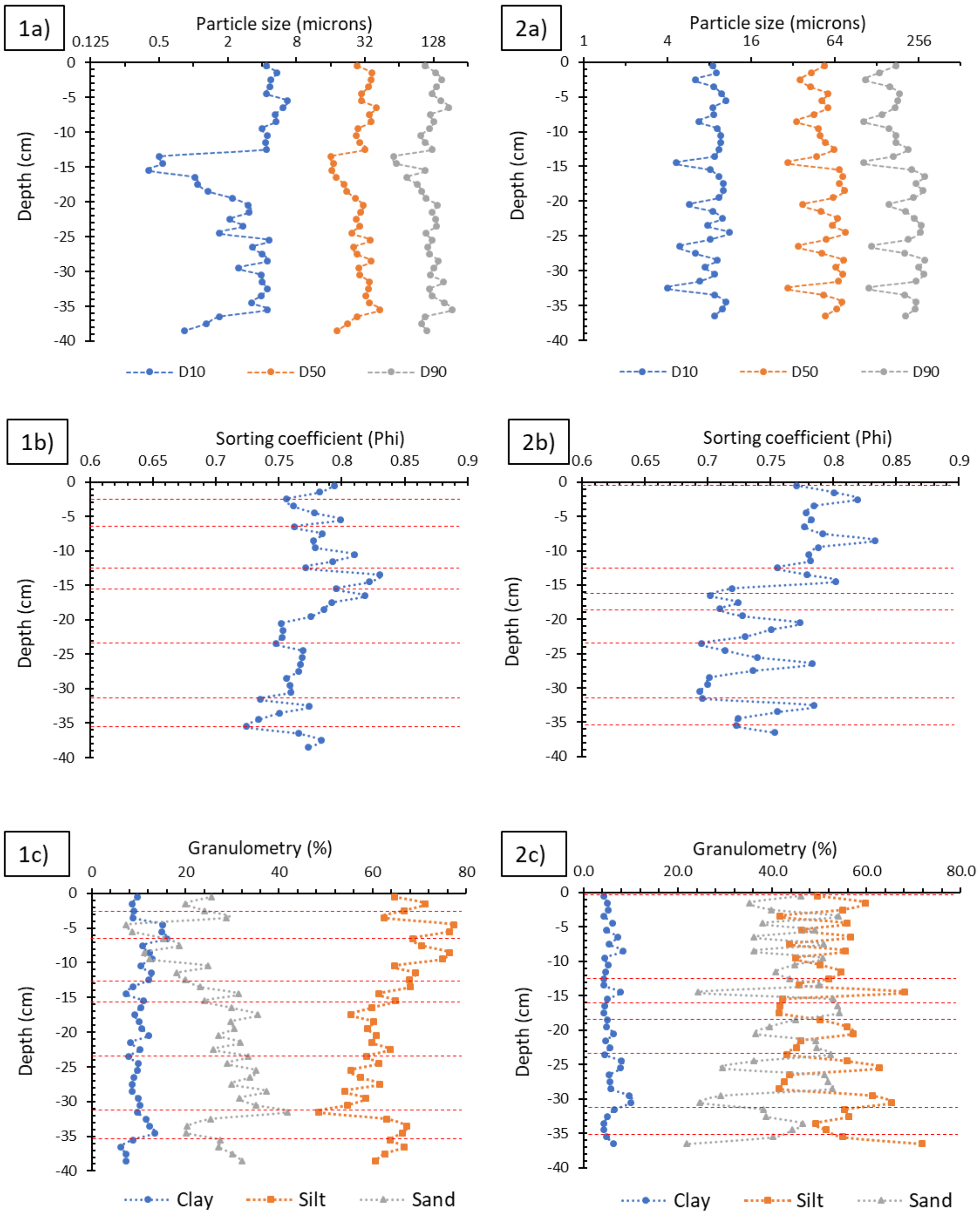

Figure 18: Characterisation of the sediment records in the Phela river mangrove ("Baam Leam"). 1) Results of the first core and 2) Results from the duplicate core. a) Variations of the D_{10}, D_{50} and D_{90}; b) Variations of the sorting coefficient; c) Variations of the percentages of clay, silt and sand. The red dashed line are markers of drops in the sorting coefficient associated to significant changes in the grain size distribution.

5.1.1.2 Mangrove cores in the Nakhon Si Thammarat Province

The core from the lower mangrove (core 1) in the Thung Sai catchment presents a D_{10} varying from 4.39 to 10.7 microns, a D_{50} varying from 30.2 to 139.4 microns and a D_{90} varying from 112 to 838.57 microns. The upper mangrove core (core 2) shows variations in the D_{10} from 5.86 to 34.05 microns, variations in the D_{50} from 59.75 to 291.26 microns and variations in the D_{90} from 312.35 to 1980.84 microns (Figure 19).

The core from the lower mangrove (core 1) in the Hin catchment presents a D_{10} varying from 0.05 to 8.11 microns, a D_{50} varying from 5.5 to 489.7 microns and a D_{90} varying from 104.24 to 1565.43 microns. The upper mangrove core (core 2) shows variations of the D_{10} from 4.4 to 52.01 microns, variations of the D_{50} from 91.07 to 291.9 microns and variations of the D_{90} from 398.07 to 1138.7 microns (Figure 20).

The core from the lower mangrove (core 1) in the Cha Mao catchment presents a D_{10} varying from 0.13 to 4 microns, a D_{50} varying from 8.4 to 33.1 microns and a D_{90} varying from 34.7 to 295.7 microns. The upper mangrove core (core 2) shows variations in the D_{10} from 0.08 to 4.77 microns, variations in the D_{50} from 8.16 to 243.26 microns and variations in the D_{90} from 108.55 to 827.15 microns (Figure 21).

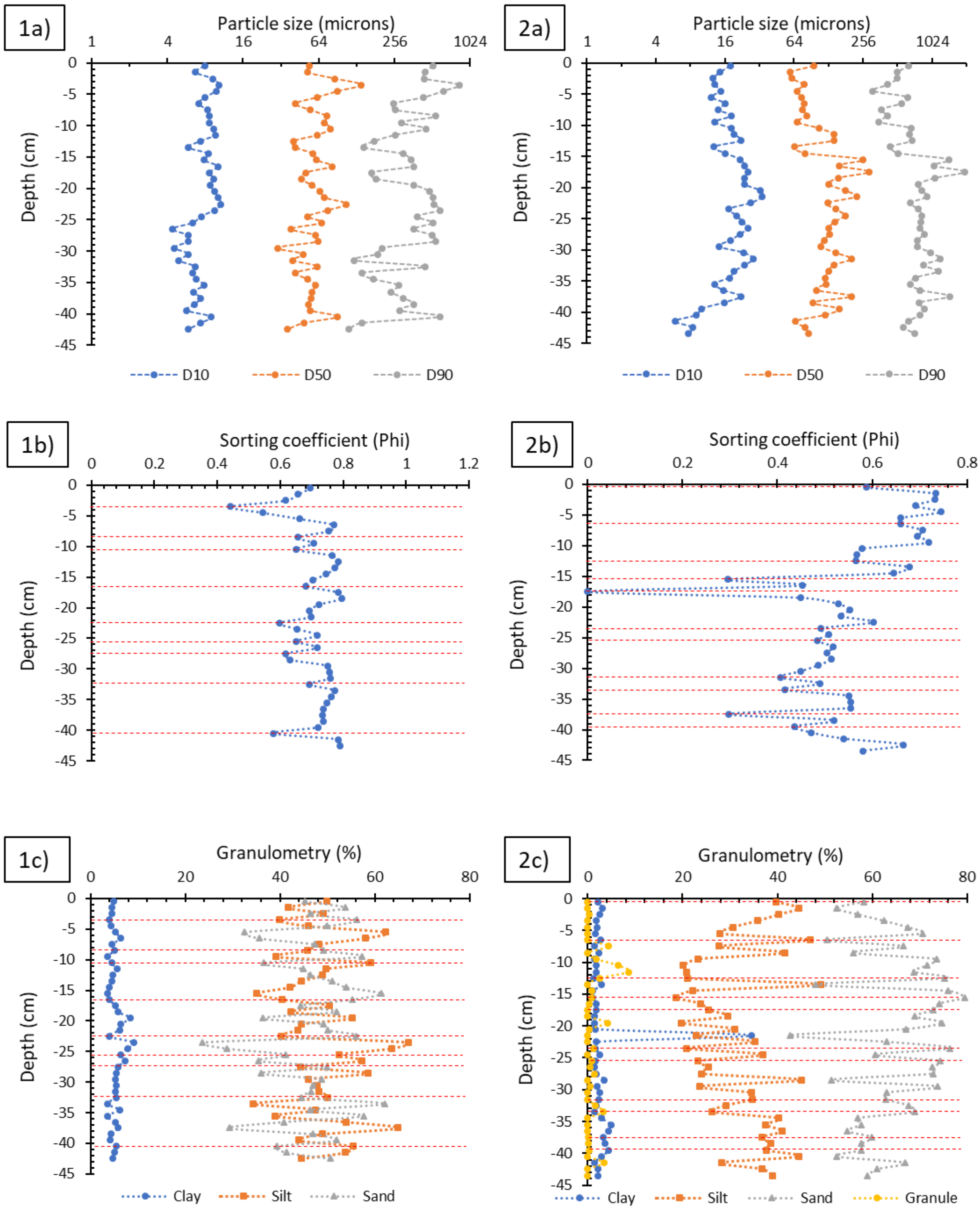

Figure 19: Characterisation of the sediment records in the Thung Sai river mangrove. 1) Results of the first core and 2) Results from the duplicate core. a) Variations of the D_{10}, D_{50} and D_{90}; b) Variations of the sorting coefficient; c) Variations of the percentages of clay, silt and sand. The red dashed line are markers of drops in the sorting coefficient associated to significant changes in the grain size distribution.

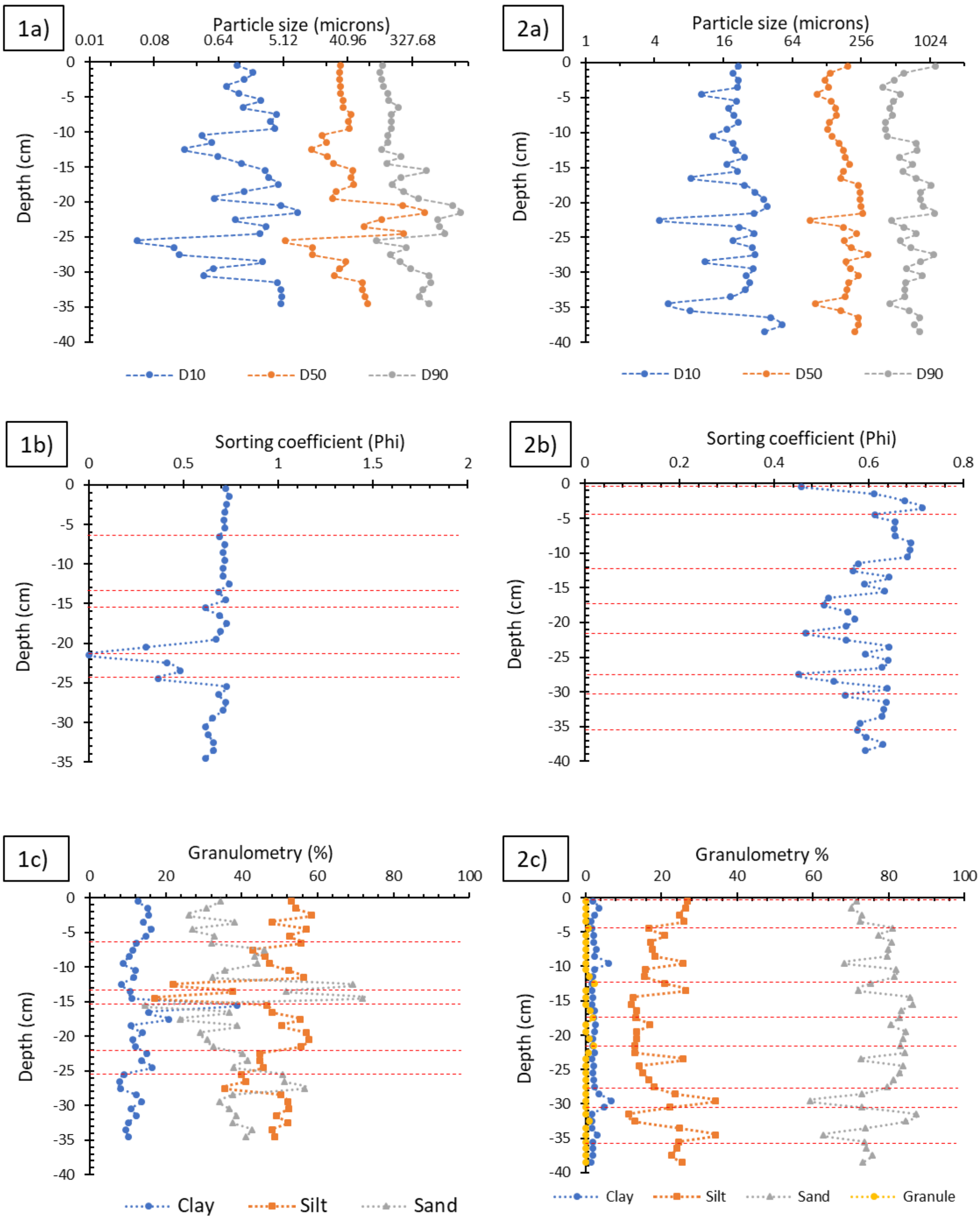

Figure 20: Characterisation of the sediment records in the Hin river mangrove. 1) Results of the first core and 2) Results from the duplicate core. a) Variations of the D_{10}, D_{50} and D_{90}; b) Variations of the sorting coefficient; c) Variations of the percentages of clay, silt and sand. The red dashed line are markers of drops in the sorting coefficient associated to significant changes in the grain size distribution.

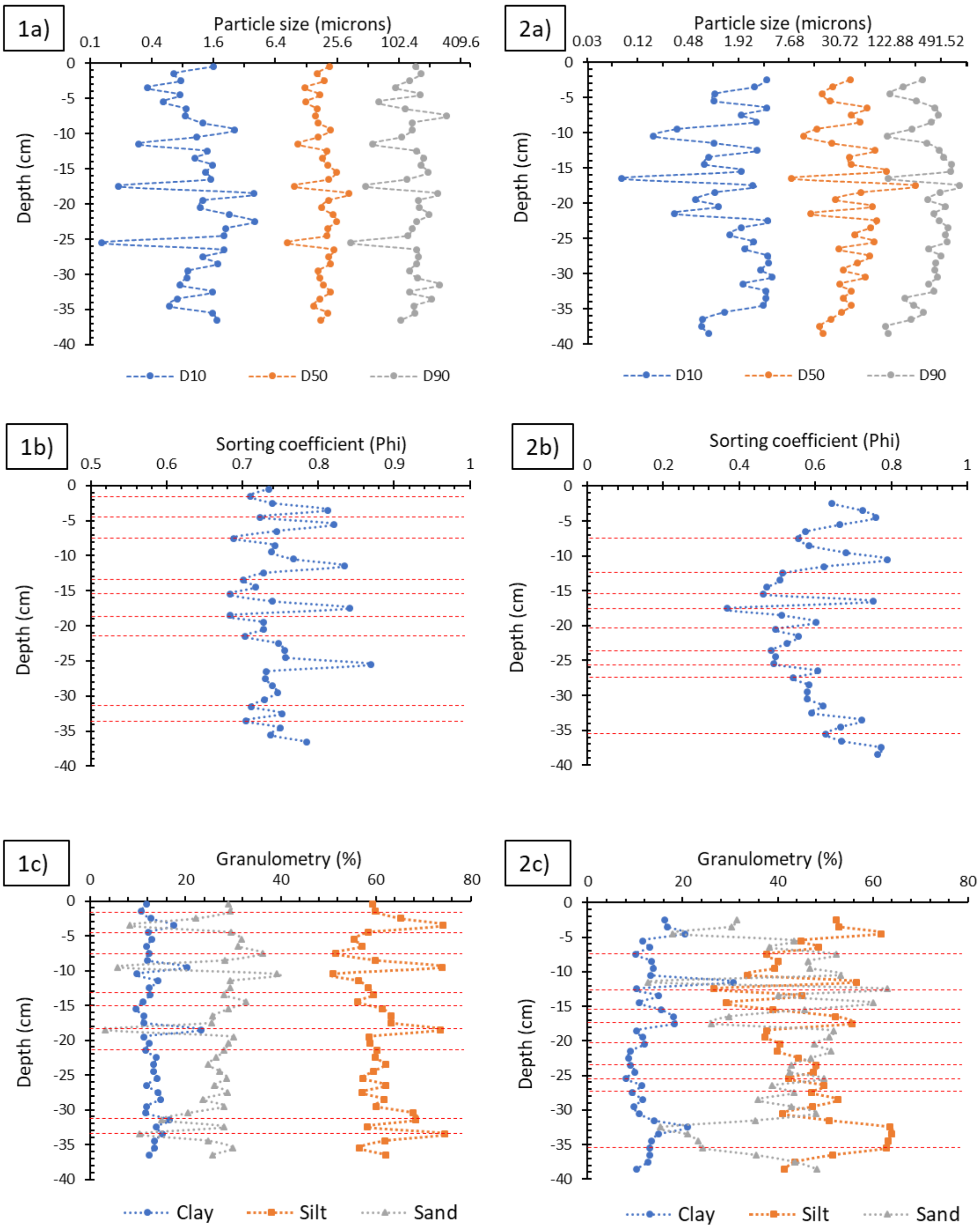

Figure 21: Characterisation of the sediment records in the Cha Mao river mangrove. 1) Results of the first core and 2) Results from the duplicate core. a) Variations of the D_{10}, D_{50} and D_{90}; b) Variations of the sorting coefficient; c) Variations of the percentages of clay, silt and sand. The red dashed line are markers of drops in the sorting coefficient associated to significant changes in the grain size distribution.

5.1.1.3 Seagrass cores in the Krabi Province

Core 1 from the seagrass at Koh Sriboya presents a D_{10} varying from 21.28 to 85.04 microns, a D_{50} varying from 115.71 to 339.48 microns and a D_{90} varying from 452.32 to 18548.23 microns. The duplicate core shows variations in the D_{10} from 14.86 to 88.5 microns, variations of the D_{50} from 186.77 to 899.4 microns and variations in the D_{90} from 584.72 to 25918 microns (Figure 22).

Core 1 from the seagrass at Koh Hang Airport presents a D_{10} varying from 29.3 to 74.6 microns, a D_{50} varying from 176.92 to 258.8 microns and a D_{90} varying from 411.4 to 479.4 microns. The duplicate core shows variations in the D_{10} from 18.13 to 74.43 microns, variations in the D_{50} from 159.16 to 223.39 microns and variations in the D_{90} from 388.17 to 463.12 microns (Figure 23).

Core 1 from the seagrass at Koh Jum presents a D_{10} varying from 26.7 to 69.1 microns, a D_{50} varying from 109.7 to 143 microns and a D_{90} varying from 217.9 to 234.6 microns. The duplicate core shows variations in the D_{10} from 11.01 to 57.51 microns, variations in the D_{50} from 93.86 to 136.93 microns and variations in the D_{90} from 209.1 to 371.56 microns (Figure 24).

As a general observation, the distribution in most of the samples is usually bi-modal. As would be expected from the hydrodynamics and sediment supply in each ecosystem, the seagrass sediment is generally coarser than the mangrove sediment.

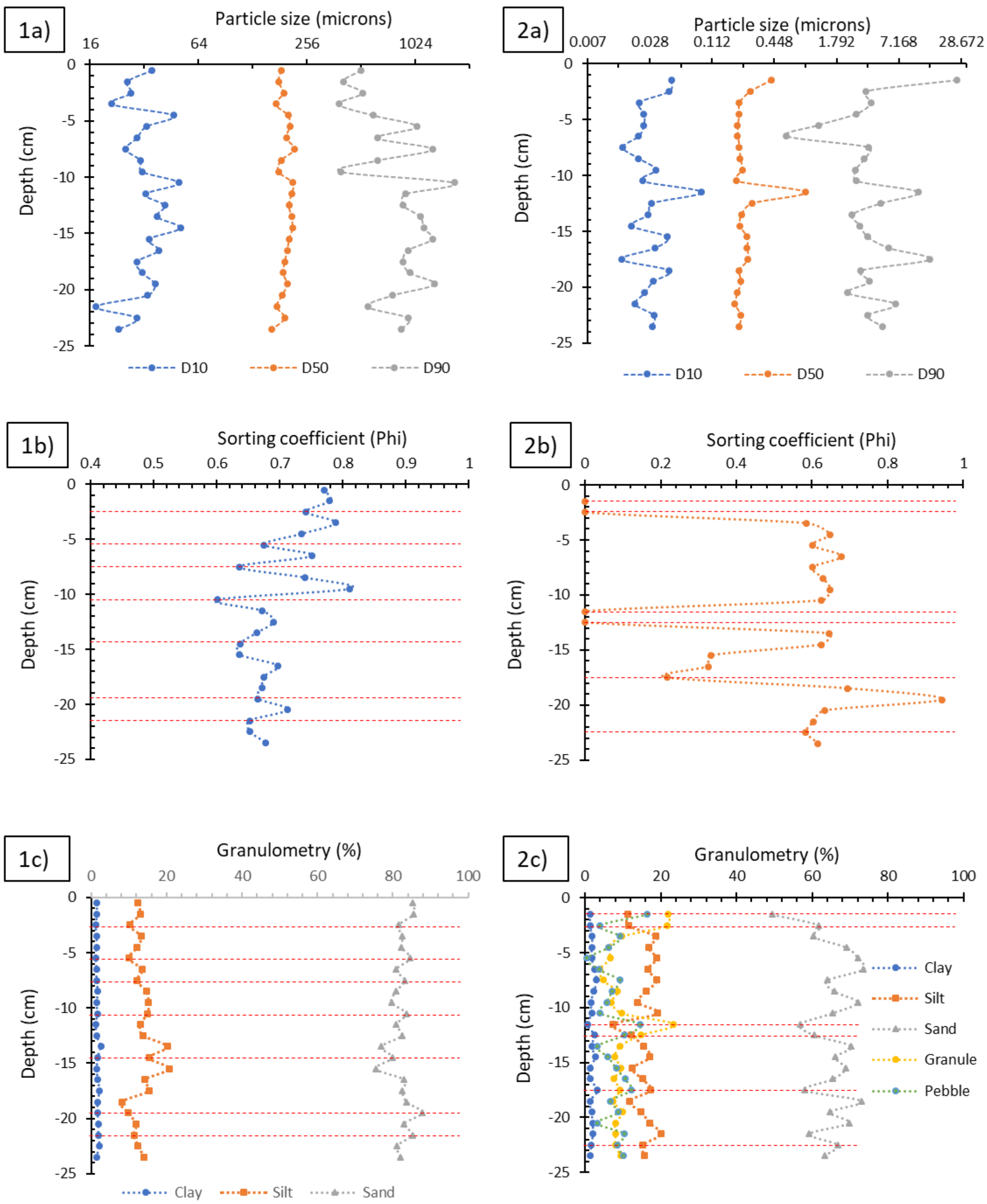

Figure 22: Characterisation of the sediment records in the seagrass at Koh Sriboya. 1) Results from the first core and 2) Results from its duplicate. a) Variations of the D_{10}, D_{50} and D_{90}; b) Variations of the sorting coefficient; c) Variations of the percentages of clay, silt and sand. The red dashed line are markers of drops in the sorting coefficient associated to significant changes in the grain size distribution.

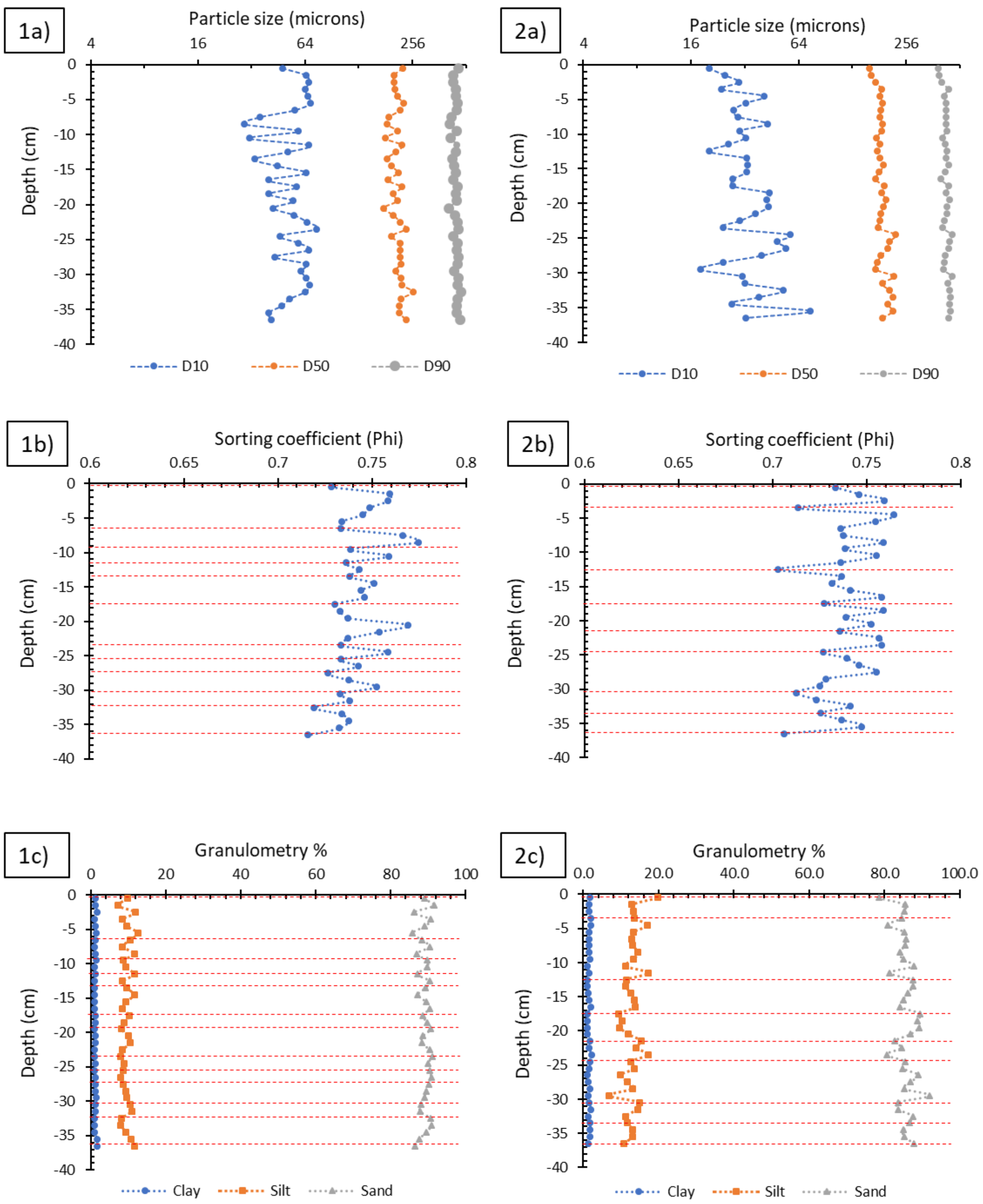

Figure 23: Characterisation of the sediment records in the seagrass at Koh Hang. 1) Results from the first core and 2) Results from its duplicate. a) Variations of the D_{10}, D_{50} and D_{90}; b) Variations of the sorting coefficient; c) Variations of the percentages of clay, silt and sand. The red dashed line are markers of drops in the sorting coefficient associated to significant changes in the grain size distribution.

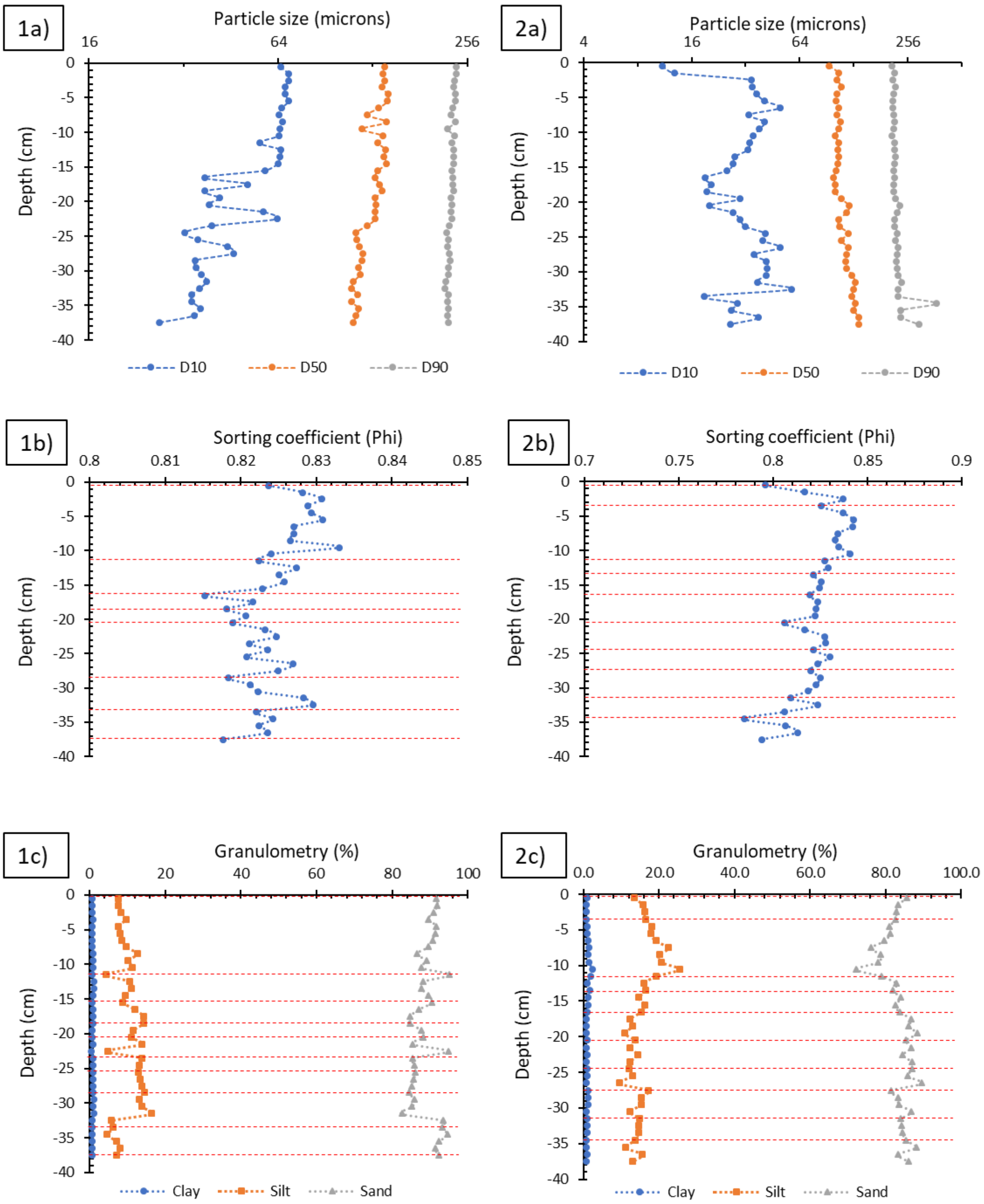

Figure 24: Characterisation of the sediment records in the seagrass at Koh Jum. 1) Results from the first core and 2) Results from its duplicate. a) Variations of the D_{10}, D_{50} and D_{90}; b) Variations of the sorting coefficient; c) Variations of the percentages of clay, silt and sand. The red dashed line are markers of drops in the sorting coefficient associated to significant changes in the grain size distribution.

5.1.2 Sorting coefficient and grain size distribution

5.1.2.1 Mangrove cores in the Krabi Province

When looking at the down core distribution of the sorting coefficient along each core, decreases in the sorting coefficient can be observed. These can be sudden or progressive. The sudden decreases represent a clear shift in depositional energy of the sediment within the mangroves.

When looking at the Krabi town first core, decreases in the sorting can be identified at various depths -1.5, -10.5, -12.5, -18.5 and -22.5 cm. These represent a coarsening of the sample typically with less clay present and an increase in the proportion of silt or sand (Figure 16).
Similar observations can be drawn with the records of the core in Krabi Airport and Baan Leam (Phela catchment) at respective depth of -0.5, -2.5, -6.5, -10.5, -14.5, -19.5 and -23.5 cm; and -3.5, -6.5, -12.5, -15.5, -23.5, -31.5 and -35.5 cm (Figures 17 and 18).

The analysis of the duplicate cores showed similar tendencies, however some of the sudden decreases in the sorting coefficient correspond to increases in the clay and slit fractions to the deficit of the sand fraction. The decreases in the sediment sorting along each duplicate core are identified at -1.5, -6.5, -11.5, -13.5, -16.5, -18.5, -21.5 and -28.5 cm for the Krabi town core (Figure 16); -0.5, -3.5, -6.5, -11.5, -13.5, -20.5, -25.5, -30.5, -35.5 cm for the Krabi airport core (Figure 17); and, -0.5, -6.5, -12.5, -16.5, -18.5, -23.5, -31.5 and -35.5 cm for the Baan Leam core (Figure 18). The clear increase in the clay and silt fractions are identified in the Krabi town core at -6.5, -13.5, -18.5, -24.5 and -28.5 cm; and in the Krabi airport core at -13.5, -17.5, -25.5 and -30.5 cm (Figures 16 and 17).

When examining the vertical variations of the grain size distribution, it can be observed that the proportion of clay throughout the core are very consistent in contrast to the portions of the sand and the silt grain sizes that appears to increase or decrease to the depend of each other describing cycles. Those cycles can be observed on all the cores sampled in the Krabi province.

5.1.2.2 Mangrove cores in the Nakhon Si Thammarat Province

In the lower mangrove core situated within the Thung Sai catchment, decreases in the sorting coefficient occur at -3.5, -8.5, -10.5, -16.5, -22.5, -25.5, -27.5, -32.5 and -40.5 cm. Again, these decreases are related to an increase in the sand fraction within the sample although some levels within the core at -10.5, -32.5 and -40.5 cm are marked more clearly by an increase in the silt fraction (Figure 19).

Decreases in sorting coefficient in the lower mangrove core of the Hin catchment can be identified at -6.5, -13.5, -15.5, -21.5 and -24.5 cm. Two of these decreases, at -15.5 and -24.5 cm, are linked to an increase in the clay fraction and the other three, at -6.5, -13.5 and -21.5cm, are marked by an increase in the silt fraction (Figure 20).

In the Cha Mao core, decreases in the coefficient of sorting are located at -1.5, -4.5, -7.5, -13.5, -15.5, -18.5, -21.5, -31.5 and -33.5 cm. Again, most of these decreases are marked by an increase of the sand or silt fraction within the sample (Figure 21).

The analysis of the upper mangrove core shows similar tendencies again however for some of the sudden decreases in the sorting coefficient correspond to increases of the granular fraction in the Hin mangrove records. The decreases in the sorting coefficient in core 2 of Thung Sai are identified at the following depths: -0.5, -6.5, -12.5, -15.5, -17.5, -23.5, -25.5, -31.5, -33.5, -37.5 and -39.5 cm. Most of these decreases in sorting correspond to an increase in sand as for the lower core, only samples at depths -6.5 and 31.5 cm correspond to an increase in silt (Figure 19).

As mentioned previously the increase of the coarser fractions of sediment (sand and granule) in the Hin records drives the drops of the sorting coefficient. Those drops are measured at -0.5, -4.5, -12.5, -17.5, -21.5, -27.5 and -35.5 cm (Figure 20).

In core 2 of Cha Mao, decreases in the sorting coefficient are located at depth -7.5, -12.5, -15.5, -17.5, -20.5, -23.5, -25.5, -27.5 and -35.5 cm. Here again, most decreases are marked by an increase of the sand or silt fraction within the sample (Figure 21).

When examining the vertical variations of the grain size distribution within the cores sampled in the Nakhon Si Thammarat province, the clay grain size is much more variable with sudden peaks of clay generally matching sudden increases in silt. In a similar way to the cores in the mangroves of the Krabi province, the variations of the grain size distribution between the silts and the sands appears to reveal cycles being witnesses of the weather variations throughout time. However, again these cycles are not specifically corresponding to any significant drops in the sorting coefficient suggesting again that both characteristics are caused by different phenomenon.

5.1.2.3 Seagrass cores in the Krabi Province

Similar observations are noted in the seagrass cores at Koh Sriboya and Koh Jum. Although the sediment in the seagrass cores is generally coarser than the mangrove cores, the decreases in coefficient of sorting are characterised by an increase of the coarser fraction of the sediment i.e. sand, silt, granule or even pebble.

In the Koh Sriboya cores, these decreases are notable at the following depths: -2.5, -5.5, -7.5, -10.5, -14.5, -19.5 and -21.5 cm (Figure 22).

In the Koh Hang cores decreases are notable at the following depths: -0.5, -6.5, -9.5, -11.5, -13.5, -17.5, -23.5, -25.5, -27.5, -30.5, -32.5 and -36.5 cm (Figure 23).

In the Koh Jum cores decreases are notable at the following depths: -0.5, -11.5, -16.5, -18.5, -20.5, -28.5, -33.5 and -37.5 cm (Figure 24).

In the upper cores (core 2), the decreases in sorting are at following depths. For Koh Sriboya: -1.5, -2.5, -11.5, -12.5, -17.5, -22.5 cm (Figure 22). For Koh Hang: -05, -3.5, -12.5, -17.5, -21.5, -24.5, -30.5, -33.5, -36.5 cm (Figure 23). For Koh Jum: -0.5, -3.5, -11.5, -13.5, -16.5, -20.5, -24.5, -27.5, -31.5 and -34.5 cm (Figure 24). Again, these decreases in sorting are mostly associated with an increase of the coarser fraction of sediment.

It is important to point out that the sediment in these cores was mixed with large, most likely autochthonous, biogenic sediment. This was sieved and not accounted within the results.

5.1.3 Discussion and Conclusions

5.1.3.1 Mangroves in the Krabi province

Within the Krabi province, the tide is semi-diurnal and the tidal range is macrotidal. The foreshore has a very gentle slope and flat landforms. Because of the flat topography and low wave energy there has been high deposition of finer sediments, clay, silt and organic matter along the coast (Paw, 1988).

Krabi Town and Krabi Airport mangroves are sheltered from tidal sediment influx and therefore most of the sediment in the mangrove is expected to come from fluvial sources. On the other hand, the Baan Leam mangrove (in the Phela catchment) is located at the river mouth and sea currents are likely to contribute to the sediment within this site.

Variations in the sorting coefficient indicate variations in sediment supply from rivers and potentially from groupings of high intensity - low frequency events such as storm surges and tsunamis. That sediment supply is also likely to be linked to changing hydrodynamic conditions within rivers and/or sediment availability in the catchment.

on close examination of the proportion of sand and silt within the sediment records, it can be observed that some sort of cyclicity with both portions growing or decreasing interdependently with little variation in clay. Sediment availability is closely linked to the occurrence of landslides, which has been reported to be linked to rainfall intensity (Iida, 2004; Soralump, 2010; Fan et al., 2016; Rangsiwanichpong et al., 2017; Komori et al. 2018). River flow is also directly linked to rainfall intensity and duration. Therefore, high rainfall periods increase river flow and bring a certain type of sediment, classically coarser, to downstream areas, potentially in mass pulses of sediment. These alternating cycles of grain class do not seem to match the cyclicity of the decreases in sorting which suggest that both the sorting and the silt – sand dominance in grain size distribution are driven by different forces. However, it is assumed that most of the decreases in sorting coefficient observed in the results are also markers of periods of increased rainfall and natural disaster events. Further insights using sediment dating will provide a clearer view on the chronology of these events and discussed later on (Section 5.3 & Section 5.5).

When visually comparing the cyclicity of the sorting coefficient decreases between each of the catchments within the Krabi province, it appears that these cycles are occurring at a comparable pace suggesting similarities in events between the cores/sites. Again, further information from the dating analysis (Section 5.3 & Section 5.5) will help draw more conclusive observations.

5.1.3.2 Mangroves in the Nakhon Si Thammarat province

Along the Nakhon Si Thammarat coast the stronger wave energy and local geomorphology, amongst other parameters such as anthropogenic influences, limits the formation of extensive mangrove forests. However, along the river mouths where muddy sediments are deposited, discrete mangrove forests are well established. The tidal range along the Nakhon Si Thammarat coast is small so tidal influence is only along a narrow strip along the coastline.

Both mangroves in Thung Sai and Hin are fairly isolated from significant marine sediment influence. On the other hand, the core within the Pak Phanang Bay (Cha Mao mangrove) is on the edge of the mangrove near the boundary between the Cha Mao estuary and the sea. It is highly probable that major events like typhoons bring marine sediment into this environment (Boromthanarat et al., 1991); however, the bulk of the sediment material brought into the Pak Phanang Bay comes from rivers (Panapitukkul et al., 1998; Boromthanarat et al., 1991; Flos, 1993).

In a similar way to mangroves in the Krabi province it is highly probable that decreases in sorting coefficient within the sediment records correspond to significant periods of increased hydrometeorological activity. Additional information from sediment dating will help identifying and verifying the chronology between these events (Section 5.3 & Section 5.5).

It is interesting to point out that the Hin and Thung Sai catchments cover smaller areas and the sources of sediment for both mangroves are much closer in these catchments than for the other studied catchments, explaining the wider range of grain size observed in the cores.

5.1.3.3 Seagrass in the Krabi province

Marine sediments around Krabi Province are mostly composed of mud, sand, silt and gravel from fluvial sediment deposits (Paw, 1988). The seagrass environments in the Krabi province are subjected to complex and seasonal marine currents that influence grain size distribution.

In a similar way as previously noted in the mangroves, sudden decreases in sorting mark mass deposition of coarser sediments, such as gravel or sand. These introductions of coarser sediments indicate a change in hydrodynamic conditions making them competent enough to transport coarser material within this environment.

That coarser material has two potential sources, from terrestrial sources via the Phela river, and from marine sources transported by changing currents.

Theoretically, similarities in grain size distribution and the frequency of events should be observed between the records from the cores in the Phela catchment and the seagrass cores. However, matching these events between the cores proves to be difficult without the sediment dating information. It will again be examined and discussed in the following sections (Section 5.3 & Section 5.5) providing more certainty about the age of the deposits.

The complexity of the changing marine currents with the seasons (Soegiarto & Birowo, 1975; Soegiarto, 1985; Kiran, 2017) certainly adds complexity to the sediment grain size distribution within the seagrass cores. Changing currents may contribute to the reintroduction/ redistribution of material not necessarily in sync with periods of more rainfall and supplies of sediment from the continent. Separating the different flux of sediments is not possible but the addition of the sediment dating information (Section 5.3) will help identify periods or events of deposition and eventually where the deposits are from (Section 6).

5.2 Organic matter (OM)

5.2.1 Mangroves in the Krabi province

Results are shown in Figure 25. Pak Nam Krabi mangrove (“Krabi Town core”): organic matter content varies from 7.5 to 11.5 % with a median of 9.6 % in core 1. Its duplicate shows a content varying from 7.1 to 9.8 % with a median of 9.2 %.

Kam mangrove (“Krabi Airport core”): organic matter content varies from 13.8 to 38.8 % with a median of 16.1 % in core 1. Its duplicate shows a content varying from 14.1 to 30.1 % with a median of 18.1 %.

Phela mangrove (“Baan Leam core”): organic matter content varies from 16.9 to 24.7 % with a median of 20.3 % in core 1. Its duplicate shows a content varying from 17.7 to 43.8 % with a median of 24.9 %.

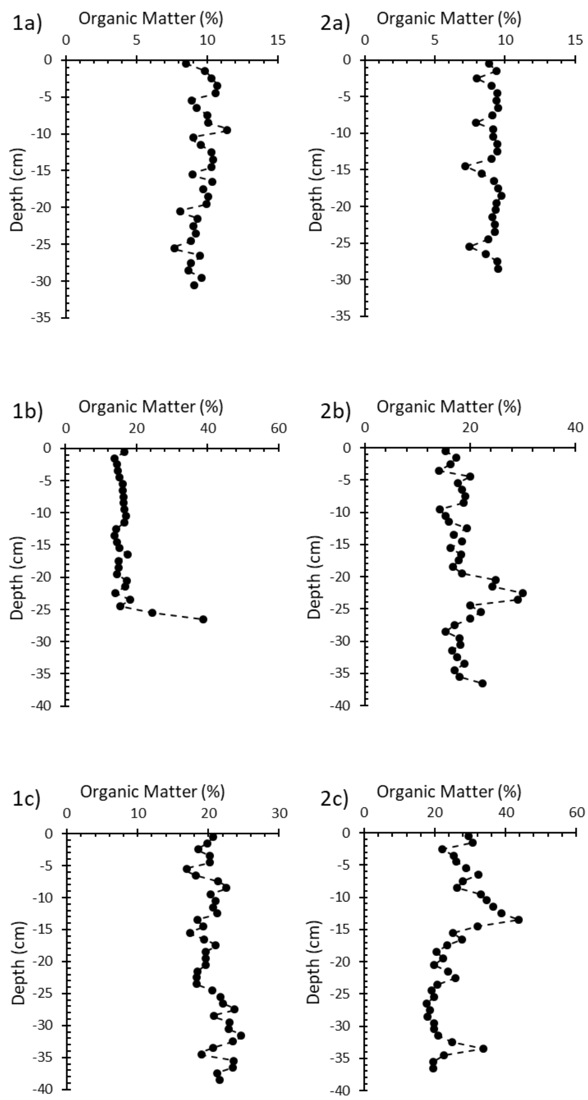

Figure 25: Variations of the percentage of OM within the sediment in the Krabi province mangroves. 1) Results from the first core and 2) Results from its duplicate. a) Mangrove within the Pak Nam Krabi catchment, b) mangrove within the Kam catchment, c) mangrove within the Phela catchment.

5.2.2 Mangroves in the Nakhon Si Thammarat province

Results are shown in Figure 26. Thung Sai mangrove: organic matter content varies from 7.94 to 49.5 % with a median of 15.92 %. Its duplicate shows a content varying from 4.7 to 25 % with a median of 8.5 %.

Hin mangrove: organic matter content varies from 2.4 to 9.6 % with a median of 6.1 %. Its duplicate shows a content varying from 3 to 6.5 % with a median of 4.8 %.

Cha Mao mangrove: organic matter content varies from 10.4 to 22 % with a median of 14 %. Its duplicate shows a content varying from 6 to 19.4 % with a median of 14.3 %.

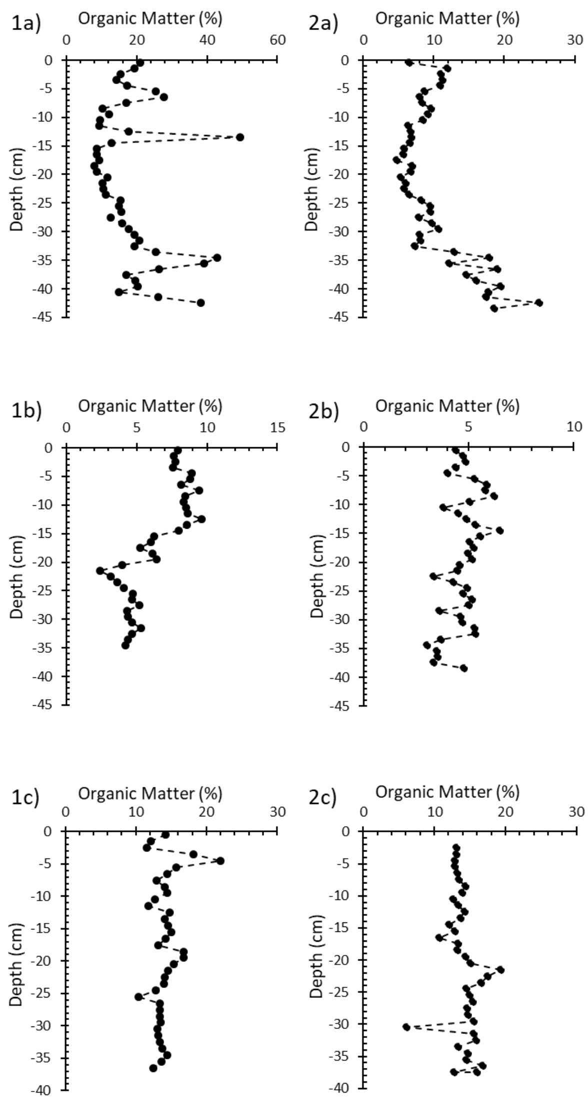

Figure 26: Variations of the percentage of OM within the sediment in the NST province mangroves. 1) Results from the first core and 2) Results from its duplicate. a) Mangrove within the Thung Sai catchment, b) mangrove within the Hin catchment, c) mangrove within the Cha Mao catchment.

5.2.3 Seagrass in the Krabi province

Results are shown in Figure 27. Koh Sriboya seagrass: organic matter content varies from 2.2 to 3.5 % with a median of 3 %. Its duplicate shows a content varying from 1 to 2.9 % with a median of 1.5 %.

Koh Hang seagrass: organic matter content varies from 0.4 to 1.3 % with a median of 0.4 %. Its duplicate shows a content varying from 0.7 to 2.2 % with a median of 1 %.

Koh Jum seagrass: organic matter content varies from 0.7 to 2.3 % with a median of 1.1 %. Its duplicate shows a content varying from 2.1 to 4.7 % with a median of 3 %.

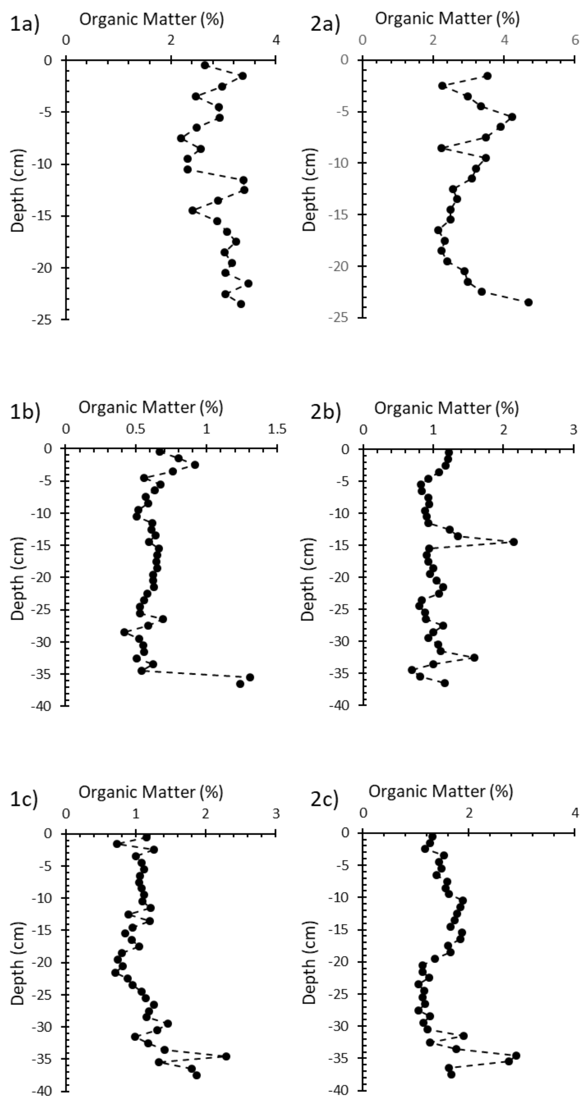

Figure 27: Variations of the percentage of OM within the sediment in the Krabi province seagrass sites. 1) Results from the first core and 2) Results from its duplicate. a) Koh Sriboya, b) Koh Hang, c) Koh Jum.

The relationship between soil organic matter and ecosystem type is quite clear when looking at the results. Mangroves have much higher stocks of organic matter than seagrass.

As mentioned earlier, the main processes controlling the percentage of organic matter within sediments are: sedimentation rates, grain size, plant material source and the decomposition processes (redox conditions, microbial populations, etc).

When examining the relationship between grain size and organic matter content, Ward (2012) and Lima et al. (2020) observed that organic matter content and particle size were strongly positively correlated. In the light of these findings, this study examined the relationship between the percentage of clay and the percentage of organic matter and the variations in D_{50} and the percentage of organic matter as a function of depth.

Relationships between the D_{50} and the percentage of organic matter proved to be successful in four study sites presenting a statistically significant regression that varies from weak to moderate (Figure 28).

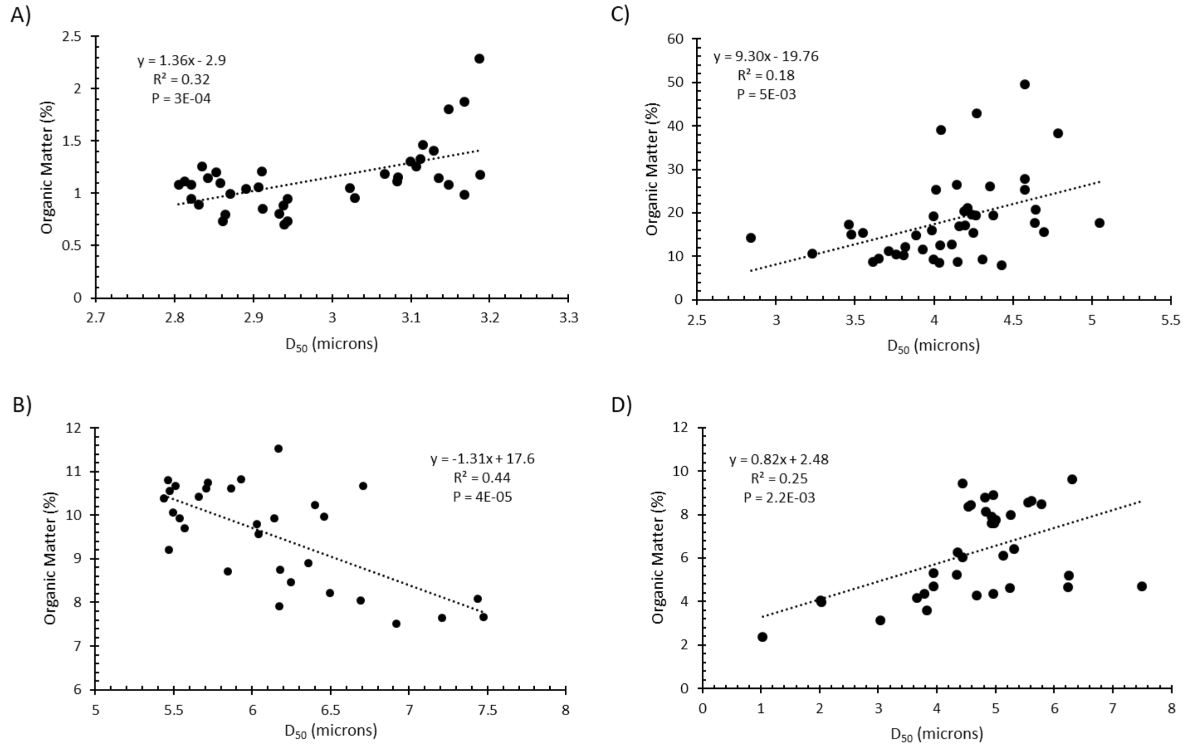

Figure 28: Statistically significant regressions observed between grain size and OM content across all the core samples. The sites showing these relationships are: A) Koh Jum (seagrass in the Krabi province), B) Krabi Town (mangrove in the Krabi province), C) Thung Sai (mangrove in the NST province) and D) Hin (mangrove in the NST province).

For most sites, Koh Jum, Thung Sai and Hin, the regression is positive, meaning that the percentage of organic matter increases with an increase of the grain size as observed by Ward (2012). In contrast, for the core sample in Krabi town, the percentage of organic matter decreases with the grain size. These results are confirmed by the duplicate cores sampled in Thung Sai and Krabi town only. Generally, organic matter has an affinity for fine sediment as it adsorbs onto mineral surfaces and the absorption processes contributes to its preservation (Hedges and Keil, 1995). A reduction in grain size typically decreases interstitial spaces in well sorted sediments, which decreases soil oxygen and thus, decomposition rates. This would explain the decrease in organic matter with the increase in grain size. However, in the Krabi Town core, with typically very fine sediment the decrease in organic matter linked to increases in D_{50} may be linked to rapid deposition of fine minerogenic sediments. Mangroves are natural sediment traps explaining rapid sedimentation rates of fine particles.

Organic productivity in mangroves and seagrasses is high in Southern Thailand as a result of the clement environment. Organic matter preservation is linked to the low oxygenation of the sediment, low bacterial activity and high sedimentation rates. In the study sites, it is assumed that most coarse sediments are deposited during high energy river flow periods where organic matter is buried rapidly contributing to its preservation. It was identified earlier that mangroves in Thung Sai, Hin and the seagrass sites generally presented a coarser vertical grain size distribution than the other study sites. It was hypothesised that the size of the catchments and the proximity of the mountain range to the mangroves in the Thung Sai and the Hin catchments were responsible for that coarsening. The presence of coarser sediment in the sediment load even during "drier" weather conditions would typically increase interstitial spaces and allow greater degradation of organic matter within the sediment. In contrast, during "rainier" periods, the rapid deposition of large amounts of coarse material would bury a large amount of organic matter which is not degraded as efficiently. This model explains the increase of organic matter content with an increase of the grain size distribution. It is hypothesised that within the seagrass environments the same assumptions of degradation and sedimentation can be made as for the Thung Sai and the Hin catchments, however hydrodynamic and sedimentation processes are much more complex because of the coastal currents.

Radio-isotopic dating and the calculation of sedimentation rates (Section 5.3 & Section 5.5) will certainly contribute to better understanding of the processes involved in the preservation of the organic matter within the sediment and the general processes of transport or deposition within the river catchments and their mangroves in the context of hydrometeorological forcing.

5.3 Radio-isotopic dating: ^{210}Pb and ^{137}Cs

The use of ^{210}Pb has been preferred to the use of the ^{137}Cs as the results obtained from the latter are very inconsistent with the typical peak of ^{137}Cs in the 1960s as described in Section 4.1. On the other hand, the ^{210}Pb activity highlights events when sedimentation rates are expected to be higher and is considered, for the purpose of this study to be more suitable. This isotope also allows to determine much more detailed sedimentation rates along the sediment column, hence it was preferred to use it for sediment dating.

5.3.1 Mangroves in the Nakhon Si Thammarat Province

The sedimentation rates measured in the duplicate core made in the Thung Sai mangrove (Figure 29) range from 0.8 to 1.6 mm/year since the 1960s and no particular peak in sedimentation rate is very clear, but as a general trend the sedimentation rate is increase throughout time from the 1960s till now.

The sedimentation rates in the Han mangrove ranges from 1.3 to 4 mm/year since the 1950s in the original core (Figure 30) and from 0.4 to 3.6 mm/year since the 1970s in the duplicate core (Figure 31). Three peaks of sedimentation can be noticed in the original core, one dated to 2015/2016 measuring 3.3 mm/year, another one dated to 1995/1996 measuring 4 mm/year and finally one in approximately 2001 measuring 3.6 mm/year. In the duplicate core, clear peaks are measured in 2007 (2.4 mm/year) and 2016/2019 (2.4 to 3.6 mm/year).

The sedimentation rates from the original core in the Cha Mao mangrove (Figure 32) vary from 1 to 5.4 mm/year from the 1960s to the present with a noticeable increase in sedimentation rates dated at 1997 (3.7 mm/year), 2007 (5.4 mm/year and 2015 (2.9 mm/year). The duplicate core (Figure 33) shows sedimentation rates varying from 0.5 to 1.4 mm/year and peak of sedimentation rate can be dated to approximately 1998.

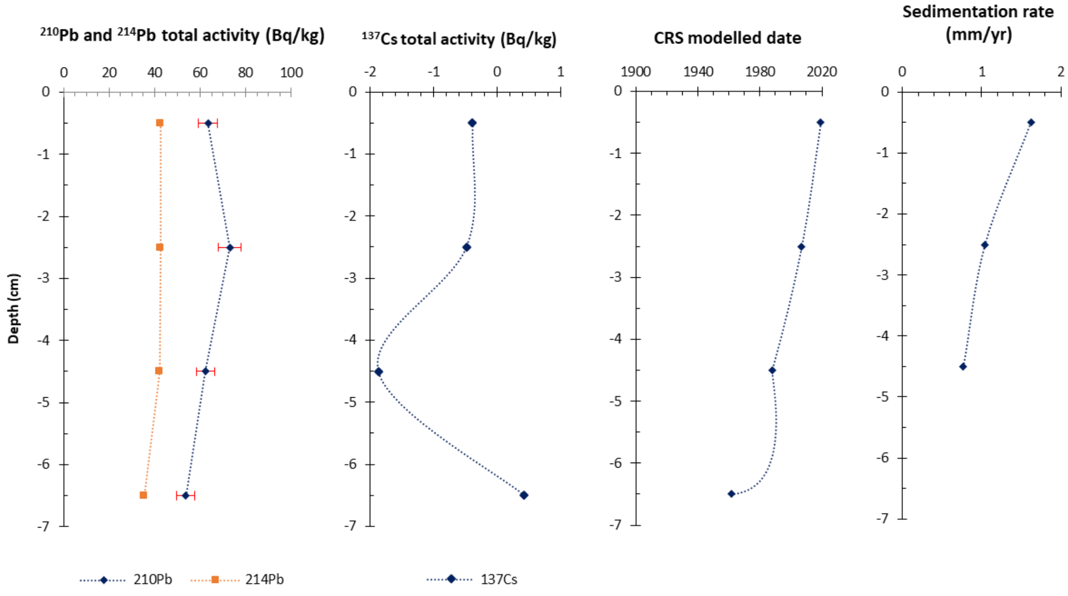

Figure 29: Radio-isotopic total activity, CRS modelled date and sedimentation rates variations according to the burial depth within the duplicate core of the Thung Sai mangrove.

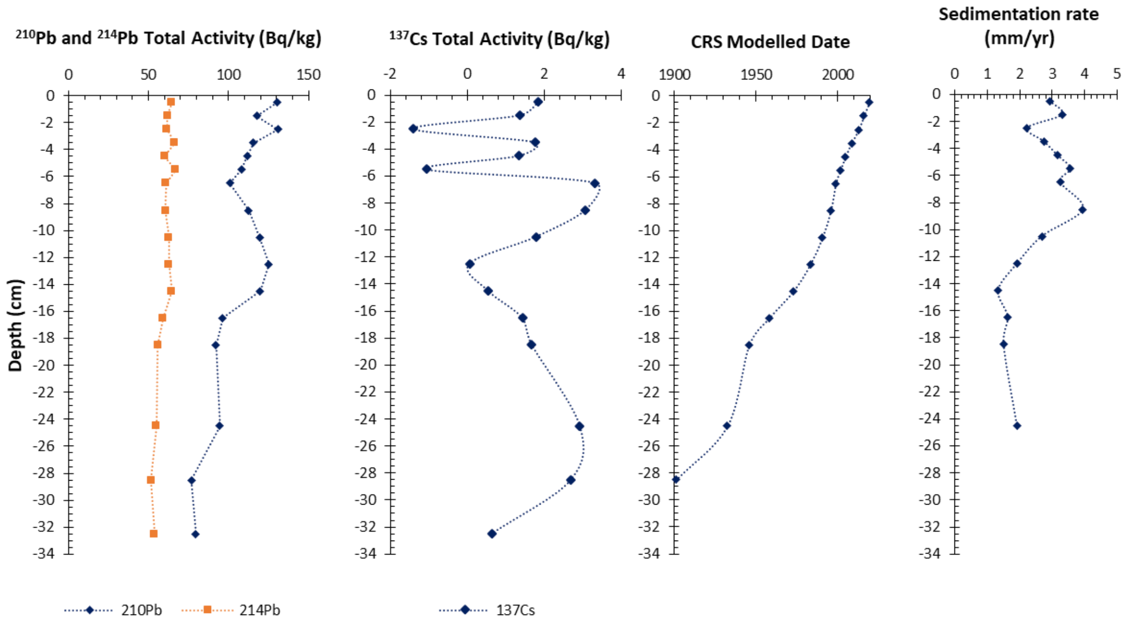

Figure 30: Radio-isotopic total activity, CRS modelled date and sedimentation rates variations according to the burial depth within the original core of the Han mangrove.

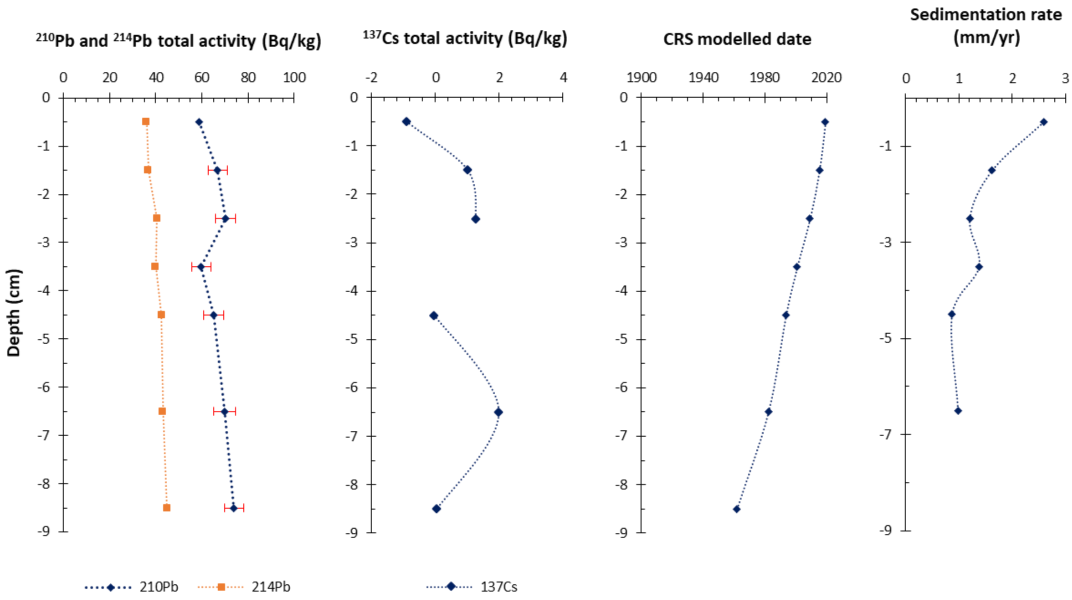

Figure 31: Radio-isotopic total activity, CRS modelled date and sedimentation rates variations according to the burial depth within the duplicate core of the Han mangrove.

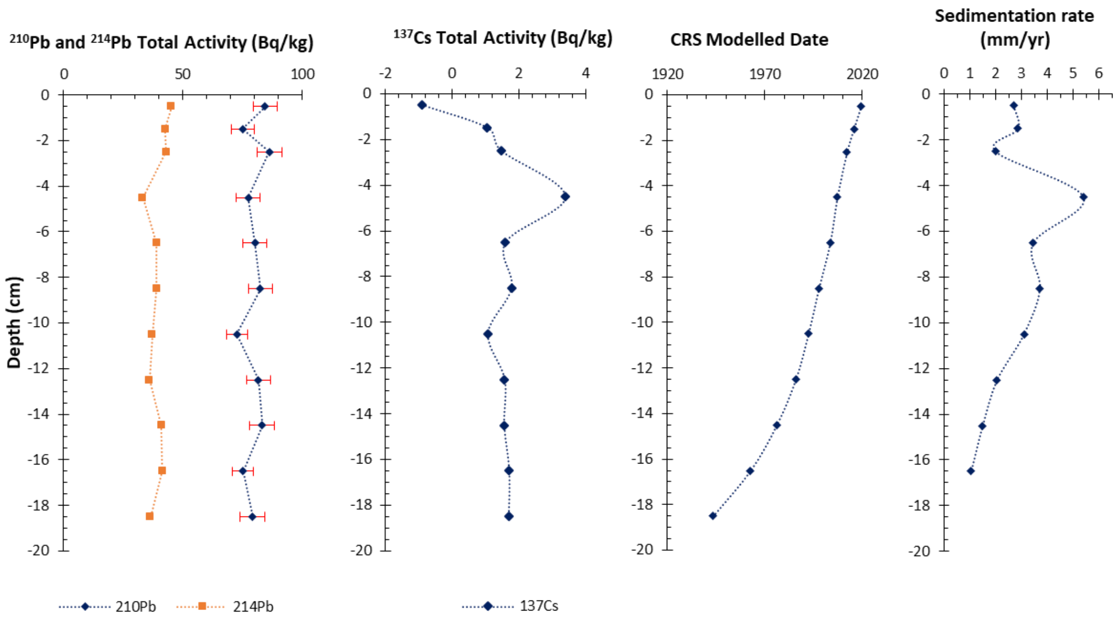

Figure 32: Radio-isotopic total activity, CRS modelled date and sedimentation rates variations according to the burial depth within the original core of the Cha Mao mangrove.

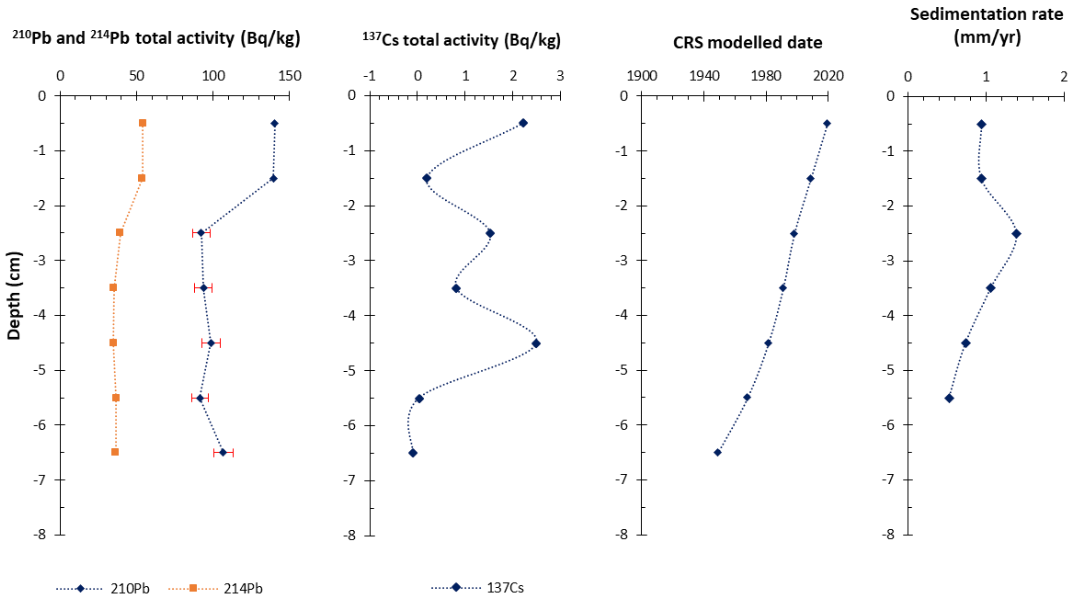

Figure 33: Radio-isotopic total activity, CRS modelled date and sedimentation rates variations according to the burial depth within the duplicate core of the Cha Mao mangrove.

5.3.2 Mangroves in the Krabi Province

The duplicate core taken in the Pak Nam Krabi's (PNK) mangrove (Figure 34) shows sedimentation rates ranging from 0.6 to 33.1 mm/year. Two sudden increases in sedimentation rates within the sedimentary column are noticeable, one dated to approximately 2006 (33.1 mm/year) and another dated to approximately 2009 (31.3 mm/year).

The duplicate core taken from the Kam mangrove (Figure 35) presents sedimentation rates varying from 1.5 to 5.4 mm/year from the 1970s. During this time period, three noticeable increase in sedimentation rates can be identified, one dated at 1985 (1.9 mm/year), a second dated at 2004 (3.3 mm/year) and a third one dated at 2009 (5.4 mm/year).

Both core in the Phela river's mangrove delivered sedimentation rates varying from 1 to 3.8 mm/year for core 1 (Figure 36) and 0.4 to 2.4 mm/year for its duplicate (Figure 37) since the 1950s/1960s. Both cores also displayed sudden peaks of sedimentation rates. In the original core those sudden peaks were dated at approximately 1991 (2.3 mm/year), 2003 (2.9 mm/year) and 2019 (3.8 mm/year). In the duplicate, those peaks were dated at approximately 1976 (1 mm/year), from 1992 to 2008 (1.9 mm/year) and 2012 (2.4 mm/year).

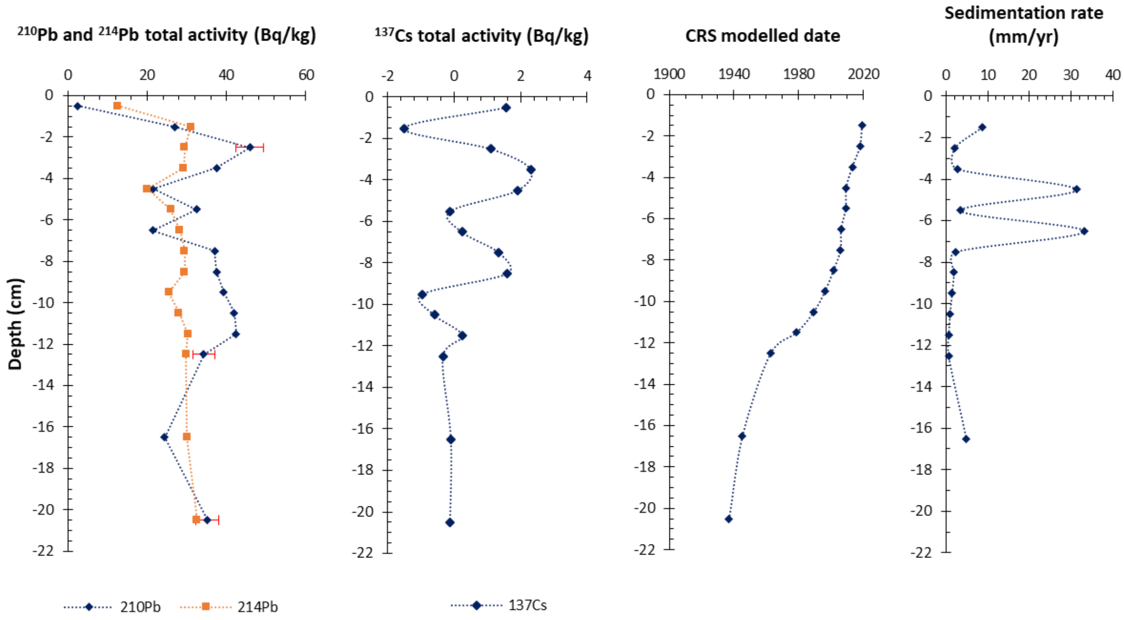

Figure 34: Radio-isotopic total activity, CRS modelled date and sedimentation rates variations according to the burial depth within the duplicate core of the PNK mangrove.

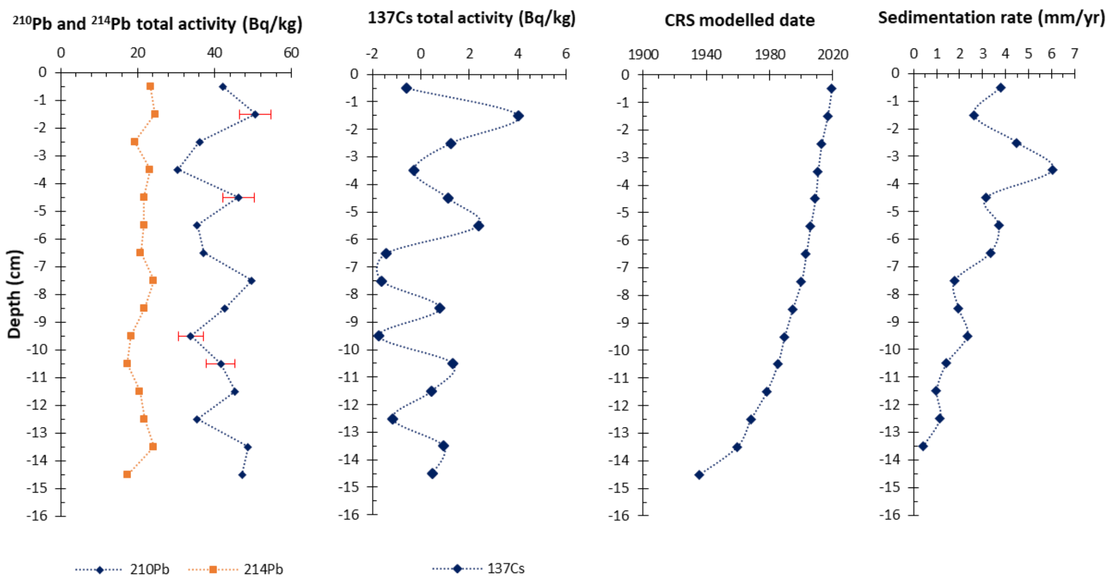

Figure 35: Radio-isotopic total activity, CRS modelled date and sedimentation rates variations according to the burial depth within the duplicate core of the Kam mangrove.

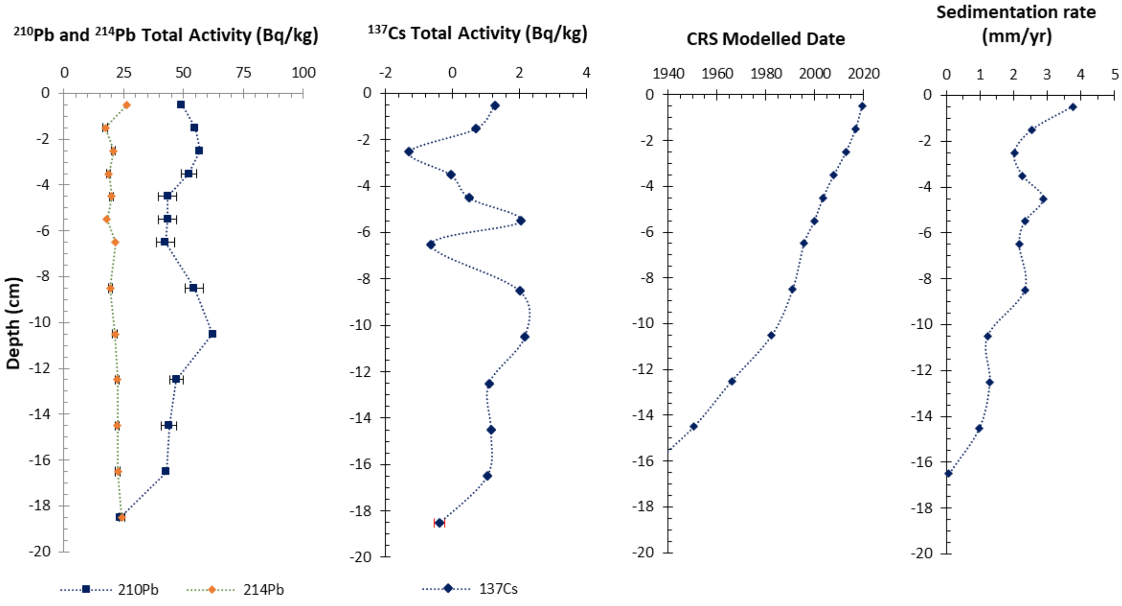

Figure 36: Radio-isotopic total activity, CRS modelled date and sedimentation rates variations according to the burial depth within the original core of the Phela mangrove.

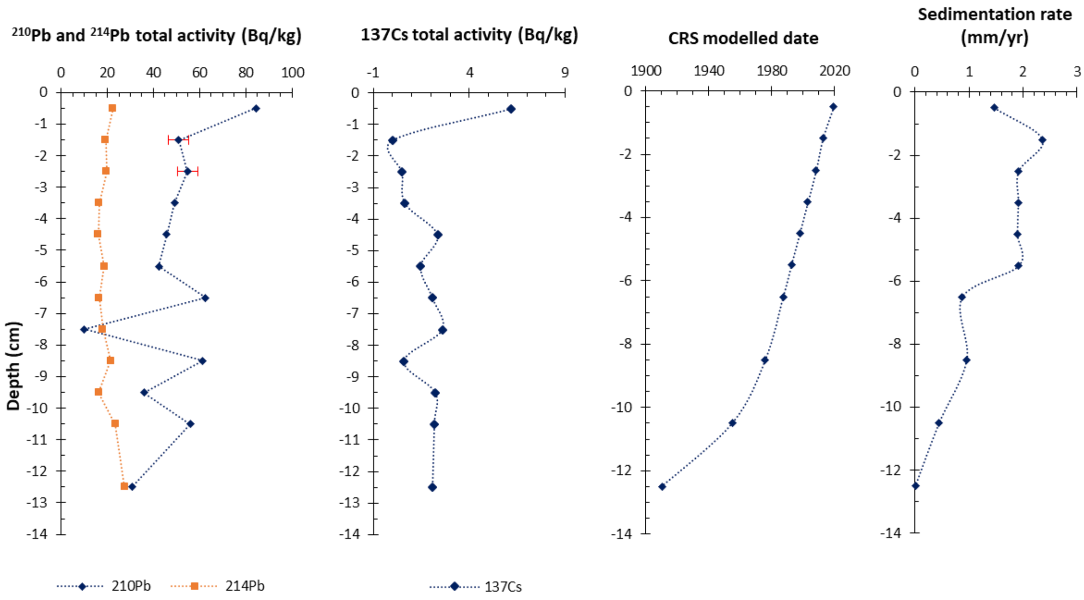

Figure 37: Radio-isotopic total activity, CRS modelled date and sedimentation rates variations according to the burial depth within the duplicate core of the Phela mangrove.

5.3.3 Seagrasses in the Krabi Province

The original core (core 1) taken in the Koh Sriboya seagrass (Figure 38) presents sedimentation rates varying from 0.9 to 2 mm/year with sudden increased sedimentation rates dated at approximately 1974 and 2019.

The original core of Koh Hang (Figure 39) shows sedimentation rates varying from 0.8 to 4.7 mm/year since the 1950s. Noticeable increases in sedimentation rates throughout the core column can be dated at approximately 1985, 2007 to 2010 and 2019.

The duplicate core (core 2) taken in Koh Jum (Figure 40) shows sedimentation rates ranging from 0.8 to 2.3 mm/year since the 1970s and no sudden change of sedimentation rate can be identified however it seems that they are increasing progressively throughout time.

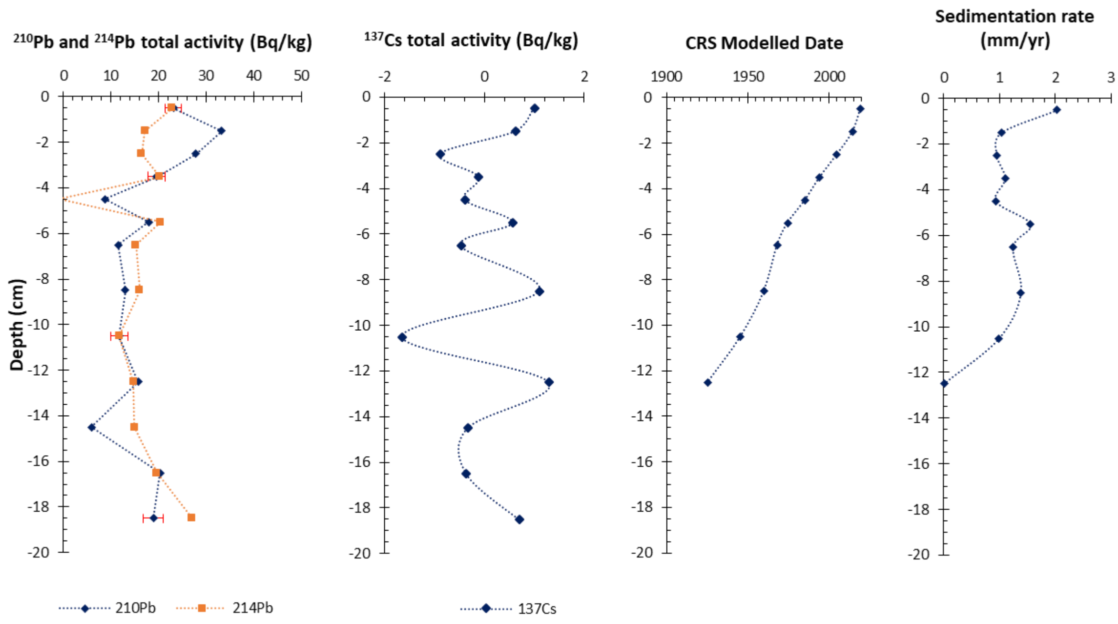

Figure 38: Radio-isotopic total activity, CRS modelled date and sedimentation rates variations according to the burial depth within the original core in the seagrass of Koh Sriboya.

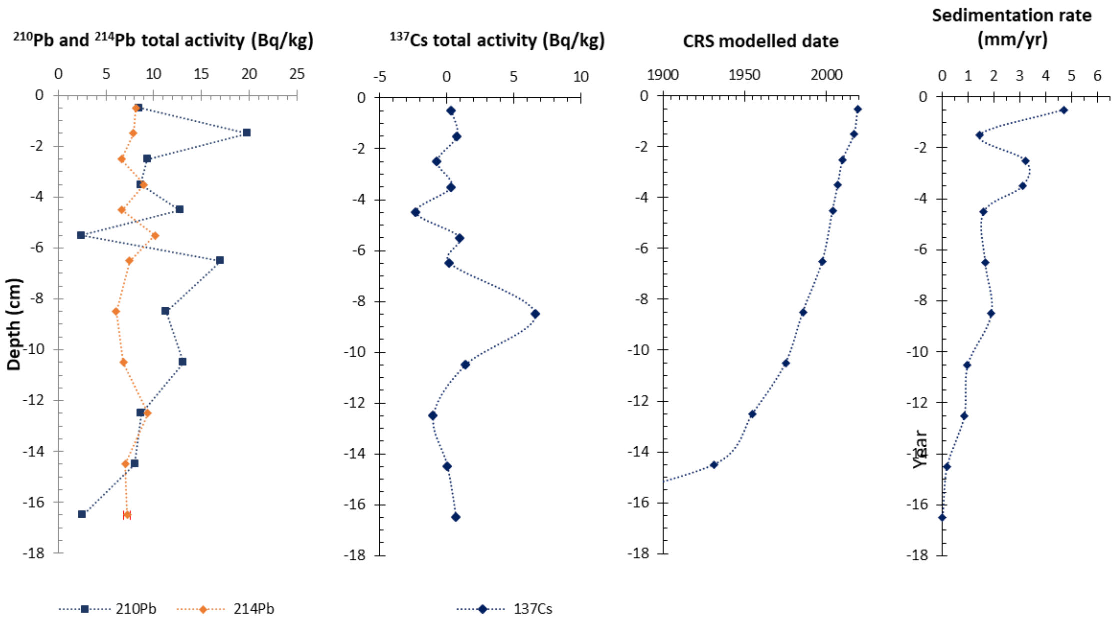

Figure 39: Radio-isotopic total activity, CRS modelled date and sedimentation rates variations according to the burial depth within the original core in the seagrass of Koh Hang.

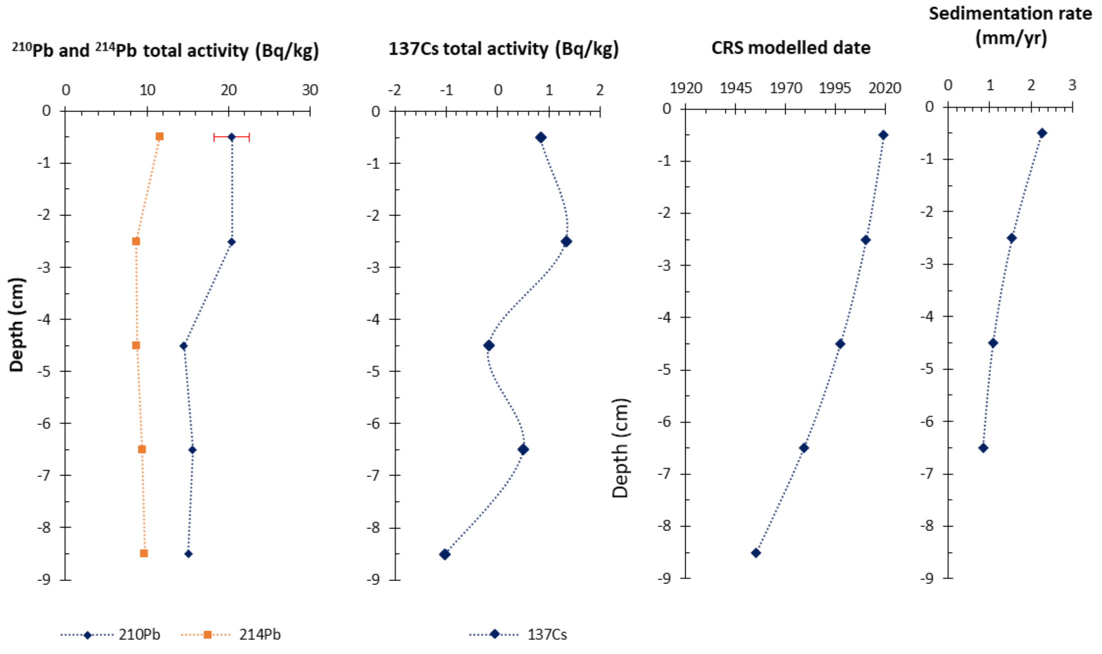

Figure 40: Radio-isotopic total activity, CRS modelled date and sedimentation rates variations according to the burial depth within the duplicate core in the seagrass of Koh Jum.

5.4 Landslide Inventories

5.4.1 Power Law equations

Frequency volumes were plotted along logarithmic axes and the tail end of the distributed data was carefully analysed as the intrinsic inaccuracy of the least squares regression (LSR) reveals itself in those areas due to under sampling in relation to data censoring. The LSR inaccuracy in the tail of the logarithmically transformed data resulting from the high-resolution data was not clear and the data was very linear, probably as a result of the ability to identify very precisely smaller size landslides in this inventory. Therefore, it was decided to keep that tail end data to extrapolate the power law equations. Figure 41 displays a typical result. Correlations for all the results have high correlations coefficients (R^2) higher than 0.7.

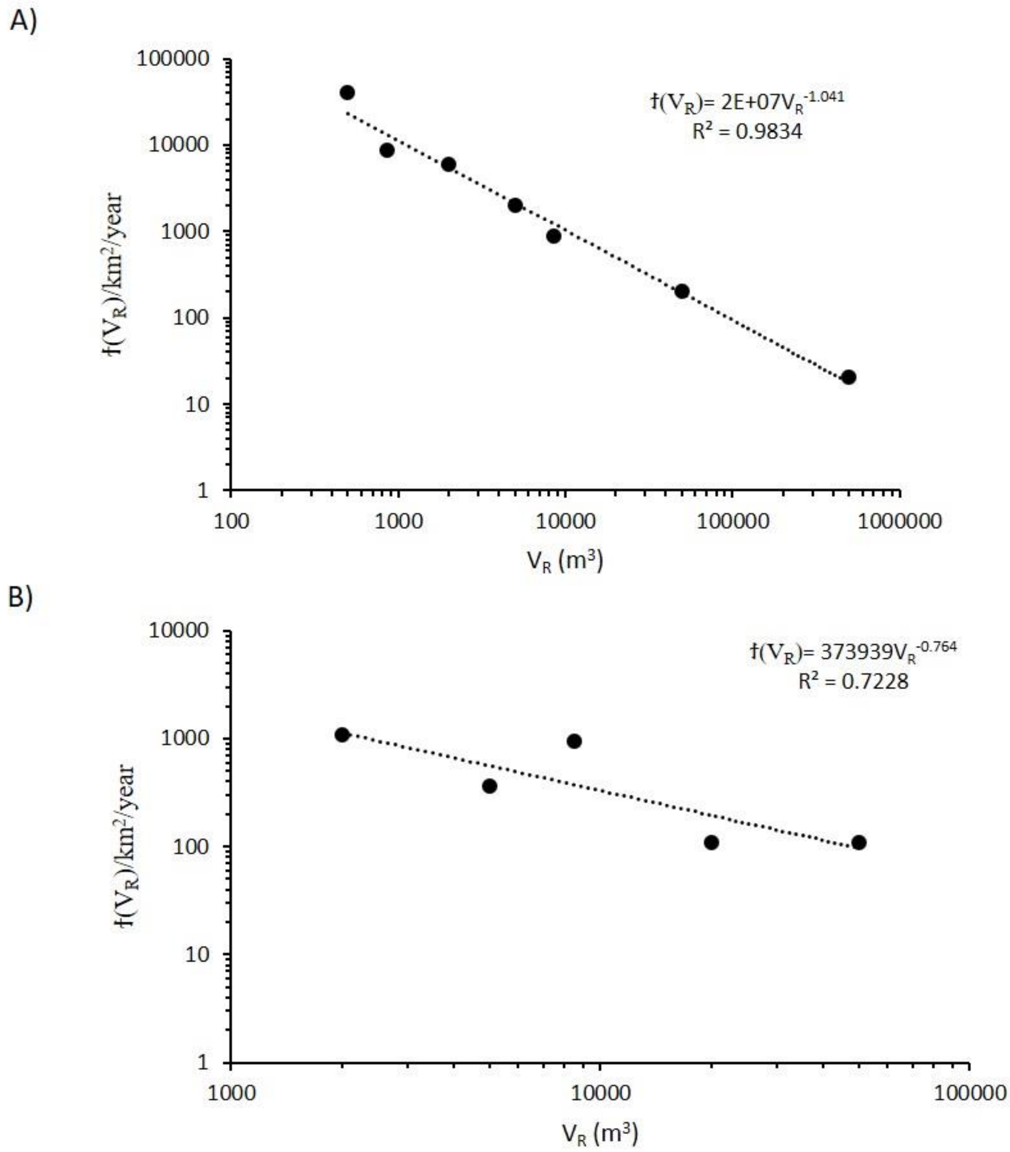

Figure 41: Best (A) and worst (B) power scaling correlation observed for the high-resolution imagery from the catchments of Pak Nam Krabi in January 2015 (A) and Cha Mao in July/August 2017 (B).

5.4.2 s and β variations

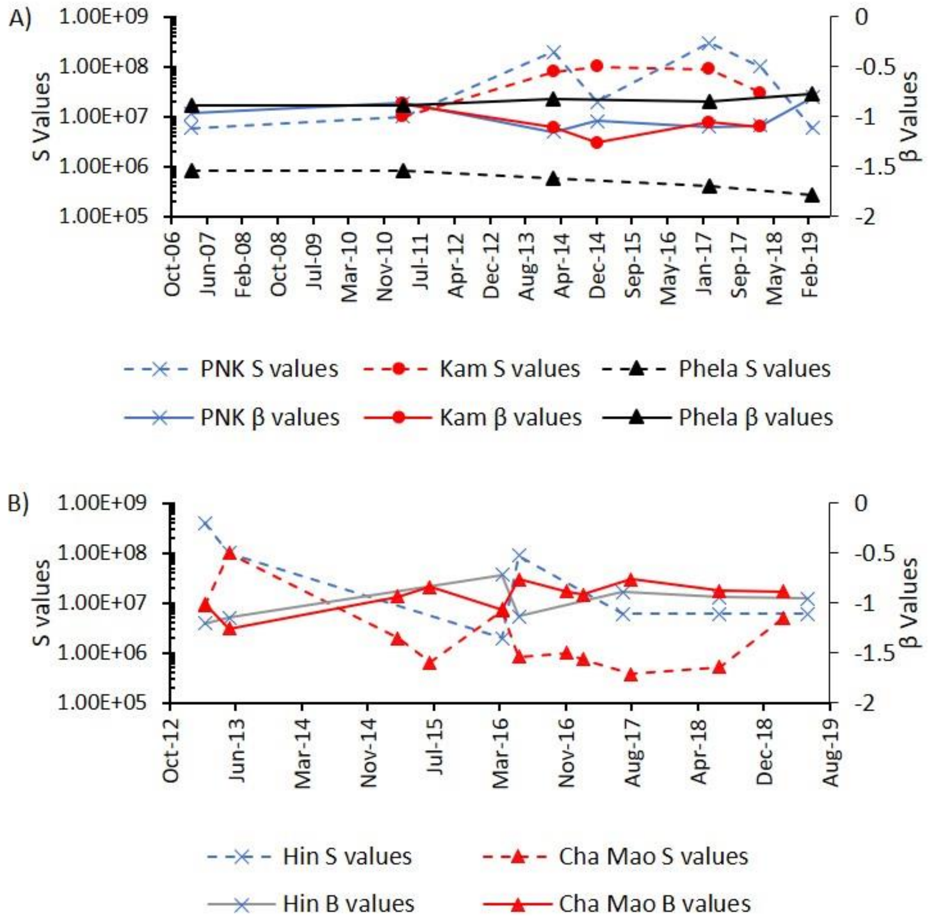

Figure 42: Variations of the s and β values from the study sites in A) the Krabi Province and B) the NST Province during the surveyed time period using High Resolution Remote Sensing Imagery.

Please note that there were insufficient data to determine enough power equations within the Thung Sai catchment within the time series available. This can be explained by two possibilities: (1) this area experiences very little mass movement events, or (2) the high-resolution imagery time series was not sufficient to appropriately capture these events. It is assumed by the study that the first assumption is more likely the reason as the resolution of the imagery available for the Thung Sai area is comparable to the other catchments in Nakhon Si Thammarat.

When looking at variations of s and β across the surveyed period within the PNK catchment, clear peaks or high values of both variables can be identified. All measurements within this catchment were collected during the same season for different years i.e. the dry season that has been described as starting from November/December to March/April. Two peaks in the s values can be identified in 2014 and 2017 whereas three clear peaks for the coefficient β can be identified in 2011, 2015 and 2019 (Figure 42).

For the Kam catchment, similar observations can be drawn regarding the timing of the sampling with imagery acquired during the dry season after the winter and supposedly more rainy conditions. High values of the multiplier s can be observed in 2014, 2015 and 2017 and peaks in the coefficient β are observes in 2011 and 2017 (Figure 42).

In contrast, in the Phela catchment, variations of the values s and β across the range are very low not highlighting any noticeable changes (Figure 42).

Measurements of the s and β values within the catchments of interest in NST were acquired across two seasons, the dry season as identified earlier and the monsoon season starting in April/May to September/October. Fluctuations of the power law regression parameter s in the Hin catchment describe peaks in the dry season 2016 and the wet season 2017. In that same catchment, variations of the coefficient β show peaks in the dry season 2013, the wet season 2013 and the wet season 2016.

When looking at the Cha Mao catchment, peaks of the s multiplier are noticeable in the dry season of 2013 and the wet season of 2015, 2016, 2017. On the other hand, high values within the β variations are identified during the wet season of 2013 and the dry seasons of 2016 and 2019 (Figure 42).

5.4.3 Frequency volume vs rainfall

To match adequately to the pattern of the seasons, yearly averages were calculated from November to October of the following year. Best correlations between rainfall and volume frequencies were obtained when the wettest month prior to the data imagery within the same season is subtracted to the early average rainfall. The wettest month of each season is used to have a good representation of the intensity of the rainfall of the season before the observation of mass movements. The subtraction of the wettest month to the year's average intensifies the differences between wettest and dryer seasons during the survey period.

Better correlations between rainfall and volume frequencies were obtained when using local weather stations (AWS) in the Krabi province whereas the regional weather stations (RID) near the Hin catchment is showing better results.

Overall correlations in the Krabi province are very good. Between the coefficient β and rainfalls, the R^2 values vary from 0.76 to 0.97 and between the multiplier s and rainfall, the R^2 values vary from 0.69 to 0.77 (Figure 43).

In the NST province, correlations were a bit more moderate with R^2 varying for 0.22 to 0.29 when using β and very poor with an R^2 nearing 0 when using s (Figure 44). When looking at these preliminary results, it can be seen that some points are outcast of the bulk results and by redrawing the results discarding these "extreme" values, correlations increase greatly for both β and s with R^2 values respectively varying from 0.3 to 0.55 and 0.46 and 0.99 (Figure 45). It is important to acknowledge that the correlations between β rainfall using the local AWS weather stations in NST was showing promising results but the relatively low amount of data points for these relationships and the very poor correlations with the s values led this study to prefer the use of the RID stations.

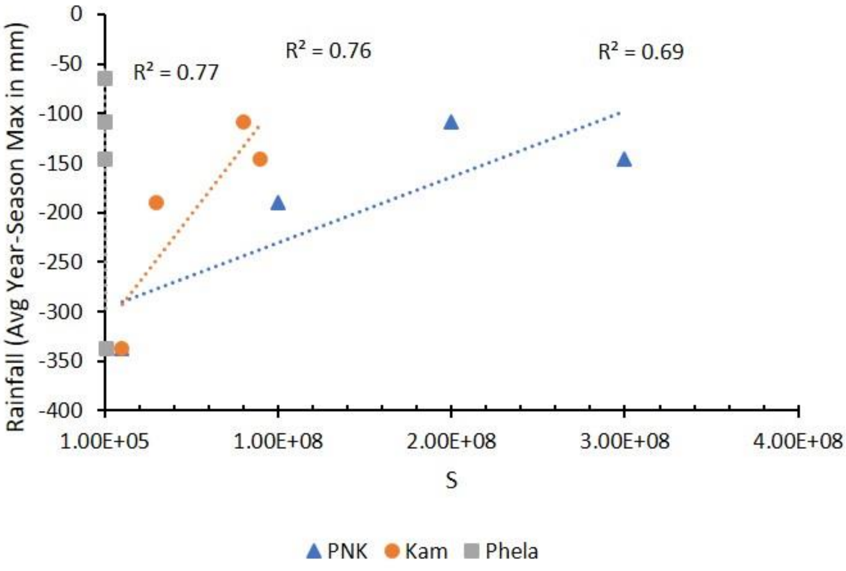

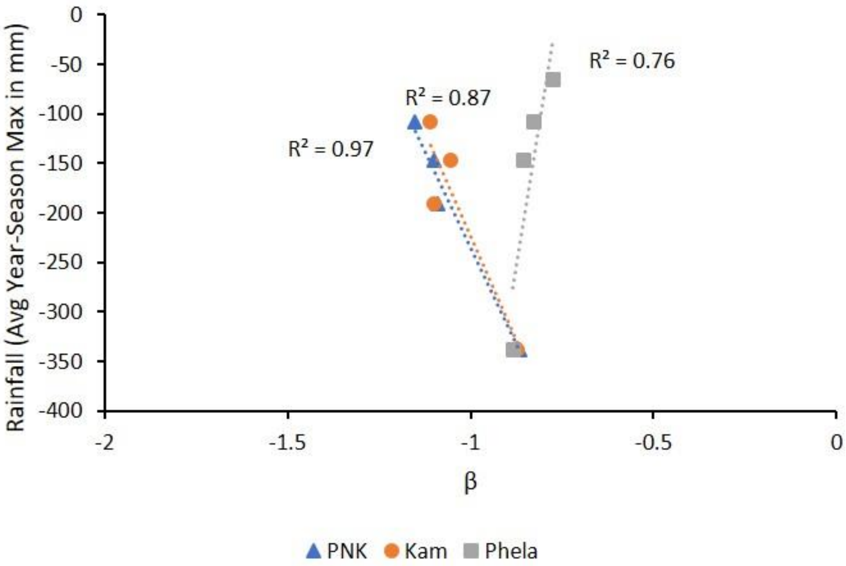

Figure 43: Correlations measured between rainfall and the parameters of the landslides β and s for the study sites in the Krabi province using rainfalls recorded by the AWS weather station in Krabi.

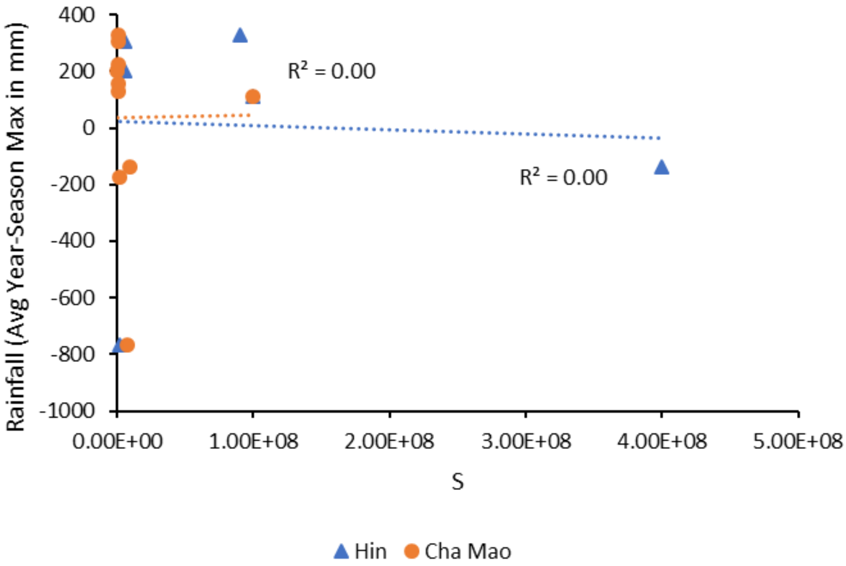

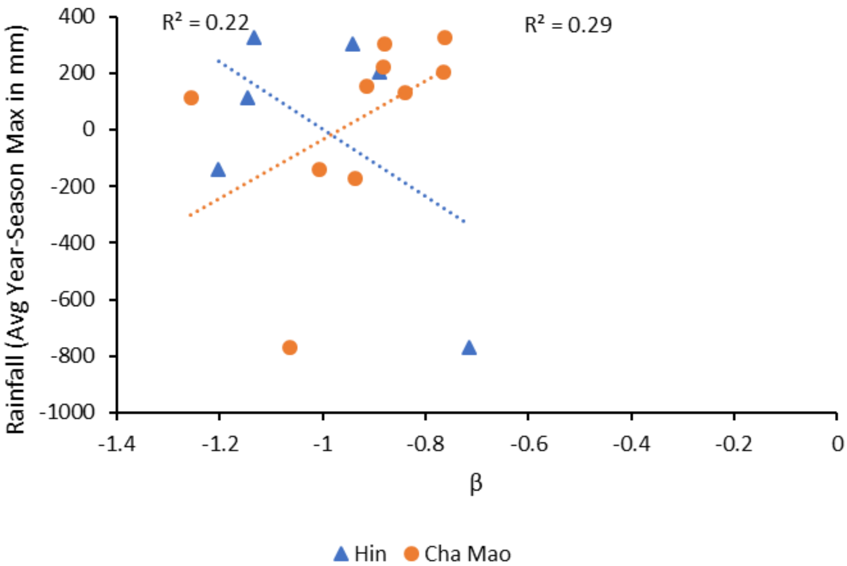

Figure 44: Correlations measured between rainfall and the parameters of the landslides β and s for the study sites in the NST province using rainfalls recorded by the RID weather station near the Hin catchment.

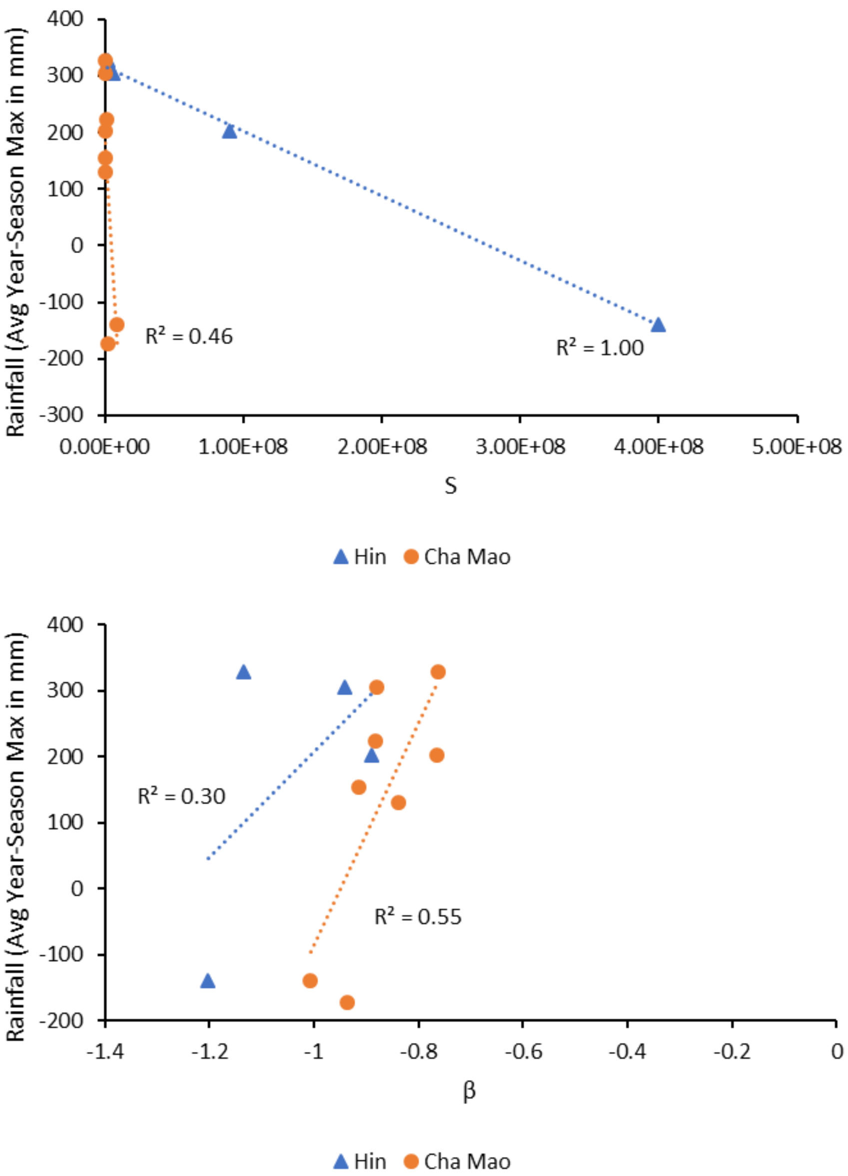

Figure 45: Revisited correlations measured between rainfall and the parameters of the landslides β and s after deleting extremes values for the study sites in the NST province using rainfalls recorded by the RID weather station near the Hin catchment.

5.4.4 Derivation of the sediment volumes made available

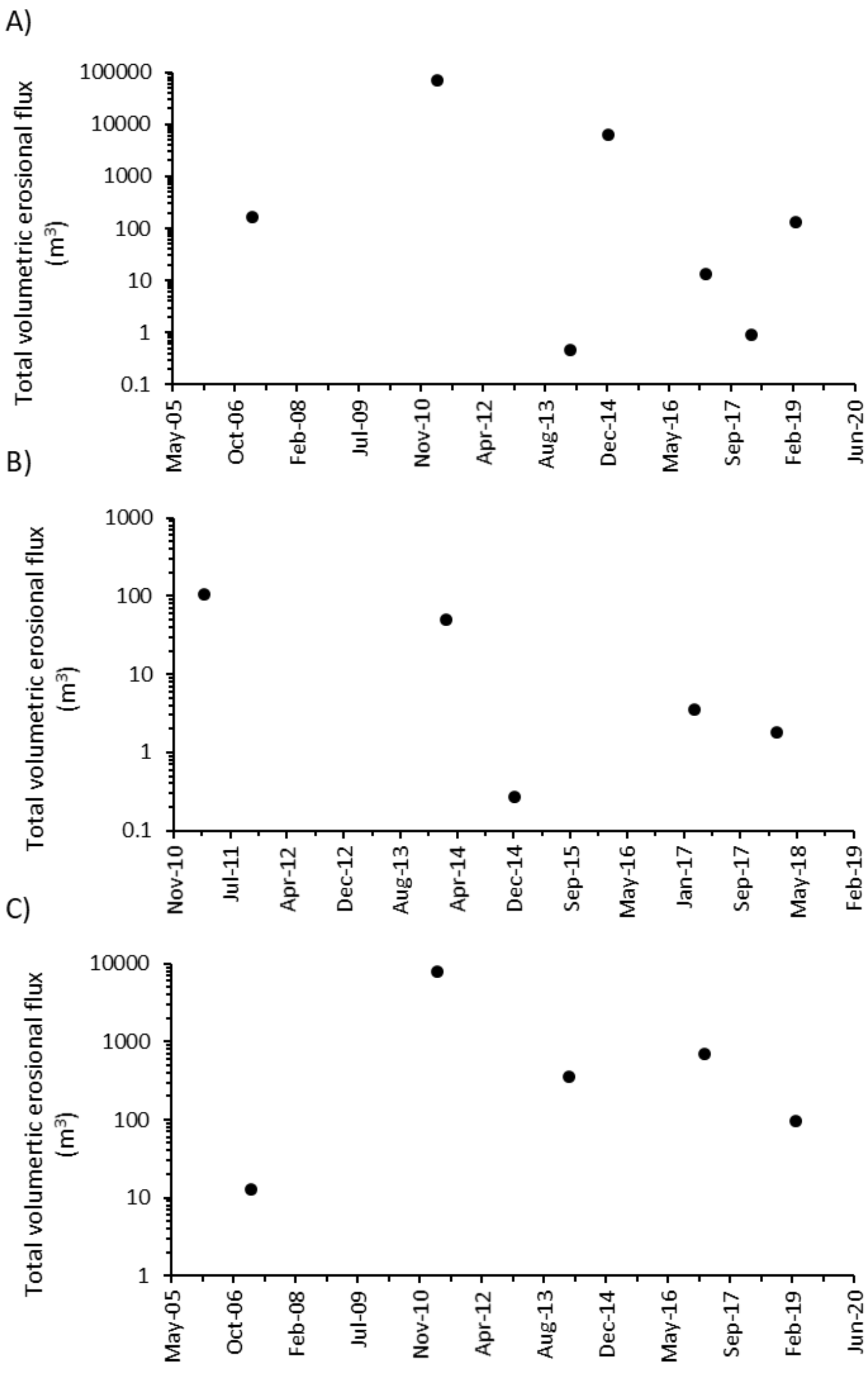

Figure 46: Krabi Province. Total volumetric erosional flux derived from the power law equations obtained for A) the Pak Nam Krabi, B) the Kam and C) the Phela river catchments over time.

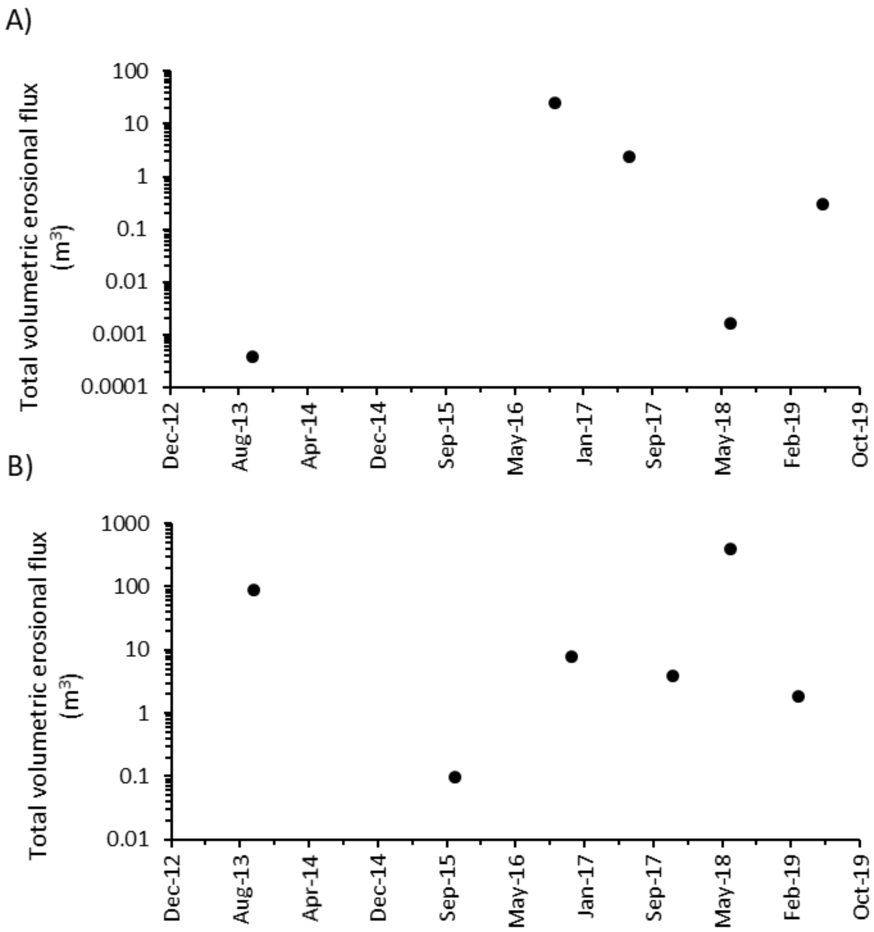

Figure 47: NST Province. Total volumetric erosional flux derived from the power law equations obtained for A) the Hin, B) the Cha Mao river catchments over time.

The calculation of the volume of sediment made available to the river catchment in the Krabi province during the survey period clearly highlights that the catastrophic landslides of 2011 in this region had made available volumes of sediment that are significantly higher than any other recent year. For example, in the PNK's catchments the volumes released in 2011 from the landslides are calculated at 68295.3m^3 which was then followed by 2015 with 6100.6m^3. In the Kam's catchment, 105.6m^3 where released in 2011 followed then by 49.8m^3 in 2014. In the Phela's catchment, 7997.5m^3 were released in 2011 and the second highest volume release was in 2017 with 706.6m^3.

In the Nakhon Si Thammarat province, the largest volumes of sediments created in the Hin catchment over the most recent period were made in 2016 with 24.4m^3, while the largest sediment volume contributions from the landslides in the Cha Mao catchment seemed to be made in 2018 with 385.9 m^3 followed then by 87.7 m^3 in 2013.

5.5 Synthesis of the sediment flux results

5.5.1 Krabi province

By crossmatching all the information collected from the vertical grain size variations, the occurrence of landslides, the inventory of extreme weathers and the analysis of the ^{210}Pb dating, the history of the sediment flux within each catchment can be retraced with an understanding of the general climate conditions at the time. It is assumed that the cores sampled in the Krabi province must have some sort of sedimentary records of the 2004 tsunami, shown either by an increase in sedimentation rate or a clear change in sediment distribution. As such, considering the intrinsic inaccuracy of the sampling methodology (1cm thick sampling increments along the sedimentary core) and the normally low rates of sedimentation (millimetric), it is believed the peaks of extreme sedimentation rates dated at approximately 2006 in the PNK mangrove (Figure 48) is the marker of the 2004 Tsunami (33.1 mm/year). Based on that assumption, it is highly probable that the peak dated at approximately 2009 is a marker of the 2011 mass landslides event (31.3 mm/year) as it is the only explanation for another sudden increase of sedimentation rate around that chronology. That assumption is supported by the cores sampled in the other mangroves. In the Kam ‘s mangrove (Figure 49), the peaks in sedimentation rate dated at 2004 (3.3 mm/year) and 2009 (5.4 mm/year) are most certainly respectively markers of the 2004 tsunami and the 2011 natural disaster. The most likely natural hazard events matching the sediment pulse dated at 1985 would be the floods, landslides and storms affecting the South in 1988/1989.

In the Phela mangrove (Figure 50 and 51), the 2004 tsunami is certainly characterised by the sudden increase of sedimentation rate dated at 2003 (2.9 mm/year) in the original core (Figure 50) while the sudden increase of sedimentation rate dated at 1991 (2.3 mm/year) is most likely an expression of the extremely intense rainfalls in the late 1980s/early 1990s (November 1988, November 1989, October 1989, October 1990 and November 1993). In the duplicate core (Figure 51) from that same mangrove, both of these peaks are in some respect part of the increased sedimentation rate observed between 1992 and 2008 (1.9 mm/year). The peak in the duplicate column dated at 2012 (2.4 mm/year) is not identified in the original core, however its chronology is most likely to be a marker of the extremely intense rainfalls and landslides of 2011. The lack of that record in the original core may be a sign of sedimentary disturbance within the records or localised sedimentary segregation. Another peak of sedimentation rate was identified in the original core in 2019 (3.8 mm/year) that is not present in the duplicate core letting this study consolidate the hypothesis that the sedimentary records from the original core might have been affected by disturbance, compaction or segregation.

Based on that chronology of events and sedimentation rates in the mangroves of the Krabi province, it is interesting to point out that only the most extreme landslide events like the one in 2011 are able to influence significantly the sedimentation rates. Records of other mass landslide events measured in the landslide survey (Section 5.4.4) do not seem to affect sedimentation rate as clearly. It was indicated early that the volumes of sediment realised during the 2011 event where significantly higher than “normal” sometimes 10 times greater than any other landslide event surveyed in those catchments. Such sudden increase in sediment release must be seen to significantly influence sedimentation rates.

Similarities are found in two of the seagrass environments, Koh Hang and Koh Jum (Figure 53 and 54), where the 2011 mass landslide is clearly marked by an increase of the sedimentation rate, respectively 3.2 and 3.8 mm/year. It reinforces the assumption that only the most extreme landslide events are able to produce significantly high sediment flux within the catchments to the mangroves and to the sea. The fact that the seagrass core in Koh Sriboya (Figure 52) is not showed any significant increase of the sedimentation rate around 2011 also suggest that the continental flux of sediment is driven in a southward direction from the Phela estuary, which appears to be in accordance with the orientation of the main channels within the network of tributaries coming from the estuary.

Interestingly, the 2011 landslide event is consistently characterised by an increase of the silt fraction across all cores. This indicates that the occurrence of mass landslides is more likely to realise large amounts of silt within the catchments or at least retained in the nearshore zone. That increase in silt as opposed to sand is more likely to be linked to characteristics of the soils and the type of landslides in the upper catchment of rivers in Southern Thailand. The landslides are generally of the debris and mudflow types, very mostly shallow and entraining the top soil (Ono et al., 2014) into very step valleys towards the lowest parts of the catchments.

The relatively very high synchronicity between the occurrence of the 2011 mass landslide event and it the record in the mangrove and seagrass sediments, bearing in mind the margin error of the ^{210}Pb dating, would indicate that the time necessary for the sediment to travel within the catchments from its upper parts to its lowest is very fast. This is certainly linked to the combined effect of the topography, being very steep in the upper part of the catchments, and the extreme rains, which rapidly increase the competency of the rivers ultimately leading to flash flooding.

When combining the ^{210}Pb sediment dating information and the cyclicity of the vertical variability of the grain size distribution described earlier in Section 5.1, it can be concluded that those cycles do not correspond to singular short-term events but are the result of much longer-term weather events. This observation is also supported by the fact that those variations do not match changes in sedimentation rates. Based on the previous findings that an increase of landslide activity leads to an increase in the silt fraction (See just above) and that landslide activity is triggered by increasing rainfalls (Fowze et al., 2012; Section 5.4.3), it is assumed that the periods of time when the silt portion increases are markers of periods of time with increased rainfall, triggering more sediment release and transport down the river catchments. The El Nino Southern Oscillations (ENSO) have been reported as influencing the climate of Thailand (Singharattna et al., 2005; Gale and Saunders, 2013; Kirtphaiboon et al., 2014). These studies have concluded that there is an increase in rainfall during La Niña periods. Based on the ^{210}Pb dating and the ENSO cycles chart, the periods of time when the silt fraction increase in the sediment column seem to be coincidental or just at the very end of periods of time when La Niña events are predominant, suggesting that it is very likely that sediment supply in those catchments is influenced by ENSO cycles (https://origin.cpc.ncep.noaa.gov/products/analysis_monitoring/ensostuff/ONI_v5.php).

Fluctuations in the sorting coefficient do not match the cycles of the fluctuations of the grain size distribution suggesting very little influence of the ENSO cycles on the sorting coefficient. Specific weather events could potentially be the origin of these decreases in sorting by potentially allowing sediment from a different source to influence grain size distribution. By using the ^{210}Pb dating information again, the analysis of the synchronicity of these decreases in sorting and the occurrence of natural disasters since the 1980s show a linkage between decreases in the sorting during the 2011 landslide events and the 2004 tsunami in the Pak Nam Krabi (Figure 48) and the Kam (Figure 49) catchments. Tropical storm Pabuk is likely to be the cause of the decrease in sorting observed in 2019 within all the Krabi mangroves. Attributing weather events to sedimentation is very difficult and should be approached with caution but the strong linkages to extreme weather events or periods of events show an interesting linkage although this becomes problematic prior to the 1980s due to the lower resolution and reliability of the climatic, remote sensing and geochronological data.

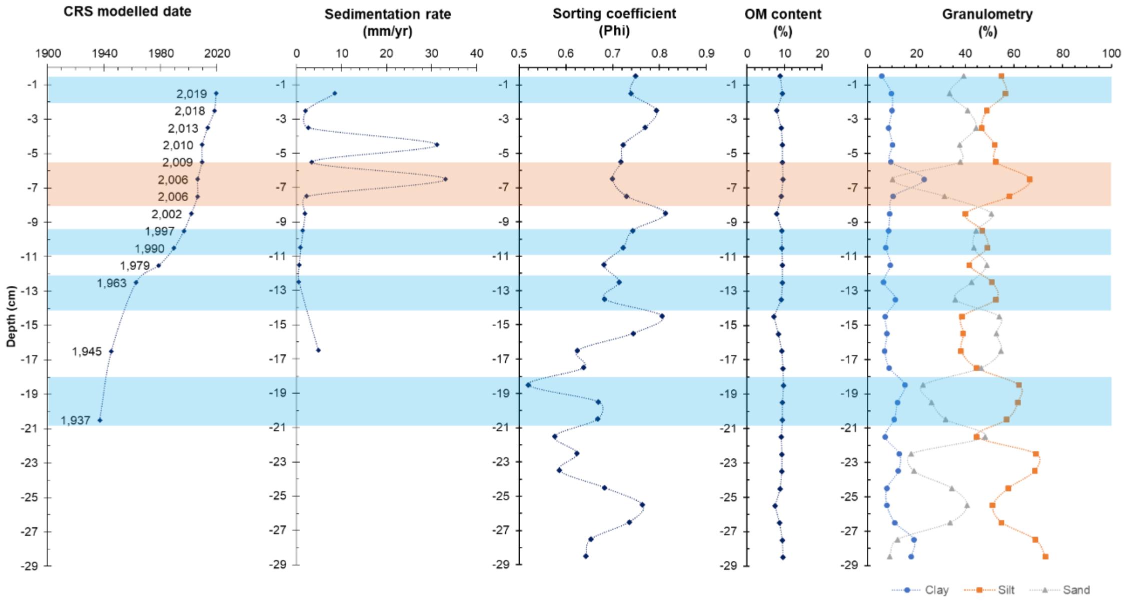

Figure 48: Cross-matching of all the measured information extracted from the duplicate core sampled in the PNK mangrove. The red shaded area corresponds the layer of sediment identified as a marker of the 2004 tsunami. The blue shaded area corresponds to a clear shift between the portion of silt/clay and sand identified as markers of La Niña periods.

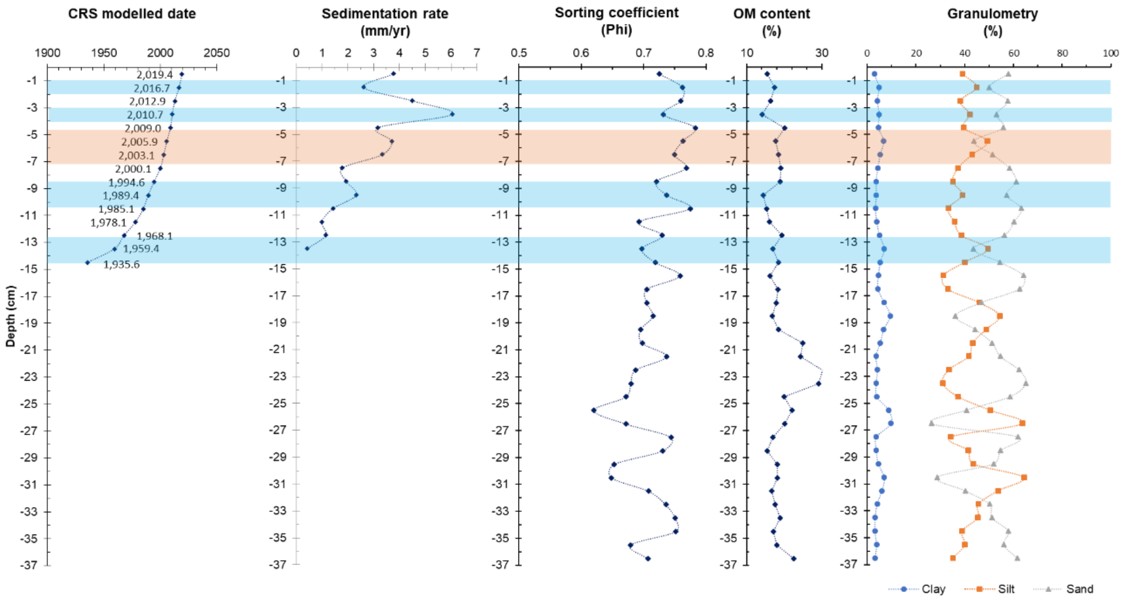

Figure 49: Cross-matching of all the measured information extracted from the duplicate core sampled in the Kam mangrove. The red shaded area corresponds the layer of sediment identified as a marker of the 2004 tsunami. The blue shaded area corresponds to a clear shift between the portion of silt/clay and sand identified as markers of La Niña periods.

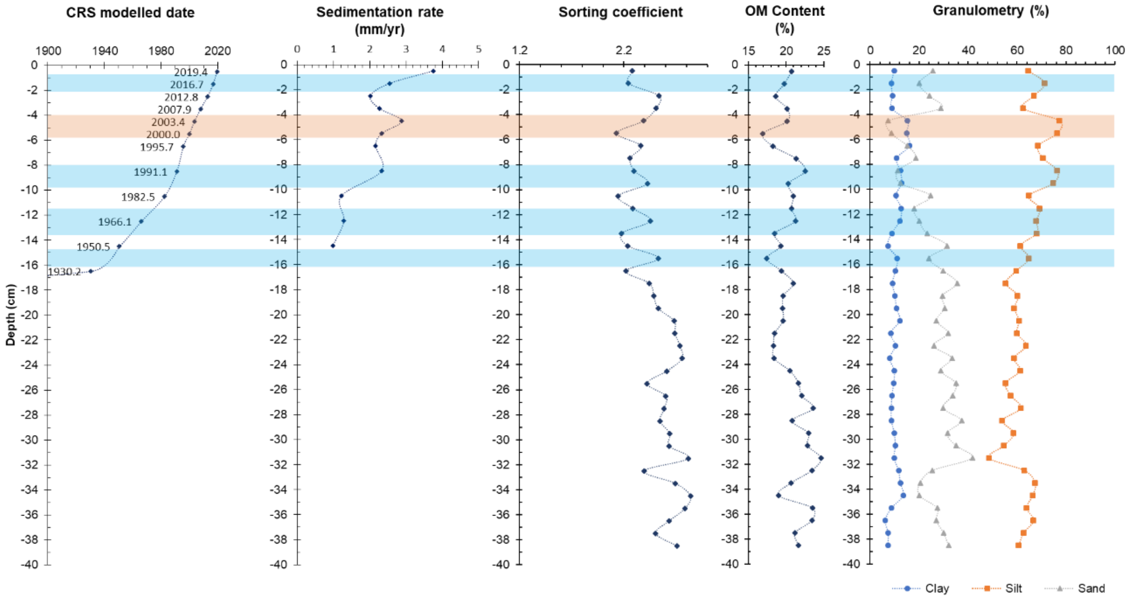

Figure 50: Cross-matching of all the measured information extracted from the original core sampled in the Phela mangrove. The red shaded area corresponds the layer of sediment identified as a marker of the 2004 tsunami. The blue shaded area corresponds to a clear shift between the portion of silt/clay and sand identified as markers of La Niña periods.

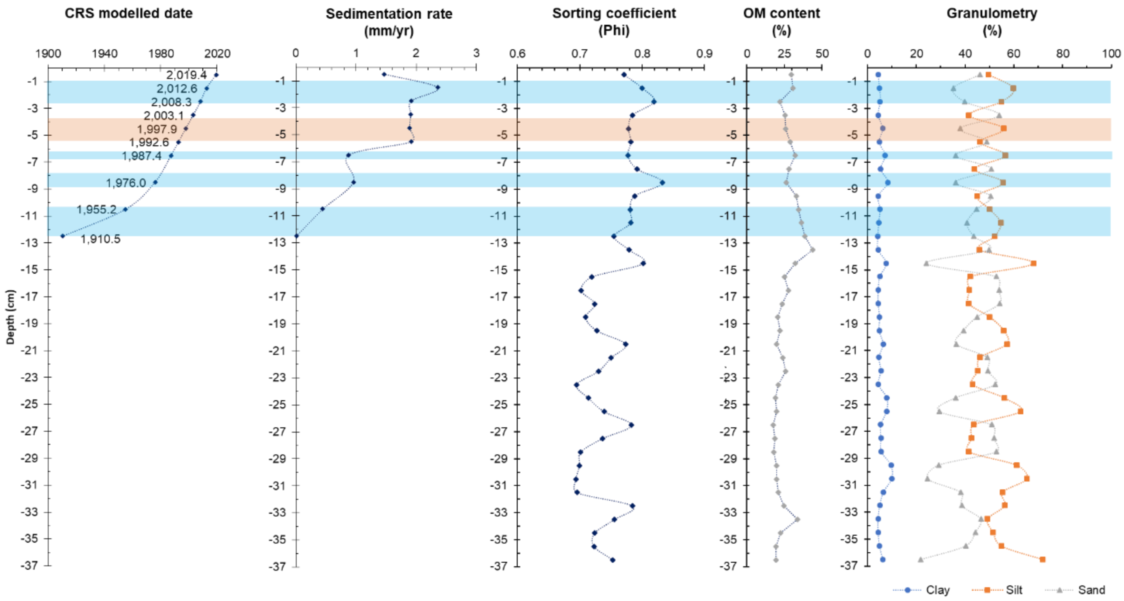

Figure 51: Cross-matching of all the measured information extracted from the duplicate core sampled in the Phela mangrove. The red shaded area corresponds the layer of sediment identified as a marker of the 2004 tsunami. The blue shaded area corresponds to a clear shift between the portion of silt/clay and sand identified as markers of La Niña periods.

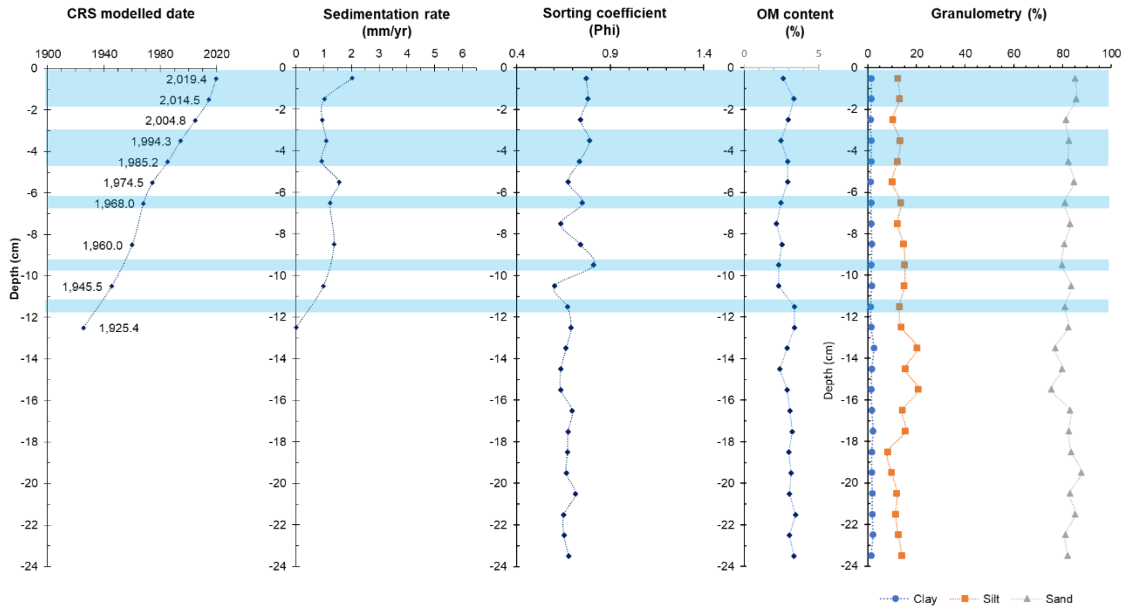

Figure 52: Cross-matching of all the measured information extracted from the original core sampled in the Koh Sriboya seagrass. The blue shaded area corresponds to a clear shift between the portion of silt/clay and sand identified as markers of La Niña periods.

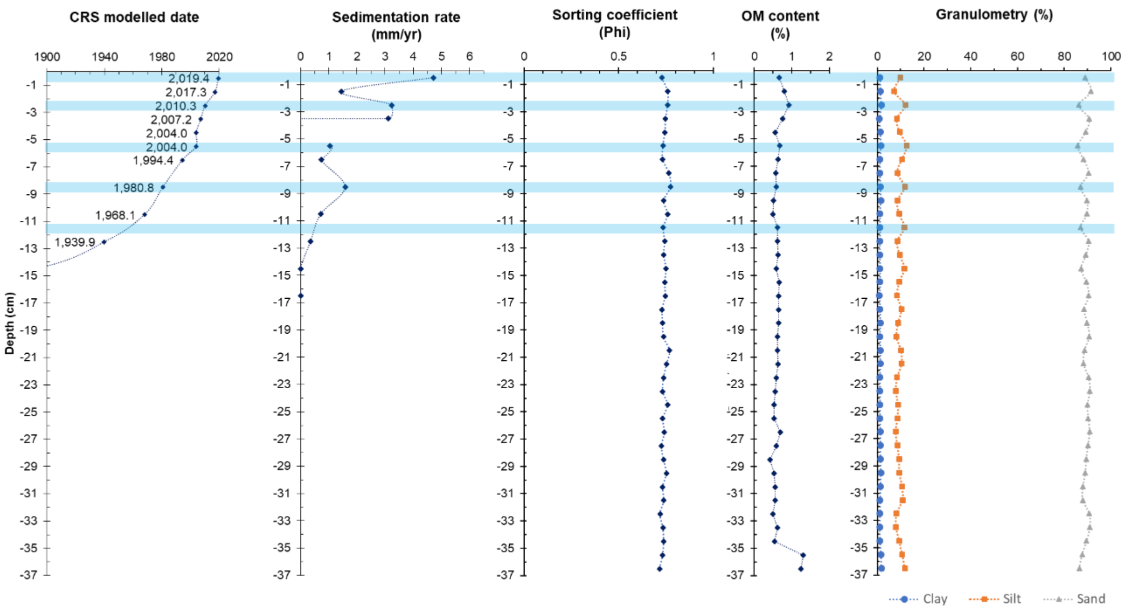

Figure 53: Cross-matching of all the measured information extracted from the original core sampled in the Koh Hang seagrass. The blue shaded area corresponds to a clear shift between the portion of silt/clay and sand identified as markers of La Niña periods.

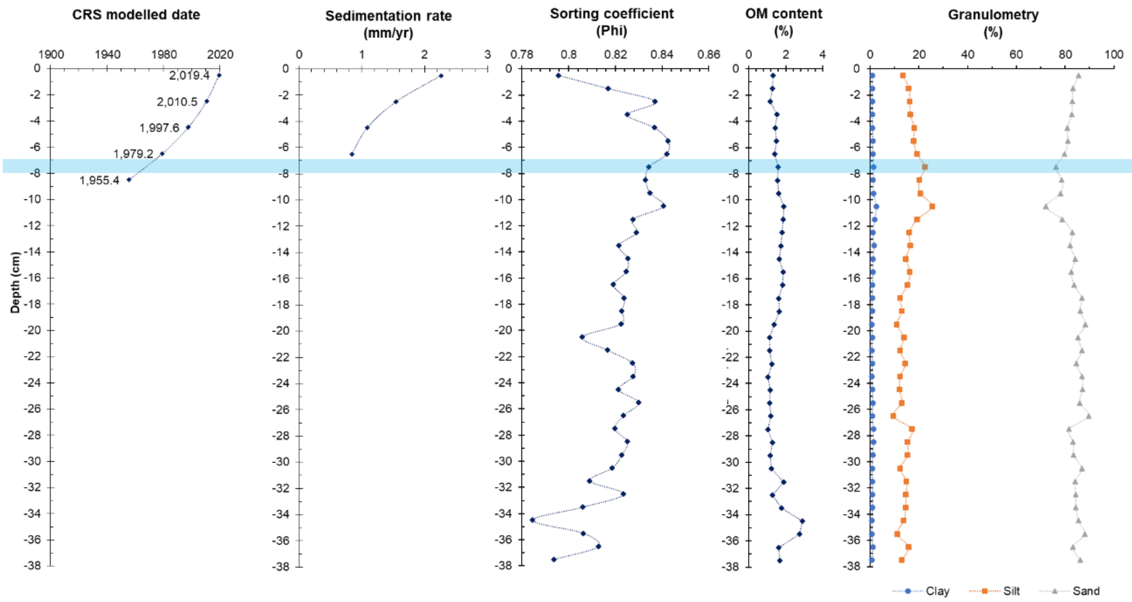

Figure 54: Cross-matching of all the measured information extracted from the duplicate core sampled in the Koh Jum seagrass. The blue shaded area corresponds to a clear shift between the portion of silt/clay and sand identified as markers of La Niña periods.

5.5.2 Nakhon Si Thammarat

Within Nakhon Si Thammarat similar cycles are noted as for the Krabi mangrove cores alternating between the fine fractions, clay and silt dominance and coarser fraction, sand (Figure 55, 56, 57, 58 and 59). The ^{210}Pb dating revealed lower sedimentation rates than in the Krabi mangroves. For example, cycles observed in the core sampled in the Thung Sai mangrove show sedimentation rates of 1.1 mm/year and the cycles of the changes in grain size distribution are much longer. The most recent shift representing a peak of the silt fraction dated between 2007 and 2019 on that specific core and the one just before that was dated to the early 1960s (Figure 55). Considering the similarities in geology and topography between the Krabi province and the NST province, it seems appropriate to assume that the periods of time showing an increase of the silt fraction and decrease of sand corresponds to wetter conditions too. These periods correspond to periods of time when La Niña is predominant for a few consecutive years during which it reached a strong index. However, a reciprocity cannot be applied. In fact, between the 1960s and 2012/2013, other pluri-annual La Niña events with a strong index occurred, with no shift in sediment distribution observed in the core. It is very likely that it is only a very local effect of the core location as when looking at vertical variations in grain size distribution on the other core sampled (original core, Figure 19) on that same site, cycles are much shorter considering the depth of the shifts along the core. This would suggest a lag in the sediment record of the duplicate core.

Similar observations can be made between the original and its duplicate in the Han's mangrove, where the duplicate core displays much longer cycles than the original core based on the ^{210}Pb dating (Figure 56 & 57). The ^{210}Pb dating information from the original core had allowed the identification of four peaks of sedimentation rates, in approximately 1995, 2001 (peaks observed in the duplicate core), 2015 and 2019. Bearing in mind the margin error associated to ^{210}Pb dating, these peaks in sedimentation rates can respectively be related to: (1) the tropical depression of 1993 and tropical depression Linda in 1997, (2) heavy rainfall in 2001, (3) the landslide inventories presented in Section 5.4.4 allowed this study to identify an increase in landslide activity in 2015/2016 and (4) three large tropical storms occurred in 2018 (Son-Tink, Toraji and Pabuk). Here again, the decreases in sorting do not match increases in sedimentation rates suggesting that another driving force is at the origin of those sudden decreases in sorting.

Finally, both cores in the Cha Mao mangrove (Figure 58 and 59) describe cycles showing alternations between the portions of the finer grain size, clay and silt, and the portions of the coarser fraction, sand. Based on the ^{210}Pb dating on the original core, the cycles corresponding to an increase in the fraction of silts match periods of time when La Niña is predominant. The same observation is not as clear on the results from the duplicate core the rates of sedimentation are very low here again with an average of 1.1 mm/year against 2.8 mm/year for the original core.

Fluctuations in sedimentation rates in the original core revealed three peaks, one dated approximately to 1997, another at 2006 and a third one dated at approximately 2015 (Section 5.3). Based on information collected from the landslide inventories (Section 5.4), natural disasters and extreme weather event inventories (Figure 15), it can be assumed that these increases are related to the occurrence of (1) the tropical storm Linda in 1997, (2) the year 2006 was marked by a series of heavy rain events and storminess as well as typhoons in Thailand (typhoon Xangsane being the most devastating), and finally (3) this landslide inventories showed noticeable landslide activity around 2014 to 2016 in Nakhon Si Thammarat that is likely to be a contributing factor in the increase in sedimentation rates around that time. It is important to bear in mind that since 1996 the bay of Pak Phanang has been the subject of stronger conservation policies and mangrove restoration plans that may have had an impact on sedimentation rates observed in this area. The duplicate core clearly displays an increase in the sedimentation rate dated at around 1998 (Section 5.3). It is assumed to correspond to the increase of sedimentation rate noticed on the original core which was dated to 1997 and associated to the impact of the tropical storm Linda (1997).

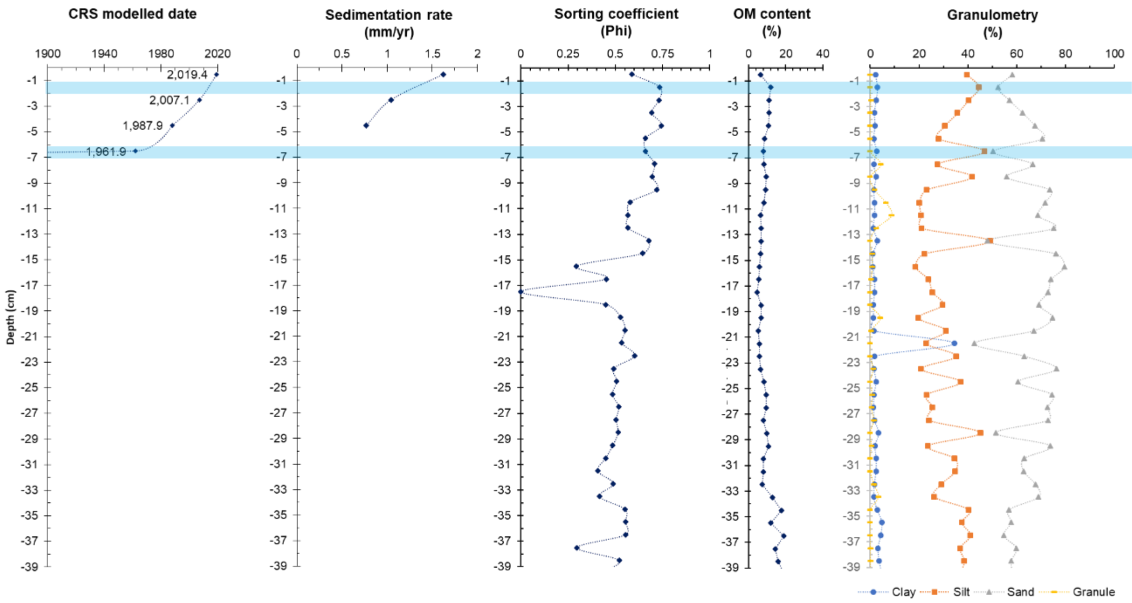

Figure 55: Cross-matching of all the measured information extracted from the duplicate core sampled in the Thung Sai mangrove. The blue shaded area corresponds to a clear shift between the portion of silt/clay and sand identified as markers of La Niña periods.

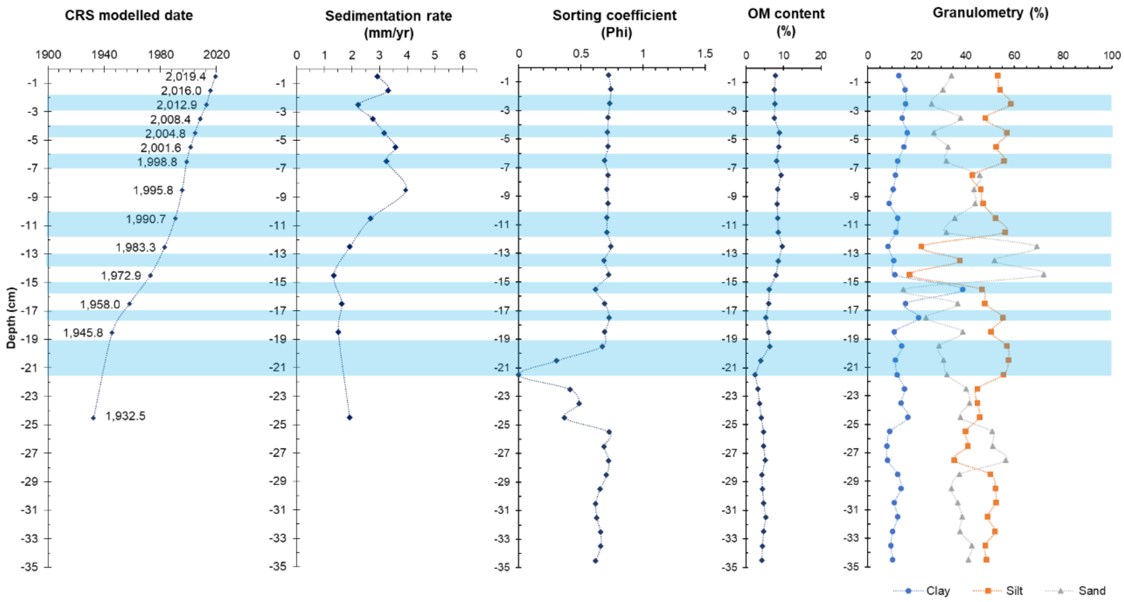

Figure 56: Cross-matching of all the measured information extracted from the original core sampled in the Han mangrove. The blue shaded area corresponds to a clear shift between the portion of silt/clay and sand identified as markers of La Niña periods.

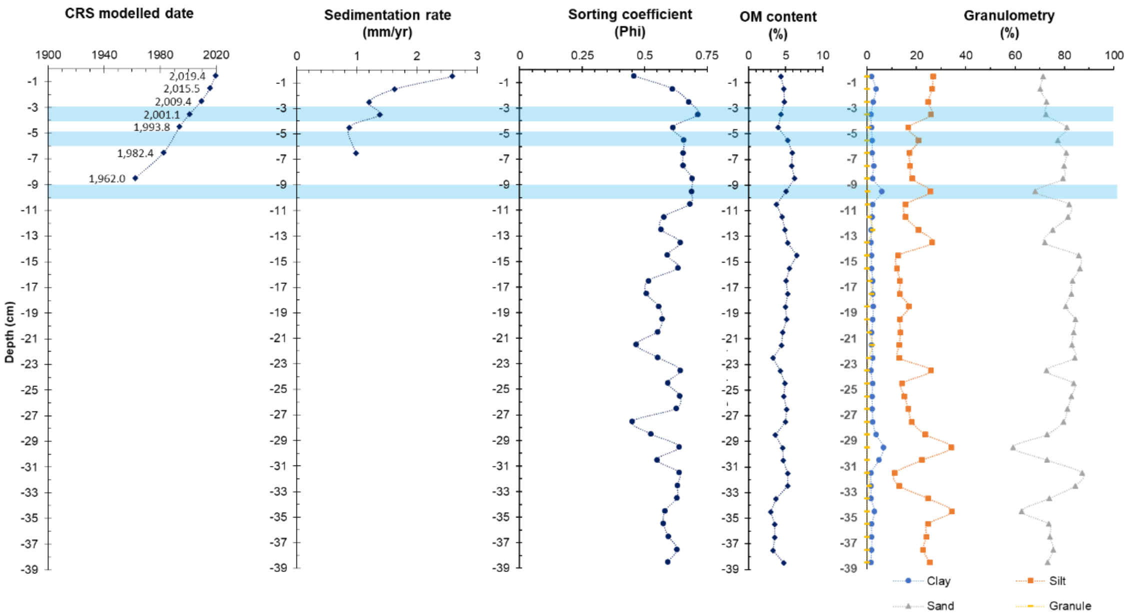

Figure 57: Cross-matching of all the measured information extracted from the duplicate core sampled in the Han mangrove. The blue shaded area corresponds to a clear shift between the portion of silt/clay and sand identified as markers of La Niña periods.

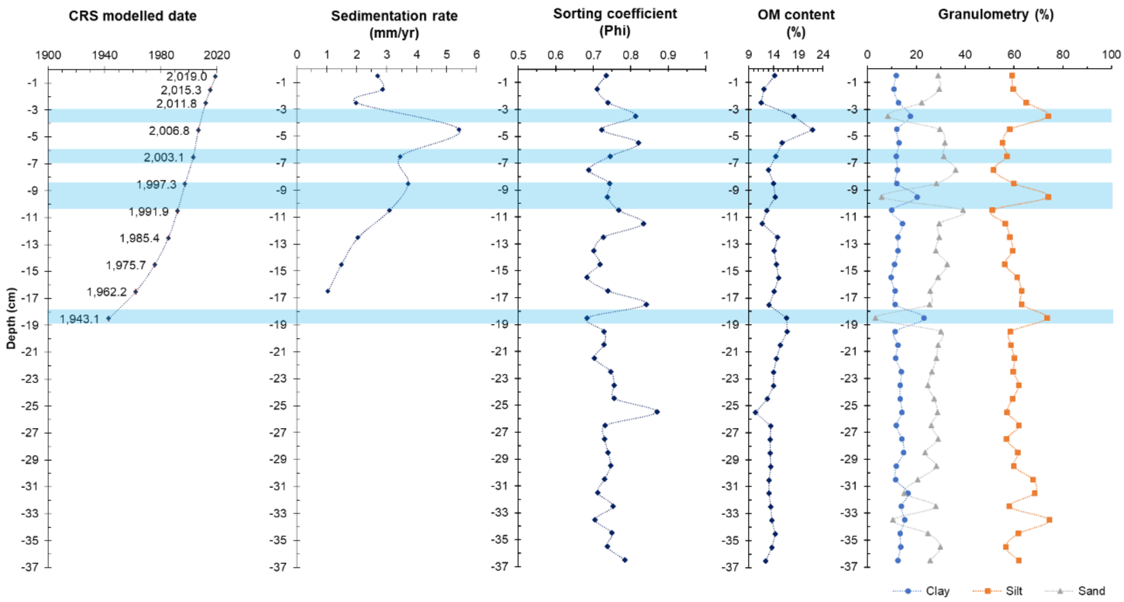

Figure 58: Cross-matching of all the measured information extracted from the original core sampled in the Cha Mao mangrove. The blue shaded area corresponds to a clear shift between the portion of silt/clay and sand identified as markers of La Niña periods.

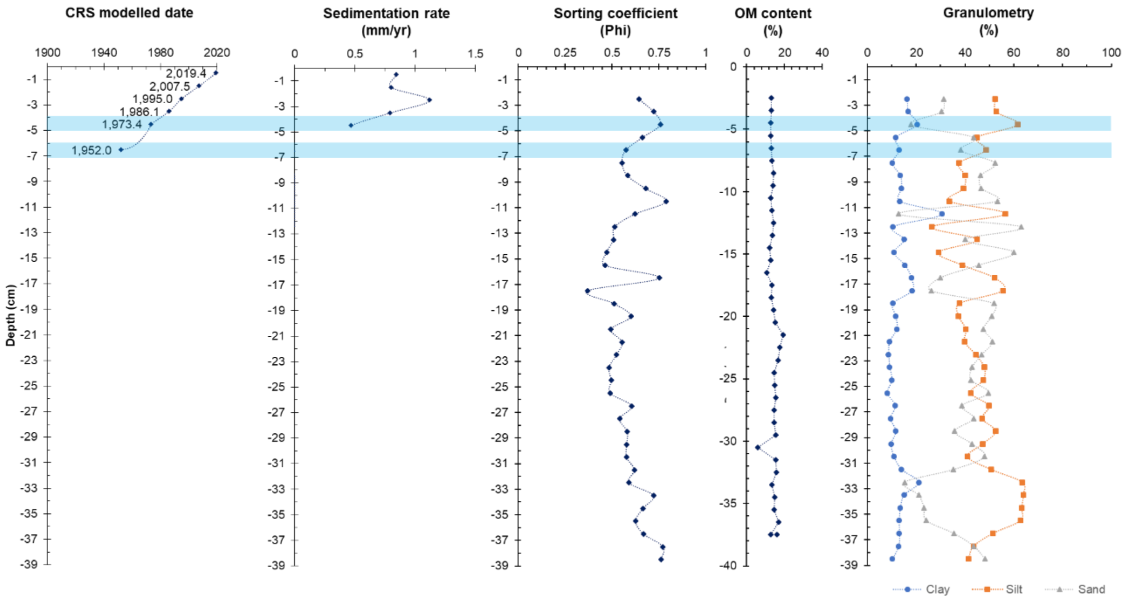

Figure 59: Cross-matching of all the measured information extracted from the duplicate core sampled in the Cha Mao mangrove. The blue shaded area corresponds to a clear shift between the portion of silt/clay and sand identified as markers of La Niña periods.

6 Final conclusion and policy making.

- Mangrove environments in Southern Thailand are much more susceptible to erode suddenly and on a greater spatial scale than sandy beaches in both provinces. Conservation efforts made by the Thai government and local authorities since the 1990s have greatly helped in restoring part of those lost environments but their coverage is still far away from what they used to be, hence those efforts are still very important to pursue, especially with their huge potential of carbon storage.
- The reactivation of old geomorphologic features (old lagoons or channels) or anthropic features (shrimp ponds) have a dramatic effect on the shoreline position at the origin of sudden rapid erosion rates. The development of more sustainable, robust and durable shrimp farm walls would certainly help in mitigating some of those dramatic shoreline retreats.
- Mangrove environments recover a lot slower than sandy beaches when they have a chance to. Hence, promoting restoration in those environments after damage is important.
- The Southern part of NST (from Tha Sala to the Songkhla province border in the South) is the most erosional sandy coastline across all areas surveyed. Despite large efforts in the development of coastal defences and shoreline realignment along this coastline, the shoreline is still suffering from erosion. More attention on shoreline realignment is required along that coast.
- When comparing the coastlines of the NST province and the Krabi province, the coastline along the NST province is extremely reactive to the occurrence of storminess and extreme weather events resulting in large erosion movements whereas the coastline along the Krabi province presents significantly lower erosional movements, most probably due to the combined geomorphology of the coastline and the efficiency of the seafloor dissipating wave energy as they approach the Krabi coast.
- The calculation of the landslides' volume per year permitted to identify that the volumes of sediment released during the catastrophic event of 2011 were by an order of magnitude of 10 times greater than any other surveyed year. Generally speaking, sedimentation rates in the mangroves are very slow (<1cm/year). Based on that information and the general observation of coastal erosion along both provinces, this suggests that the average amount of sediment transported from the mountains to the coast is not sufficient to counter-balance sediment transport along the coastlines.
- The results from the landslide inventory in the Krabi province suggest a strong relationship between the size of the landslides or their frequency and the intensity of the rainfalls. However, these results are not as strong in NST despite showing similar trends. Further data to build a more exhaustive landslide inventory over time is necessary to confirm and consolidate those results. Within the context of climate change and the increase of rainfall more landslides are expected in Southern Thailand and potentially events like the 2011 natural disaster are to be expected on a shorter return period, which was originally estimated at approximately 20 to 30 years by Gale and Saunders (2013). The Thai government has invested a lot of time and money in developing mitigating solutions to landslide and flooding occurrence. However, those pressures are set to increase as a result of climate change.
- Cores in the mangrove environments reveal valuable information on the climate cycles driving sedimentation in the Southern parts of Thailand|:
    - Sediment grain size for each core seems to be largely influenced by ENSO cycles.

- Sedimentation rates, however, do not seem to be influenced by ENSO cycles but by much more spontaneous and large scale events such as the 2004 tsunami and the 2011 catastrophic landslide events in the Krabi province and the occurrence of very heavy rain, flood and typhoon periods in the NST province. Extreme heavy rainfall and typhoons are expected to be exacerbated in the context of climate change. This increase will allow river catchments to carry more sediment from the continent to the coast but the effects of these events will be devastating to local communities and their welfare (flooding, mass movements etc.). It is also well established that a rapid increase in sedimentation may be detrimental to mangroves sustainability and development. Continual monitoring of those environments and the impact of increased sedimentation is becoming a necessity.

7 References

Appleby, P.G. & Oldfield, F. (1978). The calculation of 210Pb dates assuming a constant rate of supply of unsupported 210Pb to the sediment. Catena, 5, p1-8.

Aungsakul, K., Jaroensutasinee, M., Jaroensutasinee, K. (2007). Numerical Study of Principal Tidal constituents in the Gulf of Thailand and the Andaman Sea. Walailak Journal of Science and Technology, 4(1), p95-109.

Barlow, J., Lim, M., Rosser, N., Petley, D., Brain, M., Norman, E., Geer, M. (2012). Modelling cliff erosion using negative power law scaling of rockfalls. Geomorphology, Volumes 139–140, 2012, p416-424.

Boromthanarat, S., Cobb, S., Lee, V. (1991). Coastal Management in Pak Phanang: A Historical Perspective of the Resources and Issues. Hat Yai, Thailand: Coastal Resources Institute, Prince of Songkla University.

Brown, B. (2007). Coral reefs of the Andaman Sea: An integrated perspective. In: Gibson, RN, Atkinson, RJA and Gordon, JDM (eds.) Oceanography and Marine Biology: An Annual Review. Taylor & Francis. 45, p173-197.

Brunetti, M.T., Guzzetti, F., Rossi, M., 2009. Probability distributions of landslide volumes.

Nonlinear Processes in Geophysics 16, p179–188.

Buranpratheprat, A. and Bunpapong, M. (1998). Two-Dimensional Hydrodynamic model for the Gulf of Thailand. Proceeding of the IOC/WESTPAC Fourth International Scientific Symposium, Okinawa Japan, p469–478.

Choowong, M., Phantuwongraj, S., Charoentitirat T. (2008) Beach recovery after 2004 Indian Ocean tsunami from Phang-nga, Thailand. Geomorphology 104, p134–142.

Esmail, M., Mahmod, W.E., and Fath, H. (2019). Assessment and prediction of shoreline change using multi-temporal satellite images and statistics: Case study of Damietta coast. Egypt Appl. Ocean Res., 82, p274-282.

Fan, L., Lehmann, P., and Or, D. (2016). Effects of soil spatial variability at the hillslope and catchment scales on characteristics of rainfall-induced landslides. Water Resour. Res., 52, p1781–1799.

Flos, S.J. (1993). Estimations of freshwater flow through the Pak Phanang River. M.Sc. Thesis, University of Humberside, England, 63p.

Fowze, J.S.M., Bergado, D.T., Soralump, S., Voottipreux, P., Dechasakulsom, M. (2012). Rain-triggered landslide hazards and mitigation measures in Thailand: From research to practice, Geotextiles and Geomembranes, 30, p50-64.

Gale, E.L. and Saunders, M.A. (2013). The 2011 Thailand flood: climate causes and return periods. Weather, 68, p233-237.

Ganin, S. (1991). Study of tide characteristics on coastline of the Gulf of Thailand and Andaman Sea in the south region of Thailand. MA Thesis, Kasetsart University, Bangkok.

Gariano, S. L., Fausto Guzzetti, F. (2016). Landslides in a changing climate, Earth-Science Reviews, 162, p227-252.

Grismer, L., Grismer, J., Perry, W. Jr, Ngo, V.T., Thy, N., Onn, C. (2011). Herpetology on the fringes of the sunda shelf: A discussion of discovery, taxonomy, and biogeography. Bonner Zoologische Monographien, 57, p57-97.

Hakkou, M., Maanan, M., Belrhaba, T., El Khalidi, K., El Ouai, D., Benmohammadi, A. (2018). Multi-decadal assessment of shoreline changes using geospatial tools and automatic computation in Kenitra coast, Morocco. Ocean and Coastal Management, 163, p232–239.

Hegde, A.V., Akshaya B.J., 2015. Shoreline transformation study of Karnataka Coast: Geospatial Approach. Aquatic Procedia 4, p151-156.

Himmelstoss, E.A., Henderson, R.E., Kratzmann, M.G., and Farris, A.S. (2018). Digital

Shoreline Analysis System (DSAS) version 5.0 user guide: U.S. Geological Survey Open-File Report 2018–1179, 110 p.

IFRC, 2011. International Federation of Red Cross and Red Crescent Societies annual report 2011, 28p.

Iida, T. (2004). Theoretical research on the relationship between return period of rainfall and shallow landslides. Hydrological Processes, 18, p739-756.

Iyaruk, A., Phien-wej, N., and Giao, P.H. (2019). Landslides and debris flows at Khao Phanom Benja, Krabi, Southern Thailand. International Journal of GEOMATE, 16(53), p127-134.

Kiran, S.R. (2017). General Circulation & Principal Wave Modes in Andaman Sea from Observations.

Kirtphaiboon, S., Wongwises, P., Limsakul, A., Sooktawee, S., Humphries, U.W. (2014). Rainfall Variability over Thailand Related to the El Nino-Southern Oscillation (ENSO). Journal of Sustainable Energy & Environment, 5, p34-42.

Komori, D., Rangsiwanichpong, P., Inoue, N., Ono, K., Watanabe, S., Kazama, S. (2018). Distributed probability of slope failure in Thailand under climate change. Climate Risk Management, 20, p126-137.

Kompor, W., Ekkawatpanit, C., Kositgittiwong, D. (2018). Assessment of ocean wave energy resource potential in Thailand. Ocean and Coastal Management, 160, p64–74.

Larsen, I., Montgomery, D. & Korup, O. (2010). Landslide erosion controlled by hillslope material. Nature Geoscience, 3, p247–251.

Lima, M.A.C., Ward, R.D. & Joyce, C.B. (2020). Environmental drivers of sediment carbon storage in temperate seagrass meadows. Hydrobiologia, 847, p1773–1792.

Lo, K.F.A., Yeh, H.C.,Chen, S.H. (2015). Landslide detection using satellite remote sensing imagery. International Journal of Development Research, 5 (4), p4237-4241.

Morley, C., Charusiri, P., and Watkinson, I.M. (2011). Structural geology of Thailand during the Cenozoic. The Geology of Thailand, p273-334.

Natesan, U., Parthasarathy,A., Vishnunath, R., Jeba Kumar, G. E., Ferrer,V. A. (2015). Monitoring Longterm Shoreline Changes along Tamil Nadu, India Using Geospatial Techniques, Aquatic Procedia, 4, p325-332.

Nazaruddin, D. A., and Duerrast, H. (2018). Spatial Distribution of Shallow and Intermediate Earthquakes in Southern Thailand after the 26 December 2004 Sumatra – Andaman Earthquake. The 8th International Conference on Applied Geophysics (GeophysicsSongkhla2018) at Songkhla, Thailand, 9p.

Neelasri, C., Punpuk, V., and Radok, R. (1988). An investigation of mean sea level change in the upper Gulf of Thailand. Proceedings of International Symposium on Sea Level Rise, Bangkok, Thailand.

Niemnil, S. (2008). Sea level trend in Gulf of Thailand using tide gauge data. Proceedings of 46th Kasetsart University Annual Conference: Architecture and Engineering Natural resources and Environment, Bangkok, Thailand, p420-426.

Odin, M., Stumpf, A., Malet, J., Gosset, M., Uchida, T., & Chiang, S.H. (2018). Initial insights from a global database of rainfall-induced landslide inventories: The weak influence of slope and strong influence of total storm rainfall. Earth Surface Dynamics, 6(4), p903-922.

Ono, K., Kazama, S. & Ekkawatpanit, C. (2014). Assessment of rainfall-induced shallow landslides in Phetchabun and Krabi provinces, Thailand. Natural Hazards, 74, p2089–2107.

Özpolat, E., and Demir, T. (2019). The spatiotemporal shoreline dynamics of a delta under natural and anthropogenic conditions from 1950 to 2018: A dramatic case from the Eastern Mediterranean. Ocean and Coastal Management, 180, 104910, 17p.

Panapitukkul, N., Duarte, C.M., Thampanya, U., Kheowvongsri, P., Srichai, N., Geertz-Hansen, O., Terrados, J., Boromthanarat, S. (1998). Mangrove colonization: mangrove progression over the growing Pak Phanang (SE Thailand) mud flat. Estuarine, Coastal and Shelf Science, 47, p51-61.

Paw, J.N., Bunpapong, S., White, A.T., Sadorra, M.S.M. (1988). The coastal environmental profile of Ban Don Bay and Phangnga Bay, Thailand. ICLARM Tech. Rep., 20, 78p.

Poisuporn, P., Intongdong, S., Niamnil, S. (2003). Eye on the Ocean Unit 1: Physics in the Ocean. Bangkok: National Research Council of Thailand, p119-120.

Punpuk, V. (1992). Mean sea level rise. Proceedings of the Meeting on Application of Tidal Data on the Marine Environmental Assessment, Nontaburi, Thailand, p28-36.

Rangsiwanichpong, P., Kazama, S., Komori, D. (2017). Relationship between the probability of landslide and sediment yield in Thailand. Conference: XVI World Water Congress at Cancún, Mexico.

Ridd M.F., Barber A.J., Crow, M.J. (2011). The Geology of Thailand. London (UK): The Geological Society of London.

Ridd, M.F. (2016). Should Sibumasu be renamed Sibuma? The case for a discrete Gondwana-derived block embracing western Myanmar, upper Peninsula Thailand and NE Sumatra. Journal of the Geological Society, 173 (2):249.

Rizal, S., Damm, P., Wahid, M. A., Sundermann, J., Ilhamsyah, Y., Taufiq Iskandar, T. and Muhammad (2012). General circulation in the Malacca Strait and Andaman Sea: A numerical model study. American Journal of Environmental Science, 8 (5), p479-488.

Robbins, J.A. (1978). Geochemical and geophysical applications of radioactive lead. In: J.O. Nriagu (ed.), Biogeochemistry of Lead in the Environment. Elsevier Scientific, Amsterdam, p285-393.

Robinson, M. K. (1974). The physical oceanography of the Gulf of Thailand, Naga Expedition. In NAGA Report Volume 3: Scientific Results of Marine Investigations of the South China Sea and the Gulf of Thailand 1959–1961. The University of California, Scripps Institution of Oceanography, La Jolla, California. p5–116.

Salghuna, N.N., and Aravind Bharathvaj, S. (2015). Shoreline Change Analysis for Northern Part of the Coromandel Coast. Aquatic Procedia, 4, p317-324.

Schulte, E. E. (1995). Recommended soil organic matter tests. In Sims, J. T. and Wolf, A. M. (eds.) Recommended Soil Testing Procedures for the North Eastern USA. Northeastern Regional Publication No. 493. Agricultural Experiment Station Univ. of Delaware, Newark. p52–60.

Scheffers, A., Brill, D., Kelletat, D., Brückner, H., Scheffers, S., Fox, K. (2012). Holocene sea levels along the Andaman Sea coast of Thailand Holocene, 22 (10), p1169-1180.

Singhrattna, N., Rajagopalan, B., Kumar, K. K., & Clark, M. (2005). Interannual and Interdecadal Variability of Thailand Summer Monsoon Season, Journal of Climate, 18(11), p1697-1708.

Sinsakul, S. (1992). Evidence of Quaternary sea level changes in the coastal areas of Thailand: a review. Journal of Southeast Asian Earth Sciences, 7(1), p 23-37.

Siripong, A. (1984a). The characteristics of the tides in the Andaman Sea of Thailand. Marine Science Department, Chulalongkorn University.

Siripong, A. (1984b). Surface circulation in the Gulf of Thailand and South China Sea in 4 seasons from direct measurement. In Proceeding of the Third Seminar on the Water Quality and the Quality of the Living Resources in Thai Waters, 26–28 March 1984. National Research Council of Thailand at Marine Science Center, Srinakharinwirot University, Bangsaen, Chonburi Province, p140–148.

Siripong, A. (1985). The characteristics of the tides in the Gulf of Thailand. Report, Marine Science Department, Chulalongkorn University, Bangkok, 1p.

Soegiarto, A. (1985). Oceanographic assessment of the East Asian Seas. Environment and Resources in thePacific, UNEP Regional Seas Reports and Studies, 69, p173–184.
Soegiarto, A., & Birowo, A.T. (1975). Oceanologic Atlas of the Indonesian and Adjacent Waters. Book 1. Jakarta, Indonesia: National Institute of Oceanology.

Sojisuporn, P., Morimoto, A. and Yanagi, T. (2010). Seasonal variation of sea surface current in the Gulf of Thailand. Coastal Marine Science, 34 (1), p91-102.

Sojisuporn, P., Sangmanee, C., Wattayakorn, G. (2013). Recent estimate of sea-level rise in the Gulf of Thailand. Maejo International Journal of Science and Technology, 7, p106-113.

Soralump, S. (2010). Rainfall-Triggered Landslide: from research to mitigation practice in Thailand. Proceedings of the 17th Southeast Asian Geotechnical Conference, Taipei, Taiwan, p153–158.

Splinter, K.D., Gonzalez, M.V.G., Oltman-Shay, J., Rutten, J., and Holman, R. (2018). Observations and modelling of shoreline and multiple sandbar behaviour on a high-energy meso-tidal beach. Continental Shelf Research, 159, p33-45.

Trisirisatayawong, I., Naeije, M., Simons, W., Fenoglio-Marc, L. (2011). Sea level change in the Gulf of Thailand from GPS-corrected tide gauge data and multi-satellite altimetry. Global Planetary Change, 76, p137-151.

Vongvisessomjai, S. (2006). Will sea level really fall in the Gulf of Thailand? Songklanakarin Journal of Science and Technology, 2006, 28, p227-248.

Vos, K., Splinter, K.D., Harley,M.D., Simmons, J.A., Turner, I.L. (2019). CoastSat: A Google Earth Engine-enabled Python toolkit to extract shorelines from publicly available satellite imagery, Environmental Modelling & Software, 122, 104528, p1364-8152.

Ward, R. (2012). Landscape and ecological modelling: Development of a plant community prediction tool for Estonian coastal wetlands. PhD thesis, University of Brighton, 319p.

Wattayakorn, G. (2006). Environmental Issues in the Gulf of Thailand. In: Wolanski, E. (ed.) The Environment in Asia Pacific Harbors. Springer. The Netherlands, p249-259.

Wattayakorn, G. and Jaiboon, P. (2014). An assessment of biogeochemical cycles of nutrients in the Inner Gulf of Thailand. European Chemical Bulletin, 3 (1), p50-54.

Wentworth, C.K. (1922). A Scale of Grade and Class Terms for Clastic Sediments. The Journal of Geology, 30(5), p377–392.

Wyrtki, K., 1961. Physical oceanography of the Southeast Asian waters. 1st Ed. University of California, California, 195p.

Yanagi, T. and Takao, T. (1998). Clockwise phase propagation of semi-diurnal tides in the Gulf of Thailand. Journal of Oceanography, 54, p143–150.

Yumuang, S. (2006). 2001 Debris flow and debris flood in Nam Ko area, Phetchabun province, central Thailand. Environmental Geology, 51, p545-564.

Websites:

https://www.geothai.net/gulf-of-thailand [2016, Oct 8]. Last accessed 2021.

https://km.dmcr.go.th/, 2013. Last accessed 2021.

http://www.dmr.go.th/, 2015. Last accessed 2021.

http://www.dmr.go.th/, 2012. http://www.dmr.go.th/download/Landslide/event_landslide1.htm. Last accessed 2021.

https://brittany-kayaking.com/, 2020. Last accessed 2021.

http://www.mkh.in.th/, 2020. Last accessed 2021.

https://brittany-kayaking.com/, 2020. Last accessed 2021.

https://www.bangkokpost.com/. Last accessed 2021.

https://km.dmcr.go.th/. Last accessed 2021.

https://www.bangkokpost.com/. Last accessed 2021.

https://km.dmcr.go.th/. Last accessed 2021.

http://www.mkh.in.th. Last accessed 2021.

http://www.aws-observation.tmd.go.th/. Last accessed 2021.

https://origin.cpc.ncep.noaa.gov/products/analysis_monitoring/ensostuff/ONI_v5.php. Last accessed 2021.

https://www.usgs.gov/centers/whcmsc/science/digital-shoreline-analysis-system-dsas?qt-science_center_objects=0#qt-science_center_objects. Last accessed 2021.

EM-DAT, 2021. EM-DAT: The International Disaster Database, http://www.emdat.be/database. Last accessed 2021.

https://www.ncdc.noaa.gov/ibtracs/. Last accessed 2021.

Floodlist.com, 2020. Last accessed 2021.

Project Principal Investigators

Professor Cherith Moses, Edge Hill University (Project PI, UK PI)

Associate Professor Dr Kanchana Nakhapakorn, Mahidol University (SE Asia PI)

Project Co-Investigators

Dr Raymond Ward, University of Brighton, UK. (Work Package 1 Lead)

Dr John Barlow, University of Sussex, UK

Dr Jerome Curoy, University of Brighton

Dr Yi Wang, University of Sussex, UK. (Work Package 2 Lead)

Dr Netsanet Alamirew, University of Sussex.

Dr Uma Langkulsen, Thammasat University, Thailand. (Work Package 3 Lead)

Dr Pannee Cheewinsiriwat, Chulalongkorn University, Thailand. (Work Package 4 Lead)

Dr Chalermpol Chamchan, Mahidol University, Thailand. (Work Package 6 Lead)

Dr. Suparee Boonmanunt, Mahidol University, Thailand. (Work Package 6 co-Lead).

Professor Charles Watters, University of Sussex, UK

Project partners

Ambiental, UK

Department of Marine and Coastal Resources (DMCR), Thailand Government, Ministry of Natural Resources and Environment

National Centre for Atmospheric Research, USA